Complex Colloidal Structures by Self-Assembly in Electric Fields

Universiteit Utrecht

PhD thesis, Utrecht University, The Netherlands
ISBN: 978-90-393-5729-3

A digital (color) version of this thesis is available at http:// www. colloid. nl

Complex Colloidal Structures by Self-Assembly in Electric Fields

Complexe Colloïdale Structuren door Zelforganisatie in Elektrische Velden

(met een samenvatting in het Nederlands)

Proefschrift

ter verkrijging van de graad van doctor aan de Universiteit Utrecht op gezag van de rector magnificus, prof. dr. G. J. van der Zwaan, ingevolge het besluit van het college voor promoties in het openbaar te verdedigen op

woensdag 8 februari 2012 des ochtends te 10.30 uur

door

Hanumantha Rao Vutukuri

geboren te Zulakallu, India

Promotor: Prof. Dr. A. van Blaaderen
Co-promotor: Dr. A. Imhof

This work is part of the research programme of the 'Stichting voor Fundamenteel Onderzoek der Materie (FOM)', which is financially supported by the 'Nederlandse Organisatie voor Wetenschappelijk Onderzoek (NWO)'.

“There is Plenty of Room at the Bottom”
(Richard Feynman, Pasadena, 29 December 1959)

Contents

1

Introduction

1.1 Colloids

The term colloid originates from the Greek word "κολλα", which means glue. In 1861, Thomas Graham (1805-1869) coined the terms colloid and crystalloid to classify two types of matter he observed in his experiments. While colloidal particles form a dispersion, crystalloids form a homogeneous solution when dissolved in a solvent [1]. Wittingly and unwittingly, we encounter colloidal particles in our daily life, e.g., foods, cosmetics, detergents, inks, paints, photographic films, and papers. Colloids also play an important role in emerging technologies such as photonic crystals, advanced ceramic processing, and 3D ink-jet technology. There is no strict definition of a colloidal particle in terms of well-defined requirements on its size, shape, or composition [2, 3]. However, the upper boundary is set by the demand that the particles should be small enough to experience Brownian motion, whereas the lower limit is set by the condition that they have to be much larger than solvent molecules [2, 3].

Colloids are typically defined as objects having at least one dimension in the size range of a few nanometers to several micrometers that form a dispersed phase when suspended in a continuum solvent [2, 3]. Due to the continuous bombardment by solvent molecules, which are much smaller, the colloids experience random thermal fluctuations that cause an irregular motion of the particles through the solvent, known as Brownian motion. As a result of Brownian motion, the colloidal particles are able to explore configurational space, and eventually reach the equilibrium configuration that minimizes the free energy. These phases are analogous to the states of matter observed in atomic and molecular physics, but occur over much larger length scales, and longer time scales. The relatively large length scales, and long time scales make it easy for these phases to be studied in real space and real time. Therefore quantities that are experimentally difficult to observe in atomic and molecular systems, for instance, fundamental aspects of phase behavior [4], and dynamic processes such as the glass transitions [5, 6], can be measured with relative ease in colloidal systems through the use of direct techniques, such as bright field microscopy and confocal microscopy, or indirect techniques, such as light scattering and rheology. An important feature of the colloidal particles is the possibility of controlling the size, shape, and composition.

The interactions between the particles can also be manipulated by means chemical (e.g. charge, polymer coating) and physical (e.g. flat and rough surfaces) modification of surface of the particles and physical properties of the dispersing medium. The interactions between the colloidal particles can be altered by external fields such as electric fields, magnetic fields, and optical fields.

1.2 Complex colloidal structures by self-assembly

The assembly of colloidal particles has long been a rich and continuously growing area of materials science, with great potential for a broad range of applications including electronics, optics, and biotechnology [7–12]. Within this field, the bulk of the research has been devoted to studying the assembly of isotropic spherical particles [7–10]. For isotropic spherical particles, the interactions between them are often non-directional. As a consequence, monodisperse isotropic spherical particles commonly yield crystal phases of simple symmetry, such as face-centered cubic, hexagonal close-packed and body-centered cubic. By introducing a second species of particles of a different size into the system has already offered different stoichiometries and crystal symmetries which are strongly dependent on the size ratio and concentrations [13–15]. However, these binary structures are harder to control and grow.

Recently, there has been growing interest in the design of more complex structures to see how such a change in microstructure could influence certain material properties, especially optical properties, but also to answer the demand for more realistic model systems for molecular analogues [7–12]. The challenge is to first find and then to experimentally realize the right colloidal building blocks and interaction potentials that lead to these desired structures [11, 12]. One possible way of realizing new materials is by employing anisotropic particles as building blocks. Although a wide variety of methods are available for generating non-spherical particles [7, 9, 11, 12], most of them only yield particles with simple shapes such as dumbbells, cylinders, platelets, discs, and cubes. Only few of these methods were successful to produce monodispersed particles in large quantities. A simple way of introducing directionality into the anisotropic particles systems is by means of depletion attractions by adding a non-adsorbing polymer. Some examples include equilibrium two-dimensional (2D) fluid-like membranes composed of fd viruses [16], reconfigurable composite particle clusters including chains through shape-directed recognition based on lock- and key interactions [17], and simple close-packed cubic crystals of micron-sized hollow silica [18].

Van Blaaderen has recently introduced the elegant term of “colloidal molecules” [19], which recognizes that spherical colloids can be treated as if they were atoms, and that molecules form more complex materials than atoms do. Given the analogy between spherical colloidal particles and atoms, the most versatile and fruitful approach to achieve colloidal structures with complex, and well-controlled shapes should be achieved by self-assembly of spherical particles with complex and/or di-

rectional interactions. A different variety of methods now available for designing complex structures using different types of complex interactions as summarized in a several review papers, e.g., [7, 9, 11, 12]. Here, we shall therefore briefly describe a few methods which are some-what related to our work. Regular colloidal clusters have been reported using self-assembly of identical particles in emulsion drops, which acts as confining geometries [20]. Recently, Cho *et al*. [21] have designed composite colloidal clusters using the same technique [20] with two quite differently sized particles. More recently, some other notable methods have been reported (see review papers [9, 11, 22]) for fabricating colloidal molecules through controlled clustering routes: assisted by depletion interactions, by capillary condensation, by electrostatic interactions, by coalescence, by template directed, and by chemical bonding.

Another route one can take to obtain complex interactions is through spherical colloids containing patches of another composition or site-specific functional groups pointing in different directions. Almost two decades ago, De Gennes introduced a term called "Janus particles", which refers to micro- and nanoparticles with at least two physically or chemically differing surfaces. Nowdays, people refer to this class of particles as patchy particles of which the Janus particles are a special case. Recently, a colloidal kagome lattice structure has been reported using triblock Janus particles, which exhibit a combination of electrostatic-repulsion patch around the equator and hydrophobic attraction patches at the poles [23]. The sequence-specific binding properties of DNA methods have also been used in designing complex colloidal assemblies [24, 25].

Another possible route to tailor the interaction potential is by combining different attractive and repulsive components, or by using external fields to induce new interactions in existing systems. The latter can be achieved by introducing directional, anisotropic interactions using magnetic or electric dipoles. This is a practical strategy to impart anisotropy into self-assembled morphologies even for the most symmetric building blocks: colloidal spheres [11, 12, 26–30]. If there is a mismatch in permittivity (permeability) between the particles and the suspending medium, the colloids acquire an induced dipole moment. A major advantage of this approach is that the interactions are adjustable and fully reversible. Moreover, a large number of parameters can be used to control and tune particle interactions and subsequent self-assembly in AC electric fields, including field strength and frequency, particle shape, particle and solvent dielectric properties [26–32]. Interestingly, the relatively simple anisotropic dipolar interaction already gives rise to several new phases [31] in a uniaxial field. A combination of linker molecules and uniaxial fields can be used to design 1D linear chains with tunable stiffness (Chapter 2). Bibette *et al*. have shown that under certain conditions dynamic magnetic chains spontaneously break the symmetry of surface fluid flows and turn into self-propelled entities, which behave like artificial swimmers [33]. Biaxial fields have already proven to increase the complexity of systems and thus open up another range of novel interactions such as "inverse" dipolar interactions. This

inverse dipolar interactions offer an entirely different structures: sheets ([28], and Chapter 3). More recently, Osterman *et al*. have reported self-assembly of magnetic particles into membrane like structures in triaxial magnetic fields, which applied at a magic-angle [32]. Most studies of directed self-assembly in electric and magnetic fields have used spherical particles [26–32].

Particle anisotropy has a very strong effect on directed self-assembly in AC electric fields. For example, for Janus particles yield staggered chains [26], hetero dimer colloids, which consist of PMMA on one side and PS on the other side forms atactic like chains (Chapter 2). Fields can be used to control both the translational and orientational order of anisotropic particles (Chapters 6 & 7), and lead to structures that are otherwise unattainable using spherical particles.

1.3 Scope of this thesis

The work presented in this thesis mainly focuses on how we exploit the self-assembly of both isotropic and anisotropic particles towards the fabrication of one-dimensional (1D), two-dimensional (2D), and three-dimensional (3D) complex colloidal structures using external electric fields and/or a simple in-situ thermal annealing method. Some of these structures, for instance the 1D systems, can be used to mimic molecular systems. In Chapter 2, we present methods to produce model systems that are essentially colloidal analogues of polymer chains in all three stiffness regimes that can be observed on a single particle level, even in concentrated systems without using molecular tracers. We show our methods rely on a combination of induced dipolar interactions by external fields to assemble the particles into strings and a simple bonding step (a simple in-situ thermal annealing method or a seeded growth of a thin layer) to keep the particles together even after the field is switched off. We discuss how to obtain control over the length, and the flexibility of the bead chains. Next, we demonstrate that the flexibility of the charged strings can be tuned from very rigid (hard rod-like) to semi-flexible (as in the simplified polymer model of beads on a string [34]) by changing the ionic strength. In Chapter 3, we exploit this simple thermal sintering method further for bonding polymeric colloidal particles after they have been assembled into various three-dimensional structures. Next, we discuss the generality of our method by implementing this method to close and non-close packed structures. Moreover, we characterize these structures before and after the bonding using confocal and electron microscopy. In Chapter 4, we use our thermal annealing method to synthesize more complex shape particles such as rhombic dodecahedron particles and also we discuss the stability of the particles. In Chapter 5, the positive dielectrophoresis is exploited to direct strings of colloidal particles on a regular patterned electrode. In Chapters 6 and 7 attention is shifted to anisotropic particles. The self-assembly of gold nano-sheets as a function of salt with electric fields is studied in Chapter 6. In the Chapter 7 we concentrate on directing the self-assembly of colloidal cubes with electric fields.

References

[1] T. Graham, *Liquid difusion applied to analysis*, Philos. Trans. of the Royal Soc. **151** (1861).

[2] D. Evans and H. Wennerstrom, *The Colloidal Domain: where Physics, Chemistry, Biology, and Techonology meet*, VCH publishers, Newyork, 1994.

[3] W. B. Russel and D. A. Saville, *Colloidal dispersions*, Cambridge Univ. Press, Cambridge, 1999.

[4] V. J. Anderson and H. N. W. Lekkerkerker, *Insights into phase transition kinetics from colloid science*, Nature **416**, 811 (2002).

[5] P. K. N., A. M. Puertas, J. Bergenholtz, A. Egelhaaf, S. U. Moussaid, P. N. Pusey, A. B. Schofield, C. M. E., M. Fuchs, and W. C. K. . Poon, *Multiple glassy states in a simple model system*, Science **296**, 104 (2002).

[6] W. K. Kegel and A. van Blaaderen, *Direct observation of dynamical heterogeneities in colloidal hard-sphere suspensions*, Science **287**, 290 (2000).

[7] C. Aguirre, E. Reguera, and A. Stein, *Tunable colors in opals and inverse opal photonic cystals*, Adva. Fun. Mat. **20**, 1033 (2010).

[8] A. Stein, F. Li, and N. R. Denny, *Morphological control in colloidal crystal templating of inverse opals, hierarchical structures, and shaped particles*, Chem. Mat. **20**, 649 (2008).

[9] F. Li, D. P. Josephson, and A. Stein, *Colloidal assembly: The road from particles to colloidal molecules and crystals*, Angew. Chemie. **50**, 360 (2011).

[10] J. Galisteo-López, M. Ibisate, R. Sapienza, L. S. Froufe-Perez, and C. López, *Self-assembled photonic structures*, Adva. Mat. **23**, 30 (2011).

[11] S. M. Yang, S. H. Kim, J. M. Lim, and G. R. Yi, *Synthesis and assembly of structured colloidal particles*, J. Mater. Chem. **18**, 2177 (2008).

[12] S. C. Glotzer and M. J. Solomon, *Anisotropy of building blocks and their assembly into complex structures*, Nature Materials **6**, 557 (2007).

[13] S. Hachisu and S. Y., *Optical demonstration of crystalline superstructures in binary mixtures of latex globules*, Nature **283**, 188 (1980).

[14] K. P. Velikov, C. G. Christova, R. P. A. Dullens, and A. vanBlaaderen, *Layer-by-Layer Growth of Binary Colloidal Crystals*, Science **296**, 106 (2002).

[15] L. C. Filion and M. Dijkstra, *Prediction of binary hard-sphere crystal structures*, Phy. Rev. E **79**, 46714 (2009).

[16] B. Edward and D. Zvonimir, *Entropy driven self-assembly of nonamphiphilic colloidal membranes*, Proce. Nat. Aca. Sci. **107**, 10348 (2010).

[17] S. Sacanna, W. T. M. Irvine, P. M. Chaikin, and D. J. Pine, *Lock and key colloids*, Nature **464**, 575 (2010).

[18] L. Rossi, S. Sacanna, W. T. M. Irvine, P. M. Chaikin, and D. J. Pine, *Cubic crystals from cubic colloids*, Soft Matter **7**, 4139 (2011).

[19] A. van Blaaderen, *Anisotropy of building blocks and their assembly into complex structures*, Science **301**, 470 (2003).

[20] V. N. Manoharan, M. T. Elsesser, and D. J. Pine, *Anisotropy of building blocks and their assembly into complex structures*, Science **301**, 483 (2003).

[21] Y.-S. Cho, G.-R. Yi, J.-M. Lim, S.-H. Kim, V. N. Manoharan, D. J. Pine, and S.-M. Yang, *Self-Organization of Bidisperse Colloids in Water Droplets*, J. Ame. Chem. Soc. **127**, 15968 (2005).

[22] E. Duguet, A. Desert, A. Perro, and S. Ravaine, *Design and elaboration of colloidal molecules: an overview*, Chem. Soc. Rev. **40**, 941 (2011).

[23] C. Qian, C. B. Sung, and G. Steve, *Directed self-assembly of a colloidal kagome lattice*, Nature **469**, 381 (2011).

[24] C. A. Mirkin, R. L. Letsinger, R. C. Mucic, and J. Storhoff, *A DNA-based method for rationally assembling nanoparticles into macroscopic materials*, Nature **382**, 607 (1996).

[25] S. Y. Sung Yong Park, K. R. Lytton-Jean, B. Lee, S. Weigand, G. C. Schatz, and C. A. Mirkin, *DNA-programmable nanoparticle crystallization*, Nature **451**, 553 (1996).

[26] M. Grzalczak, J. Vermant, E. M. Furst, and M. Liz-Marzan, *Directed self-assembly of nanoparticles*,

ACS Nano **4**, 3591 (2010).

[27] H. R. Vutukuri, A. F. Demirors, P. Bo, P. D. J. van Oostrum, A. Imhof, and A. van Blaaderen, *Colloidal analogues of charged and uncharged polymer chains with tunable stiffness*, submitted.

[28] M. E. Leunissen, H. R. Vutukuri, and A. van Blaaderen, *Directing colloidal self-assembly with biaxial electric fields*, Adav. Mat. **21**, 3116 (2009).

[29] K. D. Hermanson, S. O. Lumsdon, J. P. Williams, E. W. Kaler, and O. D. Velev, *Dielectrophoretic assembly of Electrically functional microwires from nanoparticle suspensions*, Science **294**, 1082 (2001).

[30] R. M. Erb, H. S. Son, B. Samanta, V. M. Rotello, and B. B. Yellen, *Magnetic assembly of colloidal superstructures with multipole symmetry*, Nature **457**, 999 (2009).

[31] A. Yethiraj and A. van Blaaderen, *A colloidal model system with an interaction tunable from hard sphere to soft and dipolar*, Nature **421**, 513 (2003).

[32] N. Osterman, I. Poberaj, J. Dobnikar, D. Frenkel, P. Ziherl, and D. Babic, *Field-Induced Self-Assembly of Suspended Colloidal Membranes*, Phys. Rev. Lett. **103**, 228303 (2009).

[33] R. Dreyfus, J. Baudry, L. Roper, M. Fermigier, A. Howard A. Stone, and J. Bibette, *Microscopic artificial swimmers*, Nature **437**, 862 (2005).

[34] J. Baschnage, K. Binder, W. Paul, U. W. Laso, M. andSuter, I. Batoulis, W. Jilge, and T. Bürger, *On the construction of coarse-grained models for linear flexible polymer-chains - distribution-functions for groups of consecutive monomers.*, J. Chem. Phys. **91**, 6014 (1995).

2

Colloidal analogues of charged and uncharged polymer chains with tunable stiffness

A quest for colloidal particles with more complex shapes and interactions is fueled by applications in self-assembly, and advanced functional materials design, but also by the demand for more realistic model systems for molecular analogues. Here, we present a general methodology to produce model systems of colloidal analogues of (bio-)polymer chains with a tunable flexibility from smaller dielectric-colloids using electric fields and a simple bonding step. We demonstrate that permanent bead chains can be made using either thermal annealing or seeded growth on inorganic, organic and hybrid particles. The combination of soft repulsions with induced dipolar interactions gives rise to high yields and purity of the permanent bead chains or strings of the original starting particles. Additionally, we discuss how to obtain control over the length, and the flexibility of the chains. We show that chain conformations can be controlled by manipulating interactions between the particles in a chain through electrostatic repulsions, as in polyelectrolytes, and/or using depletion attractions. We demonstrate that our methodology not only leads to the possibility of achieving unprecedented single chain information of model (bio-)polymers in concentrated systems, but also offers new opportunities for advanced functional materials.

2.1 Introduction

Spherical colloids have been used successfully as condensed matter model systems in order to study fundamental aspects of phase behavior [1], and dynamic processes such as the glass transition [2, 3]. Recently, there has been growing interest in the design of colloidal particles with more complex shapes and interactions [4, 5]. Some examples include rod-like particles [6], regular clusters [7], chiral clusters [8], particles interacting with inverse dipolar interactions [9, 10], and patchy particles [11]. The assembly of colloids into polymer-like chains would constitute a significant step in the design of "colloidal molecules" [12].

Polymer science typically separates polymer stiffness into three regimes, namely rigid-rods, semi-flexible polymers and flexible polymers [13]. Biopolymers (semiflexible) such as microtubules, actin, and DNA have become useful systems for the study of fundamental aspects of polymer physics because they have several advantages over synthetic polymers [14–16]. However, even for semiflexible biopolymers the dynamics cannot be followed down to the individual monomer level by present microscopy techniques [14–16]. Previous work on making rigid colloidal bead chains was based on using a combination of the microfluidic trapping of particles in confined geometries and thermal fusing of the particles [17]. However, this technique is limited by particle size, scalability, and stiffness control between the particles. It has previously been demonstrated that the stiffness of bonds between magnetic beads in a chain can be controlled by controlling the length of a DNA-linker molecule [18–22]. However, this method relies on the specific functional groups binding to the surface of the magnetic particles and linker molecules that involve complicated chemistry [18–22]. Additionally, magnetic materials usually have a high density and strongly absorb light, making them less suitable to study concentrated systems in real space.

In this chapter we present methods to produce model systems of colloidal particle chains in all three stiffness regimes that can be observed on a single particle level even in concentrated systems without using molecular tracers. Our methods rely on a combination of induced dipolar interactions by external fields to assemble the particles into strings and a bonding step to keep the particles together even after the field is switched off. In addition, we demonstrate the generality of our method by using it to build several other colloidal polymer analogues, such as block-copolymer chains made by combining rigid and flexible strings, spherocylinders formed by heating rigid chains and both a-tactic and iso-tactic chains from dimer particles as the monomers. This approach can, in principle, be used with any type of colloidal particles. Furthermore, we demonstrate that the flexibility of the charged strings can be tuned from very rigid (hard rod-like) to semi-flexible (as in the simplified polymer model of beads on a string [23]). In addition, we have obtained control over the length, and the flexibility of the chains. Moreover, our systems can be both refractive index and density matched, so that bulk measurements in real-space are possible.

we demonstrate the generality of our method by using it to build several other colloidal polymer analogues, such as block-copolymer chains made by combining rigid and flexible strings, spherocylinders formed by heating rigid chains and both a-tactic and iso-tactic chains from dimer particles as the monomers. Furthermore, we demonstrate that the flexibility of the charged strings can be tuned from very rigid (hard rod-like) to semi-flexible (as in the simplified polymer model of beads on a string [23]). In addition, we have obtained control over the length, and the flexibility of the chains. This approach can, in principle, be used with any type of colloidal particles.

2.2 Colloids in an external AC electric field

Colloidal particles whose dielectric constant is different from that of the solvent, acquire a dipole moment parallel to an external electric field. These suspensions are called ER (electro-rheological) fluids because their rheological properties can be controlled by the external field. Induced dipolar interactions between the particles can be calculated with the point-dipole approximation [24]. The total interaction potential between the charged particles can be described as the sum of a DLVO-type screened Coulomb interaction [25], a hard-core repulsion, and an induced dipolar interaction. We neglected the van der Waals interactions, because our systems are either well index matched and/or the range of steric repulsions is sufficient enough so that the particles will never come into contact. The DLVO-type screened Coulomb interaction and the hard-core repulsion are isotropically repulsive and it can be written as follows:

$$\frac{U_{\text{Yukawa}(r_{ij})}}{k_B T} = \begin{cases} \epsilon_c \frac{exp[-\kappa(r_{ij}-\sigma)]}{r_{ij}/\sigma}, & r_{ij} \geq \sigma \\ \infty, & r_{ij} < \sigma \end{cases} \tag{2.1}$$

where $\mathbf{r}_{ij}$ is the vector separating particles *i* and *j*, k_B is the Boltzmann constant, *T* is the absolute temperature, κ is the inverse Debye screening length ($\kappa^{-1} = 1/\sqrt{8\pi\lambda_B c}$ for a number density 2*c* of a monovalent salt is given below) and σ the hard-core, or particle diameter. The value of this potential at contact (when $r_{ij} = \sigma$) is

$$\epsilon_c = \frac{Z^2}{(1+\kappa\sigma/2)^2}\frac{\lambda_B}{\sigma} \tag{2.2}$$

where *Z* is the particle charge and $\lambda_B = e^2/4\pi\epsilon_0\epsilon_m k_B T$ is the Bjerrum length of the suspending medium with dielectric constant ϵ_m; e is the elementary charge and ϵ_0 is the permittivity of vacuum. The (point) dipole-dipole contribution to the total interaction can be written as:

$$\frac{U_{dip(\mathbf{r}_{ij})}}{k_B T} = \frac{\gamma}{2}\left(\frac{\sigma}{r_{ij}}\right)^3 (1 - 3\cos^2\theta_{ij}) \tag{2.3}$$

where, θ_{ij} is the angle that $\mathbf{r}_{ij}$ forms with the z axis, which is the direction of the electric field (Figure 2.1a). The dimensionless prefactor is given by:

$$\gamma = \frac{\mathbf{p}^2}{2\pi\epsilon_0\epsilon_m\sigma^3 k_B T} \tag{2.4}$$

and $\mathbf{p} = \frac{\pi}{2}\alpha\epsilon_0\epsilon_m\sigma^3\mathbf{E}_{loc}$ is the dipole moment induced in the particle by the local electric field where $\mathbf{E}_{loc} = \mathbf{E} + \mathbf{E}_{dip}$. Here, $\mathbf{E}$ is the external electric field and $\mathbf{E}_{dip}$ is the field induced by the other dipoles. Finally, the polarizability of the particles in the medium is determined by α (the Claussius-Mossotti factor):

$$\alpha = \frac{\epsilon_p - \epsilon_m}{\epsilon_p + 2\epsilon_m} \tag{2.5}$$

where ϵ_p and ϵ_m are particle and medium dielectric constants. From these equations, it can be seen that the phase behavior basically depends on four parameters: the density of the suspension, the charge of the colloids, the screening length, and the strength of the applied field. From Eq. 2.3 it is also clear that the dipole-dipole interaction is anisotropic. It gives rise to an attraction when $\theta_{ij} < 54.7$, but repulsive interactions otherwise.

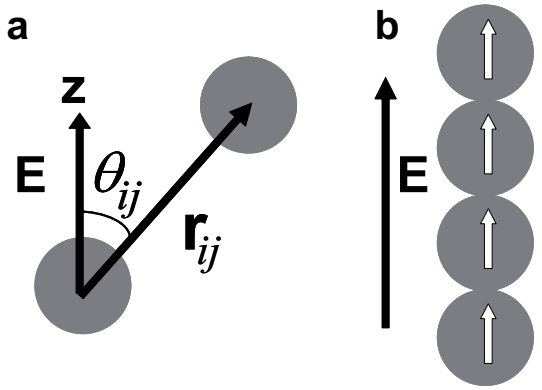

Figure 2.1: Illustration of induced dipolar interactions. **a**, Two particle centers connected by vector $\mathbf{r}_{ij}$. The vector $\mathbf{r}_{ij}$ forms an angle θ_{ij} with the direction (Z) of the external electric field. **b**, The dipole-dipole interaction favors configurations where the dipoles (denoted by the white arrows) are oriented head-to-toe fashion.

Suspensions of particles with long-range screened Coulomb interactions and induced dipolar interactions show rich phase behavior [26–28]. The dispersion

structure can be tuned from strings (1D) [29, 30], to sheets (2D) [10], and eventually to equilibrium 3D crystallites by varying the dipolar field strength [26–28, 31]. A key feature of external electric or magnetic field directed assembly is the reversibility of the interactions, which leads to a rapid return to the disordered state when the field is removed. Such effects are useful in obtaining reconfigurable and switchable assemblies, but could also be exploited to quickly anneal defects in structures by rapidly cycling the field on and off.

2.3 Experimental details

PMMA particle synthesis and suspensions

We synthesized polymethylmethacrylate(PMMA) particles by dispersion polymerization, covalently labelled with the fluorescent dye 7-nitrobenzo-2-oxa-1,3-diazol (NBD) or rhodamine isothiocyanate (RITC) and sterically stabilized with poly(12-hydroxystearic acid) [32]. Particles with a non-crosslinked core and a crosslinked shell were synthesized by the procedure of Dullens *et al* [33]. We used suspensions of 1.05 μm, 1.10 μm, 2.30 μm, and 2.60 μm diameter PMMA spheres. The 1.05 μm, 1.10 μm, and 2.30 μm particles were dispersed in a 3:1 wt/wt mixture of cyclohexyl bromide (Fluka) and cis-decalin (Sigma), saturated with tetrabutylammonium bromide (TBAB, Sigma). In this mixture, the particles were nearly density and refractive index-matched, and they behaved like hard-spheres [27]. All solvents were used as received without any further purification.

Sterically stabilized PS particle synthesis

Styrene (St, Fluka) was passed over an aluminum oxide containing column to remove the inhibitor. After the inhibitor was removed, the styrene was stored in a refrigerator. Azo-bis-isobutyronitrile (AIBN, Janssen Chemica) was re-crystallized in ethanol before use. Polyvinylpyrrolidone (PVP, Sigma) with average molecular weight 360,000 g/mol (K-90) was used as stabilizer. Dimethyl sulfoxide (DMSO, Fluka) and ethanol(Fisher) were used as supplied.

The standard recipe for post-addition dispersion polymerization of styrene [34] is listed in Table 2.1. The following procedure was used: all of the stabilizer (PVP), initiator (AIBN), one third of the monomer and half of the ethanol were added to a 250 ml three-necked flask equipped with a gas supply, a condenser, and a Teflon-coated stirring bar. After a homogeneous solution had formed at room temperature, nitrogen was bubbled through the reaction system for 30 min. The flask was then immersed in a silicon oil bath, maintained at 70 ^{o}C and stirred at 100 rpm. The remaining two thirds of monomer was dissolved in the remaining ethanol at 70 ^{o}C under nitrogen. Half of this hot mixture was added into the reaction flask after the polymerization reaction had run for 1 h, and the rest of the mixture was added after the polymerization reaction had run for 2 h. The

Chemicals	Mass (g)
Styrene	15.0
PVP	1.0
Ethanol	50.0
AIBN	0.025

Table 2.1: Preparation of sterically stabilized PS particles in ethanol.

reaction mixture was maintained at 70 ^{o}C for 24 h before cooling. The final particles suspension was washed 3 times with ethanol using a centrifuge to remove the free stabilizer. The obtained particles were dried under a nitrogen flow and stored at room temperature. The size of the particles was 1.35 μm as determined by static light scattering (SLS) and electron microscopy methods.

Electric-field setup

We used two types of sample cells: rectangular capillaries (VitroCom, UK) and home made sandwich indium-tin oxide (ITO) coated glass cells. The rectangular sample cells consisted of a 0.1 mm $\times$ 1.0 mm capillary with two 50 μm thick nickel-alloy wires (Goodfellow, UK) threaded along the side walls. All samples were confined to glass capillaries with inner dimensions of 0.1 mm $\times$ 1.0 mm or 0.1 mm $\times$ 2.0 mm. Our sandwich ITO coated glass cell consisted of two parallel no. 1 glass cover slips (130 - 160 μm thick, Menzel), which were completely coated with a conductive, semi-transparent layer of indiumtinoxide (ITO, Diamond coatings limited, UK). They were kept apart by a pair of glass spacers, which were cut out of no. 1 or no. 0 (80 - 120 μm thick) slides, and which were placed at opposite sides of the sample space. Typically, the height of the sample space, enclosed by the cover slips, was 100 - 200 μm, with an area of $\sim$ 1 cm^2. The conductive ITO layer was in contact with the suspension. The cell was constructed on top of a 1.0 mm thick microscopy slide, for extra support and easy mounting on the stage of the microscope. We glued everything together with no. 71 UV-curing optical adhesive (Norland). For the electrical contacts with the ITO electrodes we used silver paint (Jeol) and thin thermocouple alloy wire (diameter 50 μm, Goodfellow), which was then wrapped around standard electronic wire. We used a function generator (Agilent, Model 3312 OA) and a wide band voltage amplifier (Krohn-Hite, Model 7602M) to generate the electric fields. The field strength and the frequency were measured by an oscilloscope (Tektronix, Model TDS3052).

Microscopy

After filling the cell with the colloidal suspension, it was sealed at both ends with UV-curing optical adhesive (Norland no.68), and we studied particle dynamics by means of confocal laser scanning microscopy (Leica TCS SP2). We recorded xy images of 512 $\times$ 512 and 1024 $\times$ 1024 pixels. We also recorded 3D data, consisting of series of xy images at different depths (z). After drying the sample, structures that were made permanent by thermal annealing were imaged with a scanning electron microscope (FEI, XL30FEG).

Electrical conductivity measurements

Dimethyl sulfoxide (DMSO) was purified and ions were removed by contact with the mixed ionic resin beads (Bio-Rad AG 501-X8 Resin, 20-50 mesh, Biotechnology grade) for 4-5 days. We estimated the Debye screening length of our suspensions by measuring the conductivity (with a Radiometer analytical CDM 230 conductivity meter) of the normal and a strongly de-ionized DMSO and then applying Walden's rule [35].

Optical tweezers setup

Our setup for optical trapping has been described in great detail by Vossen *et al* [36]. We used a 1064 nm infrared laser (Spectra Physics) to trap the higher-refractive-index particles. In short, we applied time-sharing using acousto-optic deflectors to generate two traps and to vary their positions. Particle dynamics were followed by bright field microscopy using a charged coupled device (CCD) camera (UNIQ, UP-600).

2.4 Results and discussion

2.4.1 General behavior of dielectric particles in an AC field

Here, we used a high frequency (1 MHz) field to prevent polarization of the electric double layer. Upon application of an AC external electric field (E_{rms} = 0.30 Vμm^{-1}, f = 1 MHz, where E_{rms} is the root-mean-square field strength, and f is the frequency), the induced dipole moment in each particle favored the assembly of the particles into strings of one particle thick, aligned in the field direction in a head-to-tail arrangement with a broad distribution in the length of the chains as seen Figure 2.2a. In the low-field regime, the stable structure was a string fluid phase that consisted of chains of particles parallel to the field direction and that showed liquid like order perpendicular to the field direction [27, 28, 37]. The time scale for chain formation was on the order of a few seconds. In addition, by increasing the applied field strength, the average string length could be increased until it spanned the entire height of the gap between the two electrodes. The long

ranged repulsions are essential as they also greatly stabilize the individual strings, preventing them from forming sheets by sideways assembly of strings at higher field strengths. Furthermore, the strings became straighter and stiffer with increasing strength of the dipole-dipole interactions, which suppressed the thermal fluctuations. The string like structures rely on the presence of an external electric field, i.e., the particles disperse again when the field is switched off (Figure 2.2b).

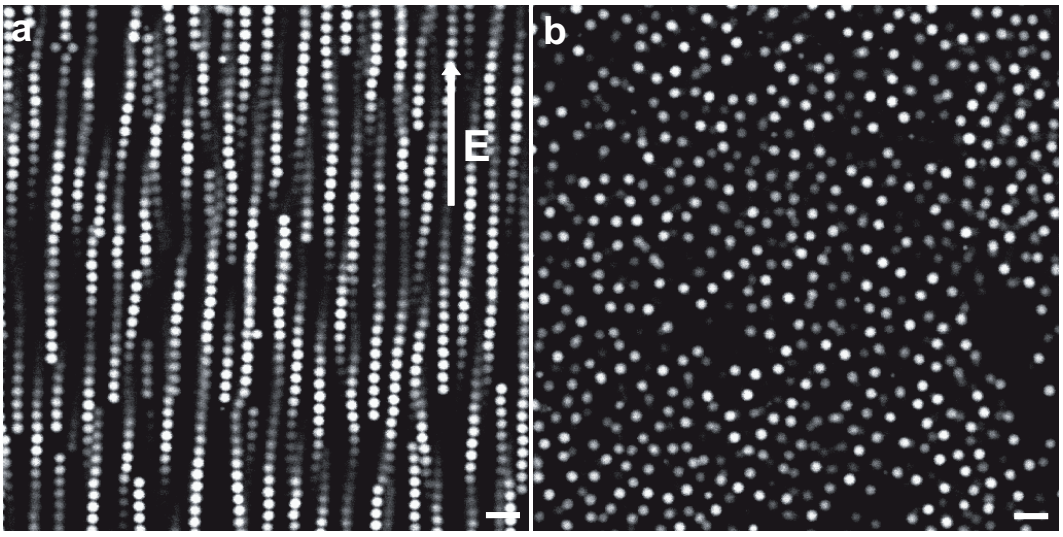

Figure 2.2: Confocal *xy* images of PMMA particles in CHB. **a**, Dielectric response of the particles in an AC field (E_{rms} = 0.30 Vμm^{-1}). **b**, Shortly after switching off the field. Scale bars are 5.0 μm.

Making use of this behavior, in the following sections, we demonstrate that permanent bead chains can be made by using eithe thermal annealing or seeded growth on inorganic, organic, and hybrid particles.

2.4.2 Rigid polymeric bead chains

In this section, we first describe a facile and flexible method for creating rigid bead chains of polymeric spheres. Our method consists of two simple steps: i) assemble the particles into 1D strings with the help of induced dipolar interactions, and ii) heat the entire sample to 70-75 ^{o}C for about 2-3 minutes. Subsequently, the method was implemented to different polymeric particles such as polymethylmethacrylate (PMMA), polystyrene (PS), and hybrid particles such as particles with a silica core and a PMMA shell.

Permanent PMMA bead chains

The dispersion was prepared at a volume fraction of ϕ = 0.04 from 1.40 μm RITC labelled PMMA particles in cyclohexyl bromide. This dispersion was then transferred into an electric capillary cell of 0.1 mm $\times$ 1.0 mm cross section with a desired length and exposed to a strong AC field (E_{rms} = 0.25 Vμm^{-1}). After

5-6 minutes, all the particles were assembled into strings of one particle wide in the field direction. The dispersion was subsequently heated to 70-75 ^{o}C, which is still well below the glass transition temperature (T_g = 140-145 ^{o}C, see Chapter 3) of PMMA, for about 2-3 minutes using a stream of hot air that was much wider than the sample cell. We kept the field on for 5 minutes while the sample cell was allowed to cool down to room temperature. The field was then removed and confocal laser scanning microscopy revealed that the particles that were in contact had bonded permanently (Figure 2.3a). After removing the field, surprisingly, more than 95 % of the dispersion was converted to permanent chains with a broad distribution in the length of the chains (Figure 2.3a). We exploit the fact that at elevated temperatures, the steric PHSA-PMMA comb-graft-stabilizer that is present on the surface of the particles, redistributes such that the particles that are in contact bond (fuse) or get entangled together permanently by the same van-der-Waals forces between the PMMA polymers that keep the uncrosslinked particles together. We believe that when the dispersion was brought back to room temperature the steric stabilizer rearranged to its original state and subsequently recovered stability. In this manner the chain structure was preserved and stable even after the field was removed. Moreover, chains remained well dispersed due to the long ranged repulsion ($\kappa\sigma \approx 0.8$, where σ is the particle diameter (1.4 μm) and κ is the inverse of Debye screening length, a measure for the range of the electrostatic repulsion). In addition, also at higher salt concentration chains were stable because the particles were still sterically stabilized. We repeated the same procedure for different volume fractions and found that the upper workable limit is 10 % by volume. In this limit, the long-range repulsion is strong enough to stabilize individual strings, preventing them from forming sheets by sideways assembly at higher field strengths [27, 28, 37].

Almost sixty years ago, Onsager predicted that a fluid of thin and long hard rods exhibits a nematic phase if it is compressed beyond a critical density [38]. Note that a nematic phase possesses long range orientational order, but no long range positional order. A nematic phase for colloidal systems has already been observed with a system of a thin and long fd virus [39], and also with inorganic rods [40, 41]. However, most of these studies have been restricted to scattering measurements due to a high refractive index nature of the particles than inhibited the index matching and thus real space microscopy deeper into a sample. Only few 3D real space studies were reported [41, 42]. Here we observed a nematic phase in a concentrated dispersion of long bead chains, which can be studied on a single particle level in three-dimensions by means of fluorescently labelled chains with confocal microscopy. Additionally, we could easily gain 3D information, for instance, the orientational order parameter (≈ 0.8) [42] for a nematic phase of long bead chains was estimated from the 3D particle co-ordinates. The nematic phase transition was accelerated by an external electric field. It was suggested by Flory and later confirmed in simulations [43, 44] that a system of hardsphere chains (length to width ratios ≥ 6) exhibit liquid crystal phases.

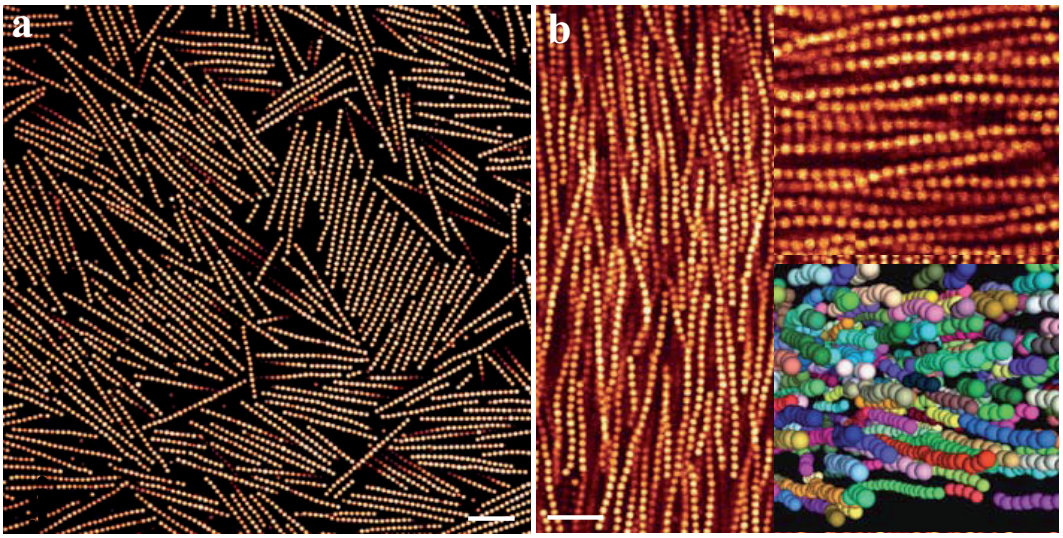

Figure 2.3: Long permanent rigid colloidal PMMA bead chains. **a**, Confocal 2D micrograph of permanent PMMA chains in CHB. **b**, Nematic phase consisting of long bead chains of PMMA in CHB. (upper inset is a magnified view and rotated in 90° degrees and lower inset is rendered particle coordinates revealing the three dimensional structure of a nematic phase of long bead chains). Scale bars are 5.0 μm.

Bead chain length control

Here, we demonstrate how fine control on the length of the permanent PMMA chains was achieved. As we discussed in Section 2.4.1, an induced dipolar strength between the particles is proportional to the square of the applied field strength. Upon increasing the field strength the average string length could be increased until it spanned the entire height of the gap between the two electrodes. Therefore, the longest bead chain in the dispersion could be the distance between the two electrodes. We varied the distance between *(S)* the two electrodes by using spacers of different thickness as shown in Figure 2.4a. Although the chains are in Figure 2.4c not monodisperse in length we did observe locally increased nematic order in the dispersion. In this fashion more monodisperse chains of the desired length could be obtained. Moreover, we estimated the polydispersity index (PDI) for a dispersion of rigid bead chains as seen in Figure 2.4d to be 1.11. Note that it is close to commercially available PDI of PS polymer chains.

Permanent PS bead chains

The same procedure (see Section2.4.2) allowed us to make rigid polystyrene bead chains in dimethyl sulfoxide (DMSO). The dispersion consisted of electrostatically stabilized PS particles (diameter $\sigma = 1.45$ μm, 1 wt%) in dimethyl sulfoxide, and the dispersion was then introduced by capillarity in a cell of 0.1 mm $\times$ 1.0 mm cross section with a desired length. Prior to the heating step, particles were

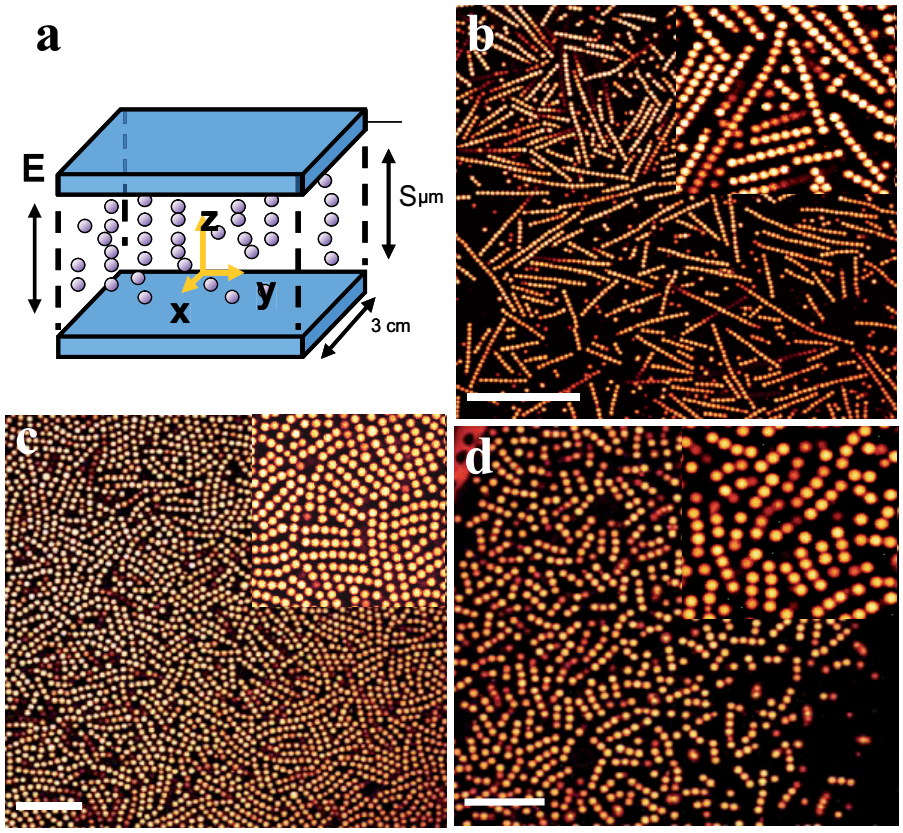

Figure 2.4: Permanent rigid colloidal PMMA bead chains. **a**, Schematic representation of the electric cell, where S is the distance between the two electrodes. **b-d**, Confocal 2D micrographs of permanent PMMA chains in CHB. **b-d**, Chains length was controlled by varying the distance *(S)* between the two electrodes , 100 μm, 10-15 μm, and 5-10 μm respectively. (**b-d**, upper inset, a magnified view of the bead chains). Scale bars are 5.0 μm.

aligned parallel to the field direction in head-to-toe manner due to induced dipolar attractions (E_{rms} = 0.15 Vμm^{-1}). The sample was subsequently heated to 70-75 °C, which is still well below the glass transition temperature (T_g = 105 °C) of PS, for about 2-3 minutes using a stream of hot air that was much wider space than the sample cell. At elevated temperatures particles which were in contact bonded (or fused) irreversibly. Then the dispersion was allowed to cool down to room temperature. Figure 2.5a clearly shows the chains are indeed permanent and rigid as well. The capillary cell was then carefully opened and the dispersion was dried on a SEM grid at room temperature.

Permanent rigid chains of silica particles

Here, we used a slightly modified method for creating rigid silica bead chains: a thermal annealing step was replaced with seeded growth of a thin silica layer

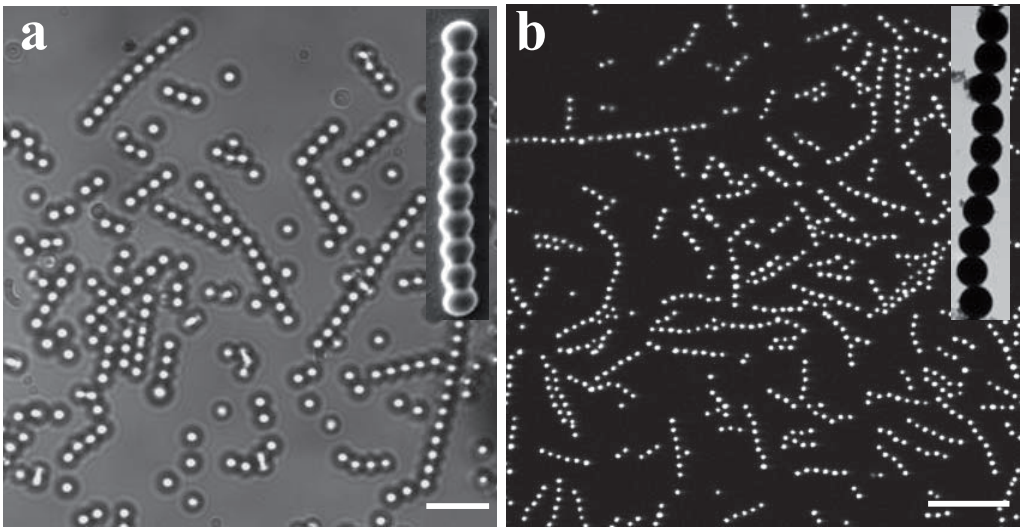

Figure 2.5: Long permanent rigid colloidal bead chains. **a**, Optical 2D micrograph of permanent PS bead chains in DMSO. Upper inset, scanning electron microscopy image of such a chain. **b**, Confocal 2D micrographs of permanent silica bead chains in water and glycerol mixture. Upper inset, transmission electron microscopy image of permanent bead chains of silica (SiO_2). Scale bars are 5.0 μm.

around the strings. 1.3 μm silica particles were synthesized with a modified Stöber method [45]. A dispersion was prepared at 0.8 % by volume of particles in a 15 %(v/v) ammonia (25 % aqueous solution) and glycerol mixture. A 10 mL portion of such a dispersion was mixed with 100 μL tetraethyl orthosilicate (TEOS, >98 % purity). Then, 5.0 μL of the final solution was transferred to an electric cell of 0.1 mm × 1.0 mm and exposed to an external AC field ($E_{rms} = 0.20\ V\mu m^{-1}$). Under these conditions, a thin layer of about 60-70 nm of silica was grown around chains which were aligned in the field direction with the help of dipolar attractions. Note that the reaction was done at room temperature and the reaction time was about 3-4 hrs. In this fashion both silica and amorphous titania colloidal chains were fixed. The strings were dried on a glass slide and then observed with TEM as shown in Figure 2.5b. If a thicker silica coating was desired, subsequent additions of TEOS were made (similar to seeded growth). During the growth step the chemical reaction increases the ionic strength of the dispersion, which can hamper the stability of these chains.

A reaction free method for fabricating permanent rigid silica chains in aqueous solution

The following is a reaction free method to produce rigid silica bead chains. Silica particles with an average diameter of 1.30 μm were prepared at 1.0 % by volume in a 0.3 % by weight of polyethyleneimine (PEI, $M_w = 750$ kg/mole) DMSO solution. The suspension was allowed to stand for 3-4 hrs. During this period of time the cationic PEI molecules adsorbed on the anionic surface of the particles. The

solution was then introduced by capillarity in an electric cell of 0.1 mm $\times$ 1.0 mm cross section and subjected to a sufficiently strong AC field ($E_{rms} = 0.25\ V\mu m^{-1}$) for 20-30 minutes. Strong dipolar attractions aligned the silica particles and subsequently allowed the PEI molecules to irreversibly link them. After removing the field, the chains structure was preserved as shown in Figure 2.6a.

Permanent rigid silica chains in apolar solvent

However, the stability of these systems is limited by the range of the repulsion ($1/\kappa$) and it is a challenge to get sufficiently long-range repulsions in aqueous suspensions. Hence to overcome this limitation, we synthesized silica chains in an apolar solvent (CHB) as well with a slightly modified method: First, a reaction was carried out between 3-methacryloxypropyltrimenthoxysilane (TPM) and silica particles to stabilize the latter in CHB. The TPM coating reaction was carried as follows: 0.34 g of 2.50 μm silica particles were dispersed in 15 mL of ethanol, 1 mL of ammonia (25 % aqueous solution) and 2 mL of TPM. The reaction mixture was allowed to react for 2 hrs. The particles were then washed a few times with ethanol and dried at room temperature. In a closed 200 mL glass laboratory flask, 15 mg of poly (12-hydroxystearic acid) soultion and 5 g of azo-bis-isobutyronitrile (AIBN, Janssen Chemica) was dissolved in 10 g of CHB. Dried TPM coated particles were transferred to that solvent mixture. 5.0 μL of suspension was placed between the two electrodes then a reaction was carried out between TPM-coated particles in the presence of an AC field ($E_{rms} = 0.20\ V\mu m^{-1}$) at 70 °C for 3-4 hrs. After the field was turned off, permanent rigid silica chains resulted (Figure 2.6b).

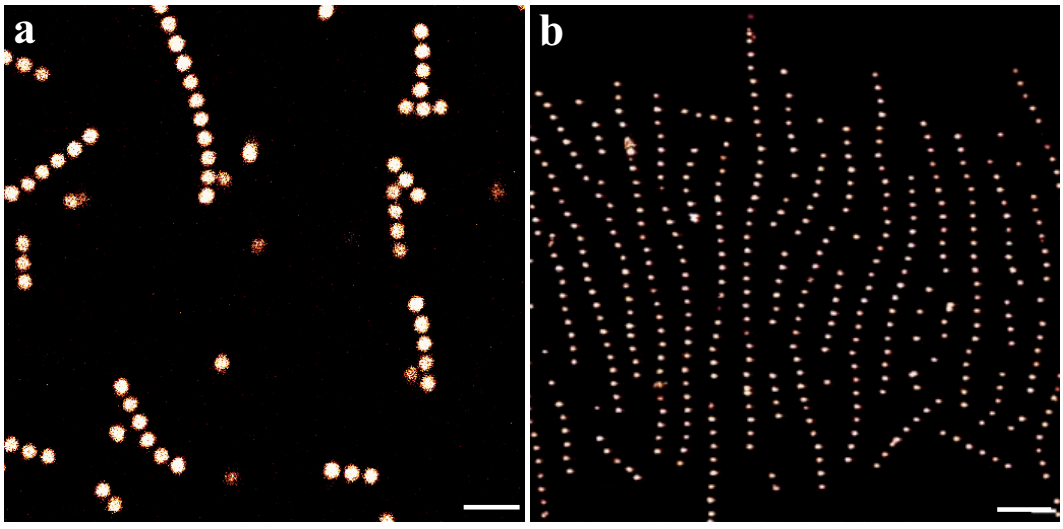

Figure 2.6: Confocal micrographs of rigid silica bead chains. **a**, Silica beads were permanently connected by the PEA molecules in DMSO. **b**, Rigid silica bead chains that were coated with TPM. Scale bars are 5.0 μm.

2.4.3 *Tuning the shape from polymer bead chains to spherocylinders*

Here, we demonstrate that our method can also be used for tuning the shape from a beads-chain to a spherocylinder. We first synthesized the rigid PS bead chains as described in Section 2.4.2 and the chains were subsequently aligned in the field direction (E_{rms} = 0.05 V/μm). The capillary cell was then immersed into a hot oil bath which had a temperature of 95 °C for a longer period of time about 3-4 hrs. Note that glasstransition temperature of PS is about T_g = 105 °C [46]. We believe that at these conditions particles which were in contact undergo a viscoelastic deformation and had bridged the gap between the beads in a chain by entanglement of polymers across the boundaries. Figure 2.7 clearly shows that bead chains transformed to spherocylinders.

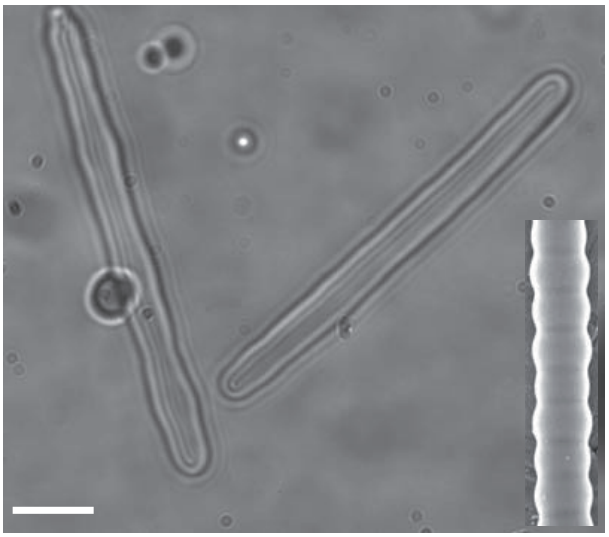

Figure 2.7: Optical micrograph of PS spherocylinders. The shape change from bead chains to spherocylinders was achieved by thermal annealing for a longer period of time (3-4 hrs). Lower inset, SEM image of such a rod. Scale bar is 2.0 μm.

2.4.4 *Flexible bead chains*

Here, we adapted our simple method to produce (semi-)flexible dielectric bead chains as well. Subsequently, the method was implemented to different systems, such as sterically stabilized particles with a cross- linked PMMA core and an uncross-linked PMMA shell, emulsion droplets of polydimethylsiloxane (PDMS), and sterically stabilized (polyvinylpyrrolidone, PVP) PS beads.

Semi-flexible chains of PMMA beads

We used RITC labelled uncrosslinked core (σ = 2.0 μm)- crosslinked PMMA shell($\approx$100 nm) particles dispersed in CHB. We repeated the same protocol as in Section 2.4.2 which resulted in semi-flexible chains as shown in Figure 2.8. Note that at elevated temperatures un-crosslinked PMMA chains might act as a linker between the beads. Figure 2.8 reveals the different conformations of such a chain in CHB.

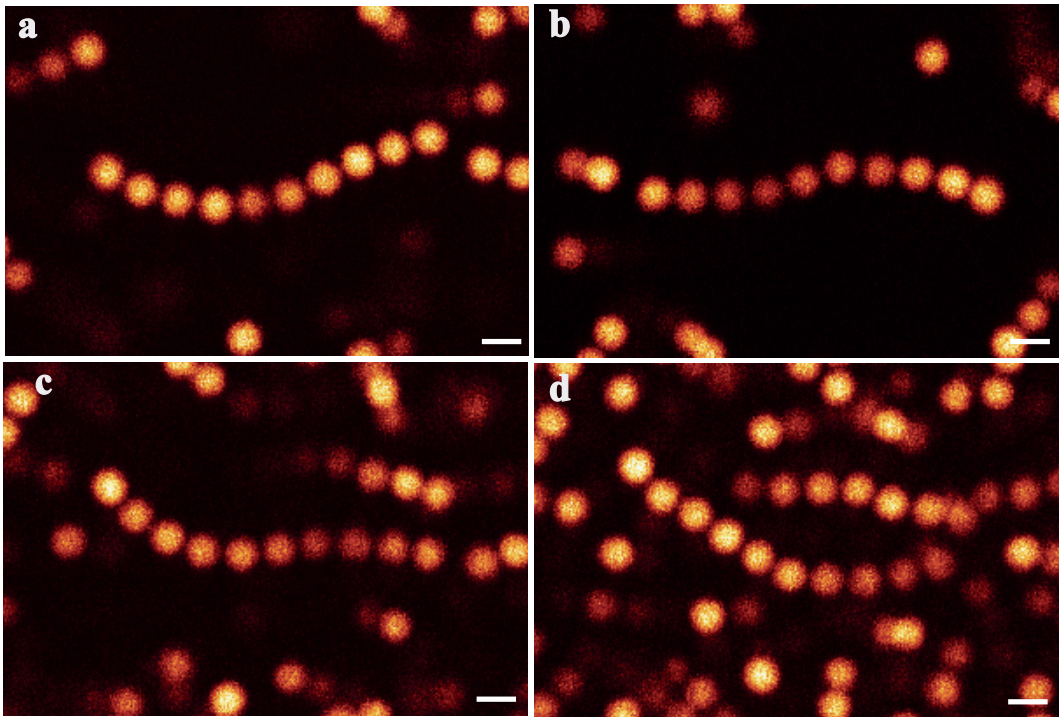

Figure 2.8: Semi-flexible PMMA bead chains, a sequence of confocal microscopy images show the different conformations of PMMA bead chains. The time-lapse between the frames is 5 sec. Scale bars are 3.0 μm.

Semi-flexible chains of silica-coated PDMS droplets

Polydimethylsiloxane (PDMS) silicone oil-in-water emulsion droplets were synthesized by base-catalyzed hydrolysis and polymerization of dimethyldiethoxysilane (DMDES, $\geq$ 97.0 %, Fulka). The whole fabrication process has been explained in detail elsewhere [47, 48]. The continuous phase of the emulsion was prepared by adding 20 %(v/v) ammonia (29.7 wt%, Merck) to de-mineralized water. Then, 5.0 % by volume was added to the aqueous solution and vigorously shaken for a few mins. The emulsion droplets formed within a few hours time, but they were allowed to grow for at least 24 h before being coated. These PDMS emulsion droplets were aligned in the field direction, a thin layer about 20-30 nm

in thickness of organo-silica was then grown around them [48]. This thin layer of organo silica has a Youngs modulus of ~ 200 MPa [48, 49] which was responsible for the flexibility as is also shown in Figure 2.9.

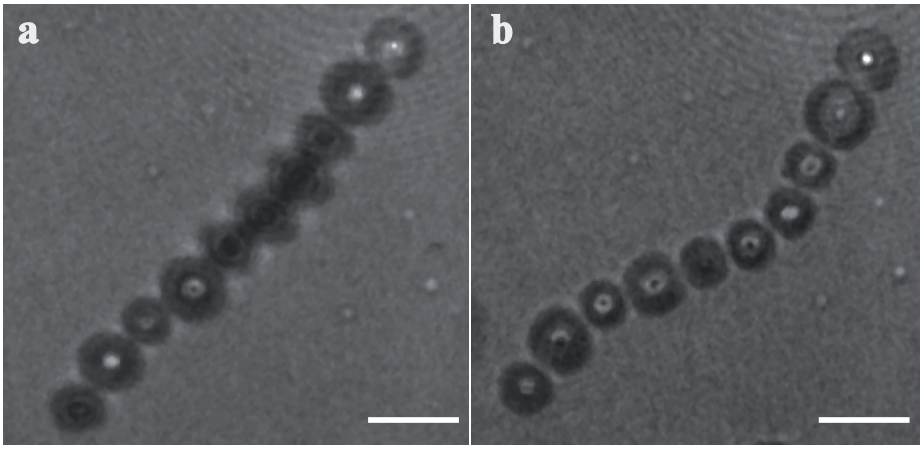

Figure 2.9: Semi-flexible silica coated PDMS droplet chains in water. Time-lapse confocal microscopy images show the different conformations. The time-lapse between the frames is 7 sec. Scale bars are 5.0 μm.

(Semi-)flexible PS bead chains

PVP (M_w = 360 kg/mol) stabilized 1.35 μm PS particles were prepared at 0.80 % volume fraction in DMSO. The suspension was then transferred to an electric cell of 0.1 mm × 1.0 mm cross section with a desired length and subjected to an AC electric field (E_{rms} = 0.10 $V\mu m^{-1}$). The entire sample was heated to 60-65 °C for about 90-120 seconds and then the suspension was cooled down to room temperature. Approximately 1-2 minutes later the field was turned off. We believe that at elevated temperatures, the steric stabilizer on the surface of the particles that is chemically connected to the polymer chains is more mobile and acted as a linker between the beads and will elaborate on this below. The longer chains exhibited different conformations, which are purely driven by thermal fluctuations as shown in Figure 2.10a-d. The persistence length (l_p) of these (semi-)flexible chains was estimated (~ 20 μm or 15 σ see Section 2.4.5) using Fourier mode analysis. Moreover, the distribution of bond angles was calculated for a flexible and a rigid 8 bead chains as seen in Figure 2.10e-f, from which we conclude that bond angle distribution is Gaussian. By comparing to a Boltzmann distribution it is seen that a bond angle of 20 degrees has an elastic energy cost of 1 k_BT. To further probe the degree of flexibility, a single bead in a chain was trapped with optical tweezers and dragged through the dispersion. Hairpin-like conformations were observed as a result of the viscous drag on the chain. In addition, ring and knot like structures could be made with a single optical trap on a long semi-flexible chain (Figure 2.10g-j). Once the optical trap was released, the electro-

static repulsion, the elastic energy and thermal motion caused the chain to relax. Note that we only observed flexible chains when the particles were stabilized with higher molecular weight PVP ($\geq$ 360 kg/mol), whereas lower molecular weights of 10 kg/mol, 40 kg/mol resulted in rigid chains.

A probable mechanism

Here, we propose a mechanism to explain the flexibility between the PVP coated PS beads in a chain. It is evident from the previous Sections 2.4.2 & 2.4.4 that when the particles were stabilized with PVP the chains became flexible, whereas rigid chains resulted in the case of electrostatically stabilized particles (see Section 2.4.2). Furthermore, only high molecular weight PVP ($\geq$ 360 kg/mol) resulted in flexibility. Therefore, we think PVP is acting as a linker between the particles to bridge the gap between the neighboring particles as shown in Figure 2.11. To further examine this we attached the one end of a chain to the wall, while the other end of the chain was trapped with optical tweezers. The chain was then folded and held in this configuration for about 10 mins (Figure 2.12b). When the optical trap was released, the chain relaxed back to its original shape in about 60 secs (Figure 2.12c-e). The instantaneous chain shape is the result of a balance between the elastic force, the screened electrostatic force, the viscous drag and thermal noise. When a chain was held in a folded state for more than 100 minutes we observed a permanent kink where the bending had taken place. A kink is retained in a chain after the trap was released as seen in Figures 2.13b-c. Hence, we surmise that the stabilizing polymers (PVP) are chemically connected or/and entangled with the PS polymer chains and subsequently acted as a linker between the beads. As illustrated in Figure 2.11, PVP molecules that connected to the PS polymers might slowly relax and then permanently rearranged. Polymeric colloids are known to possess plastic behavior. It depends on the time scale of rearrangements of the polymers within the (outer) particle layers which aspect of its visco-elastic behavior gets manifested.

2.4.5 Numerical estimation of the persistence length

In this section, we describe how we estimated the persistence length of our flexible and rigid colloidal chains using Fourier mode analysis of their curvature change due to thermal fluctuations [50–52]. The persistence length is the distance along the chain over which the local orientation of the chain is no longer correlated. Note that our chains were constrained to a plane by buoyancy. We chose a chain which was isolated from neighboring chains to ensure negligible hydrodynamic coupling. The thermal curvature fluctuation of the chain was observed using an inverted optical microscope. The images were recorded using a CCD camera (Media Cybernetics, Evolution QEi camera kit, Japan) at 2 frames per second with a 5 ms exposure time for about 20 mins. We first processed recorded images and extracted the centroid position of each particle within

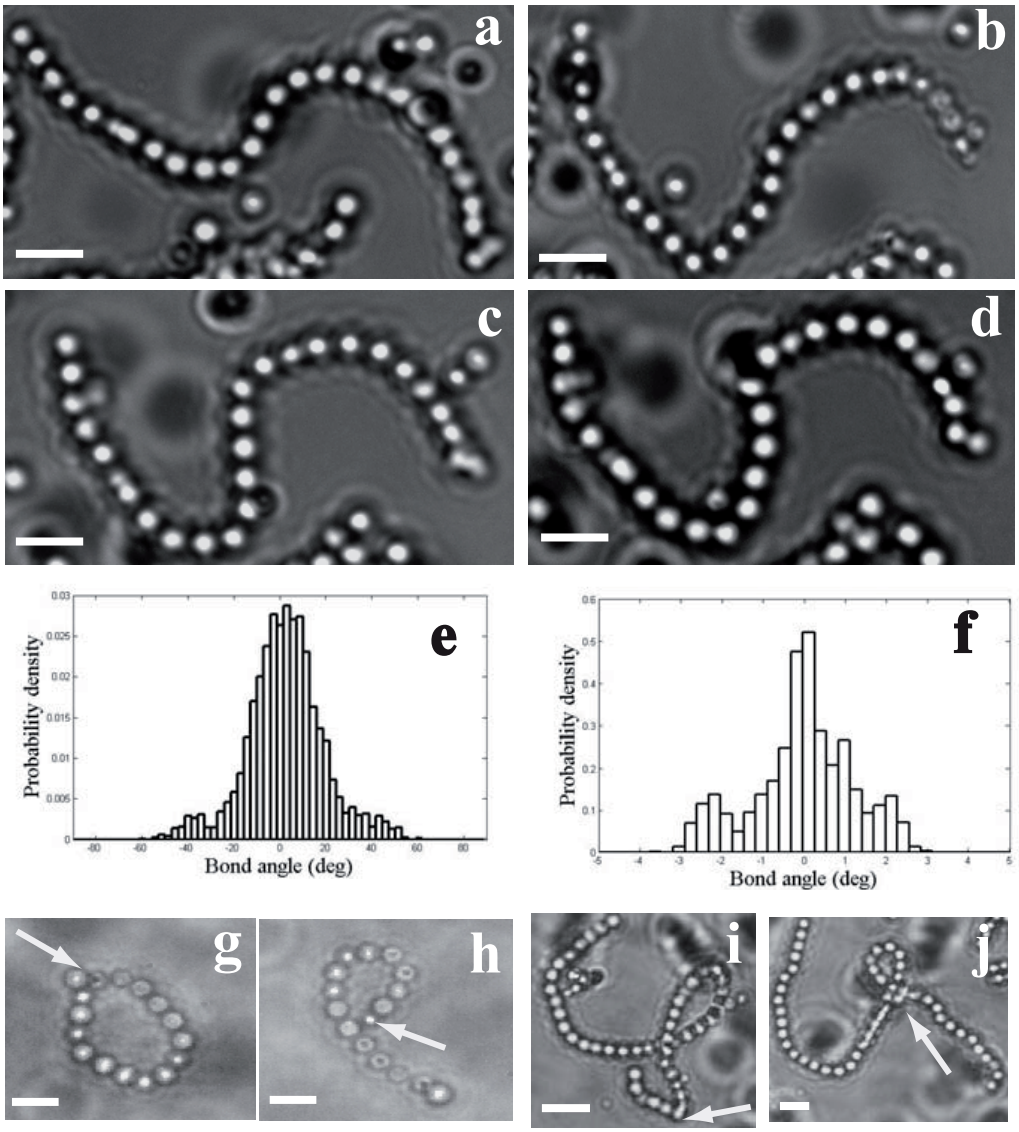

Figure 2.10: (Semi-)flexible PS bead chains in DMSO. **a-d**, Time-lapse optical microscopy images show the different conformations of a long chain in DMSO which is confined to the glass surface by gravity. The time-lapse between the frames is 5 sec. **e-f**, The distribution of bond angles for a flexible and a rigid 8 bead chain. **g-j**, A single bead in a chain was trapped with optical tweezers (indicated by an arrow) and dragged through the dispersion, a ring and knot like structures were made. Scale bars are 4.0 μm.

the chain [53]. The positions thus found are shown in Figure 2.14. From the

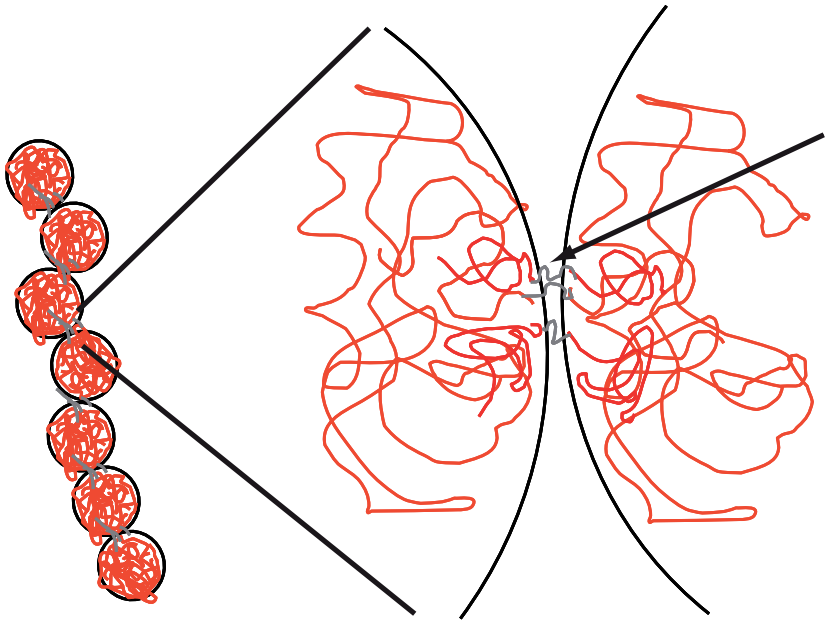

Figure 2.11: Schematic illustration of a probable mechanism: a higher molecular weight ($\geq$ 360 kg/mol) PVP (indicated by an arrow) acted as the stabilizer and also the linker molecule between the PS beads.

pixel coordinates (x_i, y_i) of the chain we calculated the tangent angle $\theta(s)$ as a function of arc length s using $\theta = \tan^{-1}((y_{i+1} - y_i)/(x_{i+1} - x_i))$ where $s = \sum_{j=0}^{i+1} \sqrt{(y_{j+1} - y_j)^2 + (x_{j+1} - x_j)^2}$.

In Fourier mode analysis, the instantaneous curvature of a chain at a given time can be decomposed into a series of Fourier modes [50–52] ,

$$\theta(s) = \sum_{n=0}^{\infty} \theta_n(s) = \sqrt{\frac{2}{L}} \sum_{n=0}^{\infty} a_n \cos\left(\frac{n\pi s}{L}\right) \tag{2.6}$$

where L is the contour length of the chain, a_n is the amplitude of the n^{th} mode. For the 8-bead chain the 7 modes are shown in Figure 2.15. The time-averaged Fourier amplitude of each mode provides an independent estimate for the persistence length at its corresponding length scale. The bending energy U of a curved filament can be expressed as an integral of its deviation in curvature from the intrinsic curvature along the filament backbone [50–52]

$$U = \frac{1}{2}\kappa \int_0^L \left(\frac{\partial\theta}{\partial s} - \frac{\partial\theta_o}{\partial s}\right)^2 ds, \tag{2.7}$$

where $\kappa = k_B T \times l_p$ is the bending rigidity, l_p is the persistence length, k_B is

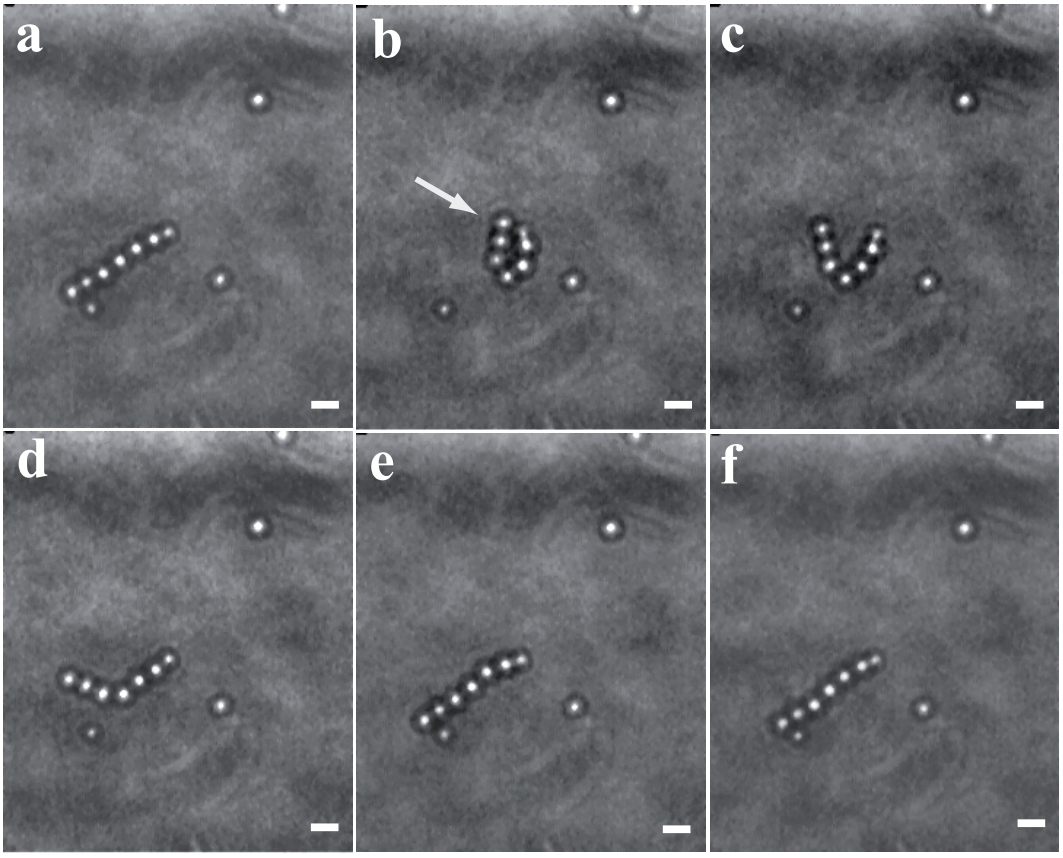

Figure 2.12: Optical micrographs of a semi-flexible PS bead chain. One end (indicated by an arrow) of the chain was trapped with a single trap by using optical tweezers. **b**, The chain was then kept in a folded form for about 10 mins. **c-f**, The trap was subsequently released, a series of microscopy images show the relaxation of the chain. The time lapse between the frames is 10 sec. Scale bars are 3.0 μm.

Boltzmann constant, and T is the temperature. Furthermore, the bending energy can be expressed as a function of Fourier mode amplitudes by differentiation of Eq. 2.6 and subsequent integration along the arc length of the chain,

$$U = \frac{1}{2}\kappa \sum_{n=0}^{\infty} \left(\frac{n\pi}{L}\right)^2 (a_n - a_n^o)^2 \tag{2.8}$$

Here, a_n^0 is the amplitude in the absence of applied or thermal forces and is non zero if the relaxed filament is not absolutely straight. In equilibrium, the equipartition theorem states that the average bending energy of each mode equals

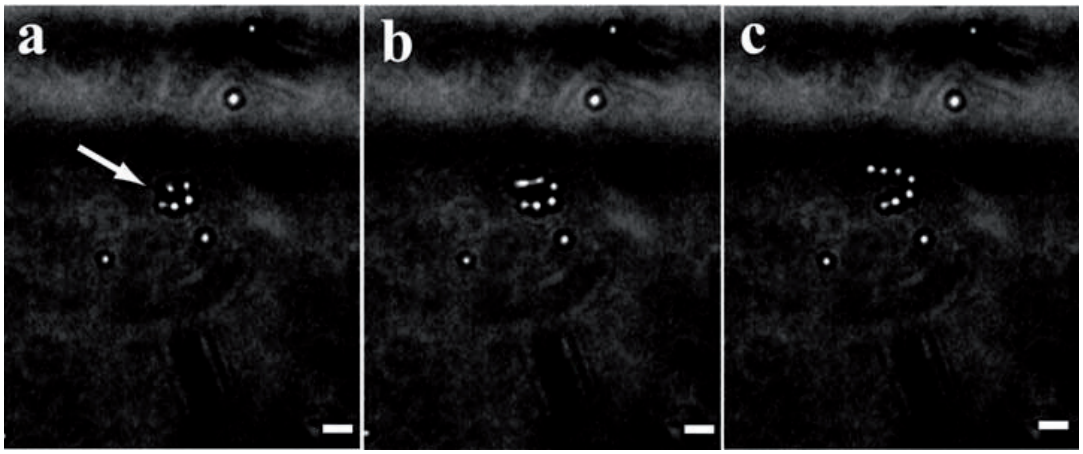

Figure 2.13: Optical micrographs of a semi-flexible PS bead chain. One end (indicated by an arrow) of the chain was trapped with a single trap by using optical tweezers. **a**, The chain was then kept in a folded form for about 100 mins. **b-c**, When the trap was released, a kink was observed in the chains. The time lapse between the frames is 10 mins. Scale bars are 3.0 μm.

to 1/2 k_BT, so that from Eqs. 2.6 and 2.8 the persistence length can be written as $l_p = 1/((\frac{n\pi}{L})^2\, var(a_n))$, where $var(a_n) = \langle (a_n(t+\Delta t) - a_n^o(t))^2 \rangle_{t,\Delta t \gg \tau_n}$, where Δt is the time lag between the different images, and τ_n the relaxation time of the n^{th} mode. We considered the first 3 modes and found that the persistence length of an 8 bead flexible PS bead chain is ~20 μm (15 σ, where $\sigma = 1.35$ μm is the particle diameter) with a standard deviation of 4.8 μm. On the other hand, the persistence length of a long rigid PS bead chain (Figure 2.5a) is 40 mm (30000 σ) with a standard deviation of 1 mm. Note that stiff chains are too rigid to display significant fluctuations. The ratio between the persistence length and the contour length (lp/lc) for our (semi-)flexible strings is on the order of 1, whereas the ratio is larger than 1000 for our rigid rods. For a comparison, this ratio for flexible polymers such as λ-DNA is much smaller than one ($l_p \approx 50$ nm, $l_c \approx 16$ μm) [50–52]. In the case of semiflexible polymers such as actin filaments, the ratio is on the order of one ($l_p \approx 16$ μm, $l_c \approx 20$ μm) [50–52]. For rigid polymers such as microtubules the ratio is of the order of 1200 ($l_p \approx 6$ mm, $l_c \approx 50$ μm). We believe that the contour length of our semiflexible chains can easily be extended to a few hundreds of particle lengths. Therefore, our PS bead chains can be considered as flexible polymer analogues.

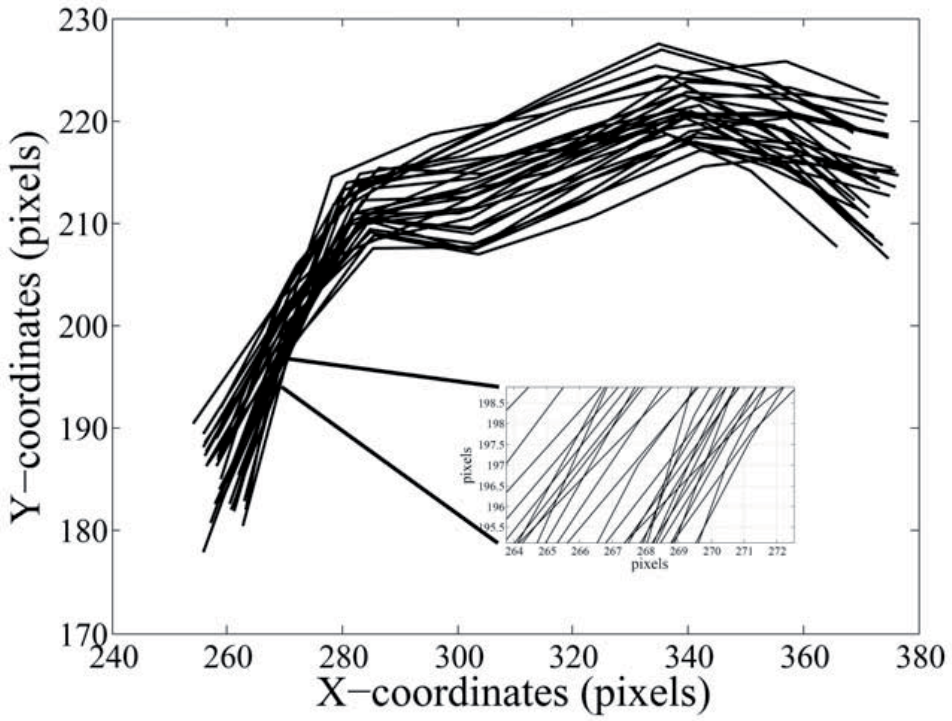

Figure 2.14: The digitized (x, y) coordinates of 8 bead (semi-)flexible PS chain in DMSO, inset, higher-magnification views of 30 consecutive chain contours from a video acquisition, which demonstrates that the filament tracking algorithm performs with sub-pixel accuracy.

2.4.6 A-tactic polymers like PMMA-PS dimer chains

We also implemented our method to a dispersion of hetero dimer colloids, which consisted of PMMA (σ = 1.0 μm) on one side and PS (σ = 0.85 μm) on the other side that were stabilized with PVP (M_w = 360 kg/mol). These chains became flexible as well as seen in Figure 2.16a. Note that the dielectric constants of both materials are close to each other (ϵ_{PMMA} = 2.6, ϵ_{PS} = 2.4) therefore no preferential dimer ordering was observed within the chain as in atactic polymers [13]. The SEM image clearly reveals the dimer particles are irregularly arranged in a chain (Figure 2.16b). Controlling the internal structure of a chain is essential for photonic applications. We exploit the charge inhomogeneity between both sides of the dimer (PS-PMMA) particle to obtain control over the internal structure of heterodimer chains. Prior to chain formation, all the particles were first aligned in a particular direction using a low DC field (2.0 V/mm) that causes the side with the most negative zeta-potential to point to the positive electrode. The particles were then exposed to an AC field, followed by a heating step. The resulting dimer chains were similar to isotactic polymers. Moreover both ends of a particle could

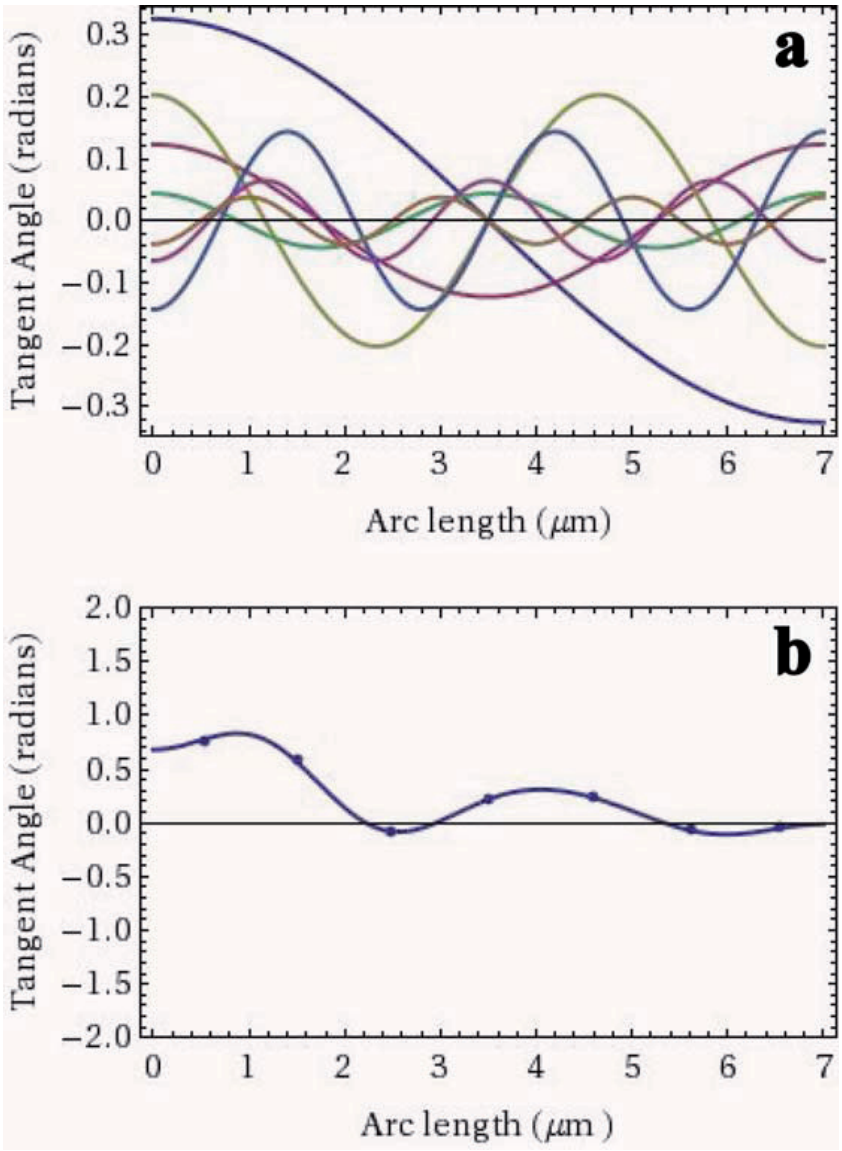

Figure 2.15: a, Curves showing the 7 cosine modes into which the tangent-angle curve was decomposed for one snapshot of the chain. **b**, sum of the 7 modes was shown as a solid curve.

easily be distinguished by exploiting the refractive index differences with optical microscopy (1.59 for PS vs. 1.49 for PMMA). Figure 2.16c clearly shows that the dark parts (PS) in this chain are all regularly distributed contrary to the previous case.

2.4.7 Tuning the flexibility between the beads in a bead chain

An interesting feature of our flexible chains is that the flexibility of already synthesized charged chains can be tuned by manipulating the interactions between

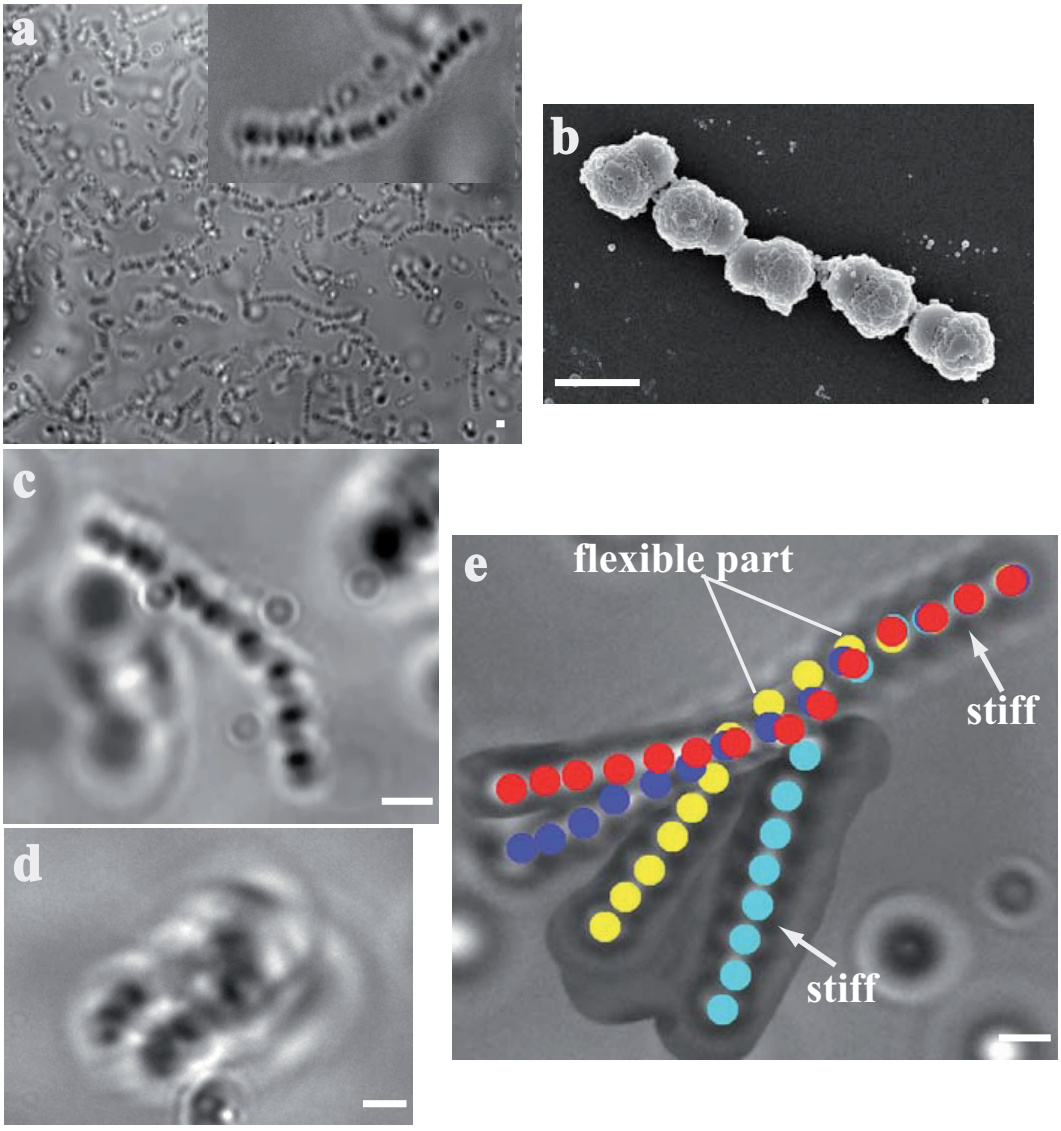

Figure 2.16: Complex strings. **a** & **c**, Optical micrograph of a permanent semi-flexible chain of hetero dimers of PMMA-PS in water (upper inset, a magnified view of a single chain). **a**, Atactic like dimer chains. **c**, Iso-tactic like dimmer chains. **b**, Scanning electron microscopy image of an atactic like chain. **d**, Optical image of a single chain of hetero dimers in the presence of depletion attractions. **e**, Overlay of time-lapse optical micrographs of a triblock copolymer like chain of PS beads with a different color coding. Note that the overlays were constructed such that in each case one of the rigid ends is in the same position and orientation. Scale bars are 2.0 μm.

the beads in the chain. So far, we described the various chemistries for creating a variety of colloidal chains. Here, we demonstrate that we could control the flexibility of already synthesized charged chains by varying the interactions between the beads in a chain. These interactions were manipulated in three ways: (i) by applying an external electric field, (ii) by varying the range of electrostatic

repulsions ($1/\kappa$), and (iii) by inducing depletion attractions.

We first synthesized (semi-)flexible PS bead chains (see Section 2.4.4) and the chains were then exposed to an external electric field (E_{rms} = 0.06 V/μm). Induced dipolar interactions between the beads in a chain forced them into a straight conformation in the applied field direction as shown in Figure 2.17b.

When the chains were transferred from a normal solvent ($\kappa\sigma \approx 5$, where σ = 1.35 μm) (DMSO) to a strongly deionized ($\kappa\sigma \approx 1$) solvent, the chains became stiff as seen in Figure 2.17c. This is in analogy to polyelectrolytes [54]. The longer ranged electrostatic repulsions between the beads forced them into a straight conformation.

Instead of increasing repulsions we can also induce attractions between the beads. We induced short-range attractions by adding a non-adsorbing polymer (1.75 wt% dextran of M_w = 5000 kg/mol) which acted as a depletant to the PS-PMMA dimer chains in water. The attractive depletion interactions between the beads induced a folded state of the semi-flexible chains (Figure 2.16d). The conformational states of a polymer are also highly dependent on the monomer-solvent and monomer-monomer interactions. The structures of the semi-flexible polymers in the globule state are complicated because they are not determined solely by the competition between entropy and monomer-solvent interaction, but also controlled by an additional elastic energy arising from backbone rigidity.

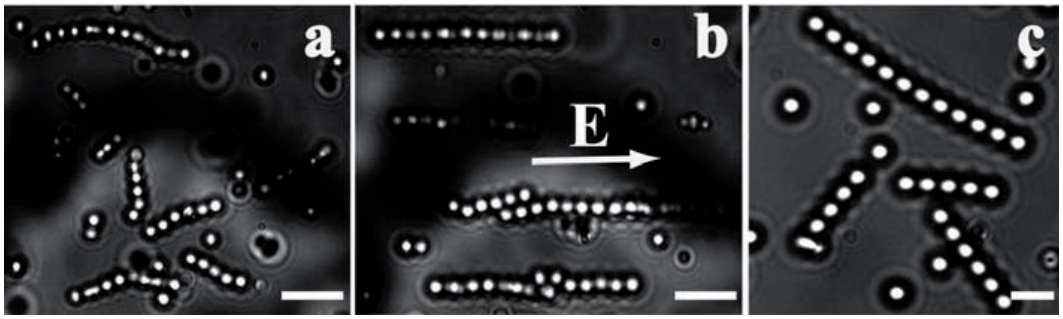

Figure 2.17: Tuning the flexibility between the beads in a chain. Conformations of PS bead chains in DMSO, **a**, absence of the field, and **b** presence of the field (E_{rms} = 0.06 Vμm^{-1}). **c**, PS bead chains were transferred from a normal solvent ($\kappa\sigma \approx 5$, where σ = 1.35 μm) (DMSO) to a strongly deionized ($\kappa\sigma \approx 1$) solvent. Scale bar are 4.0 μm.

2.4.8 Triblock copolymer like bead chains

We were also able to make chains where a part of a chain was flexible while the remaining part was rigid as in a block copolymer. We achieved this by mixing PS flexible and rigid bead chains together and repeating the same protocol of making bead chains (see Section 2.4.4). Such a chain (Figure 2.16e) consisted of a 5—bead flexible middle part and stiff end parts of lengths 3 and 6, respectively. Figure 2.16e clearly shows the conformational changes in the middle part

of chain. Note that the overlay was constructed in a way that one of the stiff ends is in the same position and orientation.

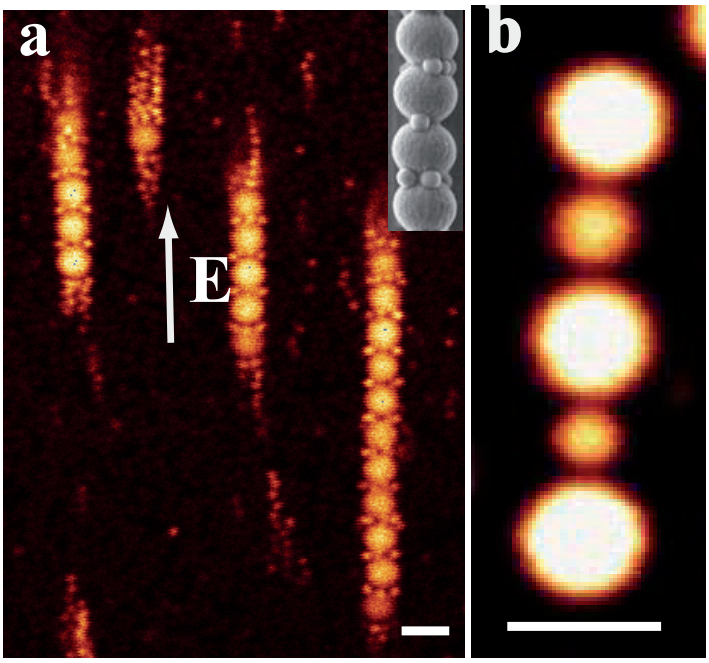

Figure 2.18: Confocal microscopy images of bi-disperse PMMA spheres in CHB under the external electric field. **a**, Several small (5-6) particles (σ_s = 0.60 μm) were arranged between every two almost touching big spheres (σ_l = 2.40 μm) in the plane perpendicular to the field direction (upper inset, SEM image of such a single chain). **b**, Large (1.5 μm) and small (1.05 μm)particles assembled alternatingly. Scale bars are 2.0 μm.

2.4.9 Binary strings

In contrast to monodisperse systems, complex structures were observed with bi-disperse systems of PMMA particles in an external electric field. For homogeneous particles of the same material, the induced dipole moments in an external electric field are proportional to their volume (see Eq. 2.3). Therefore, the dipolar interactions between the larger particles almost always are much stronger than between the smaller ones. At higher field strengths, the two particles did not form chains individually but formed together more complex string-like arrangements. Around the contact point of two larger particles an annular attractive potential well exist, where a small particle can interact favorably with two large particles. Consequently the small particles can get trapped in this well. In addition, our results are qualitatively in good agreement with simulations [55, 56].

Our dispersion consisted of equal amounts (1.8 wt%) of small and large PMMA spheres with diameters of 2.40 μm and 0.60 μm in CHB, respectively. For a small size ratio (σ_s/σ_l = 0.25) the smaller particles arranged in rings around the

strings of larger particles at the contact point between the spheres; candle flame-shaped clusters of small particles assembled at the ends of the chains (E_{rms} = 0.45 V/μm) (Figure 2.18b). Subsequently, this structure was permanently fixed by our thermal annealing method (see details in section2.4.2). The cell was then carefully opened and dried on a SEM grid.

For a size ratio of 0.7, strings composed of alternatingly small and large particles formed (Figure 2.18b). Although this system is yet to be optimized, it is a promising route to make more complex structures.

2.5 Conclusions & outlook

In conclusion, we demonstrated a general method to make dielectric bead chains with a high purity and quantity. The method is quite general as it relies only on i) a repulsive double layer interaction which is on the size range of the particles, ii) an induced dipolar attractive force in the direction of the external electric field and iii) either short-ranged attractions associated with e.g., a combination of van der Waals forces and a linker molecules (PVP) or a seeded growth of a thin layer which keeps the particles together. The results presented here also illustrate that our systems of (semi-)flexible and rigid bead chains behave in a way that is similar to a variety of polymers and/or simplified polymer models [57]. Controlling the interactions between the colloidal beads (segment-segment), bead and solvent, and molecular weight of the linker (PVP) offers exquisite control over chain conformations and the possibility to gain new real space insight into behavior on the monomer level. Moreover, we have shown that our method can also be implemented for particles of more complex shape and composition and can likely be extended to significantly smaller particles by using the giant electro-rheological effect [58].

Acknowledgements

We thank Johan Stiefelhagen for PMMA & PS particle synthesis. It is a pleasure to acknowledge Frank Smallenburg, Edwards Barry and Raghunath Chelakkot for useful assistance in the persistence length calculations. We would like to thank Mirjam Leunissen for demonstrating the electric cell construction, Ahmet Demirörs for silica particles & emulsion droplets synthesis, Bo Peng for PS particle synthesis, and Peter van Oostrum for optical tweezers measurements. We would also like to thank Stéphane Badaire & Hans Meeldijk for SEM measurements. Laura Filion is thanked for the critical reading of this chapter.

References

[1] V. J. Anderson and H. N. W. Lekkerkerker, *Insights into phase transition kinetics from colloid science*, Nature **416**, 811 (2002).

[2] P. K. N., A. M. Puertas, J. Bergenholtz, A. Egelhaaf, S. U. Moussaid, P. N. Pusey, A. B. Schofield, C. M. E., M. Fuchs, and W. C. K. . Poon, *Multiple glassy states in a simple model system*, Science **296**, 104 (2002).

[3] W. K. Kegel and A. van Blaaderen, *Direct observation of dynamical heterogeneities in colloidal hard-sphere suspensions*, Science **287**, 290 (2000).

[4] S. M. Yang, S. H. Kim, J. M. Lim, and G. R. Yi, *Synthesis and assembly of structured colloidal particles*, J. Mater. Chem. **18**, 2177 (2008).

[5] S. C. Glotzer and M. J. Solomon, *Anisotropy of building blocks and their assembly into complex structures*, Nature Materials **6**, 557 (2007).

[6] G. J. Vroege and H. N. W. Lekkerkerker, *Phase-Transitions in Lyotropic Colloidal and Polymer Liquid-Crystals*, Rep. Prog. Phys. **52**, 1241 (1992).

[7] V. N. Manoharan, M. T. Elsesser, and D. J. Pine, *Anisotropy of building blocks and their assembly into complex structures*, Science **301**, 483 (2003).

[8] D. Zerrouki, J. Baudry, D. Pine, P. Chaikin, and J. Bibette, *Chiral colloidal clusters*, Nature **455**, 380 (2007).

[9] R. M. Erb, H. S. Son, B. Samanta, V. M. Rotello, and B. B. Yellen, *Magnetic assembly of colloidal superstructures with multipole symmetry*, Nature **457**, 999 (2009).

[10] M. E. Leunissen, H. R. Vutukuri, and A. van Blaaderen, *Directing colloidal self-assembly with biaxial electric fields*, Adav. Mat. **21**, 3116 (2009).

[11] F. Sciortino, E. Bianchi, J. F. Douglas, and P. Tartaglia, *Self-assembly of patchy particles into polymer chains: A parameter-free comparison between Wertheim theory and Monte Carlo simulation*, J. Chem. Phys. **126**, 194903 (2007).

[12] A. van Blaaderen, *Anisotropy of building blocks and their assembly into complex structures*, Science **301**, 470 (2003).

[13] P. De Gennes, *Scaling Concepts in Polymer Physics*, Cornell Uni. Press, New York, 1979.

[14] T. T. Perkins, D. E. Smith, and S. Chu, *Relaxation of a Single DNA Molecule Observed by Optical Microscopy*, Science **276**, 2016 (1997).

[15] D. E. Smith, H. P. Babcock, and S. Chu, *Single-polymer dynamics in steady shear flow*, Science **283**, 1714 (1999).

[16] C. M. Schroeder, H. P. Babcock, E. S. G. Shaqfeh, and S. Chu, *Observation of Polymer Conformation Hysteresis in Extensional Flow*, Science **301**, 1515 (2003).

[17] K. E. Sung, S. A. Vanapalli, D. Mukhija, H. A. McKay, M. J. Mirecki, M. A. Burns, and M. J. Solomon, *Programmable Fluidic Production of Microparticles with Configurable Anisotropy*, J. Am. Chem. Soc. **130**, 1335 (2008).

[18] E. M. Furst, C. Suzuki, M. Fermigier, and A. P. Gast, *Permanently Linked Monodisperse Paramagnetic Chains*, Langmuir **14**, 7334 (1998).

[19] S. L. Biswal and A. P. Gast, *Mechanics of semiflexible chains formed by poly(ethylene glycol)-linked paramagnetic particles*, Phys. Rev. E **68**, 21409 (2003).

[20] S. Harpreet, P. E. Laibinis, and T. A. Hatton, *Synthesis of flexible magnetic Nanowires of Permanently Linked Core-Shell Magnetic Beads Tethered to a Glass Surface Patterned by Microcontact Printing*, Nano Lett. **5**, 2149 (2005).

[21] L. Cohen-Tannoudji, E. Bertrand, L. Bressy, C. Goubault, J. Baudry, J. Klein, J. F. Joanny, and J. Bibette, *Polymer Bridging Probed by Magnetic Colloids*, Phys. Rev. Lett. **94**, 038301 (2005).

[22] R. Dreyfus, J. Baudry, L. Roper, M. Fermigier, A. Howard A. Stone, and J. Bibette, *Microscopic artificial swimmers*, Nature **437**, 862 (2005).

[23] J. Baschnage, K. Binder, W. Paul, U. W. Laso, M. andSuter, I. Batoulis, W. Jilge, and T. Bürger, *On the construction of coarse-grained models for linear flexible polymer-chains - distribution-functions for groups of consecutive monomers.*, J. Chem. Phys. **91**, 6014 (1995).

[24] J. Jackson, *Classical Electrodynamics*, Wiley, New York, 1999.

[25] E. Verwey and J. Overbeek, *Theory of the Stability of Lyophobic Colloids*, Elsevier, New York, 1948.

[26] U. Dassanayake, S. Fraden, and A. van Blaaderen, *Structure of electrorheological fluids*, J. Chem. Phys. **112**, 3851 (2000).

[27] A. Yethiraj and A. van Blaaderen, *A colloidal model system with an interaction tunable from hard sphere to soft and dipolar*, Nature **421**, 513 (2003).

[28] A.-P. Hynninen and M. Dijkstra, *Phase diagram of dipolar hard and soft spheres: manipulation of colloidal crystal structures by an external field*, Phys. Rev. Lett. **94**, 138303 (2005).

[29] K. D. Hermanson, S. O. Lumsdon, J. P. Williams, E. W. Kaler, and O. D. Velev, *Dielectrophoretic assembly of Electrically functional microwires from nanoparticle suspensions*, Science **294**, 1082 (2001).

[30] H. R. Vutukuri, A. F. Demirors, P. Bo, P. D. J. van Oostrum, A. Imhof, and A. van Blaaderen, *Colloidal analogues of charged and uncharged polymer chains with tunable stiffness*, submitted.

[31] R. Hayward, D. Saville, and I. A. Aksay, *Electrophoretic assembly of colloidal crystals with optically tunable micropatterns*, Nature **404**, 56 (2000).

[32] G. Bosma, C. Pathmamanoharan, E. H. A. de Hoog, W. K. Kegel, A. van Blaaderen, and H. N. W. Lekkerkerker, *Preparation of monodisperse, fluorescent pmma-latex colloids by dispersion polymerization*, J. Colloid Interf. Sci. **245**, 292 (2002).

[33] R. P. A. Dullens, M. Claesson, D. Derks, A. van Blaaderen, and W. K. Kegel, *Monodisperse Core-Shell Poly(methyl methacrylate)Latex Colloids*, Langmuir **19**, 5964 (2003).

[34] J.-S. Song, F. Tronc, and M. A. Winnik, *Two-Stage Dispersion Polymerization toward Monodisperse, Controlled Micrometer-Sized Copolymer Particles*, J. Am. Chem. Soc. **126**, 6562 (2004).

[35] R. Fuoss, *Ionic association. III. The equilibrium between ion pairs and free ions*, J. Am. Chem. Soc. **80**, 5059 (1958).

[36] D. L. J. Vossen, A. van der Horst, M. Dogterom, and A. van Blaaderen, *Optical tweezers and confocal microscopy for simultaneous three-dimensional manipulation and imaging in concentrated*, Rev. Sci. Instrum. **75**, 2960 (2004).

[37] A.-P. Hynninen and M. Dijkstra, *Phase behavior of dipolar hard and soft spheres* , Phys. Rev. E **72**, 51402 (2005).

[38] L. Onsager, *The effects of shape on the interaction of colloidal particles*, Ann. N.Y. Acad. Sci. **51**, 627 (1949).

[39] M. Adams, S. L. Dogic, Z. Keller, and S. Fraden, *Entropically driven microphase transitions in mixtures of colloidal rods and spheres*, Nature **393**, 349 (1998).

[40] M. Hideatsu and M. Yoshiko, *Liquid Crystal Formation in Suspensions of Hard Rodlike Colloidal Particles: Direct Observation of Particle Arrangement and Self-Ordering Behavior*, Phys. Rev. Lett. **90**, 349 (2003).

[41] A. Kuijk, A. van Blaaderen, and A. Imhof, *Synthesis of Monodisperse, Rodlike Silica Colloids with Tunable Aspect Ratio*, J. Am. Soc. **133**, 2346 (2011).

[42] D. Mukhija and M. J. Solomon, *Nematic order in suspensions of colloidal rods by application of a centrifugal field*, Soft Matter **7**, 540 (2011).

[43] C. Vega, C. McBride, and L. G. MacDowell, *Liquid crystal phase formation for the linear tangent hard sphere model from Monte Carlo simulations. 115, 4203*, J. Chem. Phys. **115**, 4203 (2001).

[44] D. C. Williamson and G. Jackson, *Liquid crystalline phase behavior in systems of hard-sphere chains*, J. Chem. Phys. **108**, 10294 (1998).

[45] A. van Blaaderen and A. Vrij, *Synthesis and Characterization of Colloidal Dispersions of Fluorescent, Monodisperse Silica Spheres*, Langmuir **8**, 2921 (1992).

[46] S. Mazur, R. Beckerbauer, and J. Buckholz, *Particle size limits for sintering polymer colloids without viscous flow. Langmuir*, Langmuir **13**, 4287 (1997).

[47] T. M. Obey and B. Vincent, *Novel Monodisperse "Silicone Oil"/Water Emulsions*, J. Colloid Interf. Sci. **163**, 454 (1994).

[48] C. I. Zoldesi and A. Imhof, *Synthesis of monodisperse colloidal spheres, capsules, and microballoons by emulsion templating*, Adva. Mat. **17**, 924 (2005).

[49] C. I. Zoldesi, I. L. Ivanovska, C. Quilliet, G. J. L. Wuite, and A. Imhof, *Elastic properties of hollow colloidal particles*, Phys. Rev. E **78**, 51401 (2008).

[50] F. Gittes, B. Mickey, J. Nettleton, and J. Howard, *Flexural Rigidity of Microtubules and Actin-Filaments Measured from Thermal Fluctuations in Shape* , J. Cell biology **120**, 923 (1993).

[51] A. Ott, M. Magnasco, A. Simon, and A. Libchaber, *Measurement of the Persistence Length of Polymerized Actin Using Fluorescence Microscopy*, Phys. Rev. E **48**, R1642 (1993).

[52] C. Brangwynne, G. H. Koenderink, E. Barry, Z. Dogic, F. C. MacKintosh, and D. A. Weitz, *Bending dynamics of fluctuating biopolymers probed by automated high-resolution filament tracking*, Biophys. J **93**, 346 (2007).

[53] S. S. Rogers, T. A. Waigh, X. B. Zhao, and J. R. Lu, *Precise particle tracking against a complicated background: polynomial fitting with Gaussian weight* , Phys. Biol. **4**, 220 (2007).

[54] T. Odijk, *Possible Scaling Relations for Semidilute Polyelectrolyte Solutions*, Macromolecules **12**, 688 (1979).

[55] J. P. Huang, Z. Wang, and C. Holm, *Structure and magnetic properties of mono- and bi-dispersed ferrofluids as revealed by simulations*, J. Magn. Magn. Mater. **289**, 234 (2005).

[56] F. Smallenburg, H. R. Vutukuri, A. Imhof, A. van Blaaderen, and M. Dijkstra, *Self-assembly of colloidal strings in an external electric or magnetic field*, in preparation.

[57] N. C. Karayiannis, K. Foteinopoulou, C. F. Abrams, and M. Laso, *Modeling of crystal nucleation and growth in athermal polymers: self-assembly of layered nano-morphologies*, Soft Matter **6**, 2160 (2010).

[58] W. J. Wen, X. X. Huang, S. H. Yang, K. Q. Lu, and P. Sheng, *The giant electrorheological effect in suspensions of nanoparticles*, Nature Materials **2**, 730 (2003).

3

Bonding assembled colloids without loss of colloidal stability

---

Here, we present a facile and flexible one-step thermal annealing method to permanently fix non-close and close-packed polymeric structures, so that they easily survive a subsequent drying step without loss of colloidal stability. We first demonstrate the concept with fluorescently labeled and sterically stabilized polymethylmethacrylate (PMMA) particles, because this system can be readily index and density matched, allowing us to compare their structures in 3D real-space before and after the treatment by means of confocal laser scanning microscopy. In the previous chapter, we have already demonstrated this method for creating 1D colloidal bead chains by the application of an external electric field, but it is shown in the present work that it can be applied on many other self-assembly schemes. Moreover, we show that the shape and volume fraction of the particles after bonding can be varied by extended heating.

3.1 Introduction

In recent years, the diversity of self-assembled colloidal structures has strongly increased as it is fueled by a wide range of applications in materials science and also in soft condensed-matter physics [1–4]. Some potential applications include photonic band-gap (PBG) crystals, materials for plasmonic devices, high-efficiency energy conversion and storage, miniature diagnostic systems, desalination, and hierarchically structured catalysts [1–4]. Three dimensional colloidal crystals with mostly close packed (randomly or fcc stacked) have been fabricated via various methods, some of which are able to impose the orientation of these crystals, e.g., sedimentation [5], colloidal epitaxy [6], evaporative or flow controlled deposition [7], shear flow [8, 9], spin-coating [10]. Recently, several methods have been reported to generate non-close packed colloidal crystal structures, for instance, by a physical or chemical immobilization of colloidal arrays with a readily polymerizable monomer, which is dissolved in the dispersion [11–13], and by a combination of thermal sintering and etching of close-packed colloidal crystals [14]. Many recent methods are currently being developed further to fabricate more diverse crystal symmetries and non-close packed structures by tuning the interaction between the particles, namely: oppositely charged interactions [15, 16], external electric fields [17, 18], and/or non-spherical shapes [19, 20]. However, the structures thus formed are vulnerable to capillary forces that arise when the solvent is evaporated and to many other post-treatment steps, especially when the particles are non-close packed [1–4]. For example, to obtain a photonic band gap in the visible, these opals must be dried, then infiltrated with a high refractive index material, and the spheres must subsequently be selectively removed by a chemical etching [1, 14] or a thermal treatment (calcination or pyrolysis) [1–4].

Here, we present a simple in-situ thermal annealing method for bonding assembled colloids without loss of stability. Subsequently, we implemented to different colloidal structures.

The rest of the chapter is organized as follows. Experimental details are listed in Section 3.2, followed by fabrication and fixation of assembled polymeric structures in Section 3.3. We implement our bonding method to four different non-close packed assemblies and one close-packed structure: i) ionic colloidal crystals of oppositely charged particles with a CsCl morphology in Section 3.3.1, ii) external electric field induced body-centered tetragonal (bct) crystal structures in Section 3.3.2, iii) labyrinthine or maze-like sheet structures induced by uniaxial external electric fields in Section 3.3.3, iv) 2D hexagonal sheets induced by biaxial external electric fields in Section 3.3.4, and v) random hexagonal close-packed crystals in Section 3.3.5. We then demonstrate the colloidal stability of the permanently bonded structures in Section 3.4. We end with a summary of the main results in Section 3.5.

3.2 Experimental details

Particle synthesis and suspensions

We synthesized polymethylmethacrylate(PMMA) particles by dispersion polymerization, covalently labelled with the fluorescent dye 7-nitrobenzo-2-oxa-1, 3-diazol (NBD) or rhodamine isothiocyanate (RITC) and sterically stabilized with poly(12-hydroxystearicacid) [21]. We used suspensions of 1.05 μm, 1.10 μm, 2.05 μm, 2.30 μm, 2.35 μm, 2.60 μm, and 3.10 μm diameter PMMA spheres. The 2.05 μm, 2.30 μm, 2.35 μm, 2.60 μm, and 3.10 μm particles were dispersed in salt (tetrabutylammonium bromide, Sigma) saturated cyclohexyl bromide (Fluka) to achieve hard-sphere like interactions [16, 18]. In this mixture, the particles were nearly refractive index-matched. All solvents were used as received without any further purification. All samples were confined to glass capillaries with inner dimensions of 0.1 mm $\times$ 1.0 mm or 0.1 mm $\times$ 2.0 mm (Vitrocom).

Differential Scanning Calorimetry

The glass transition temperature of PMMA latex particles was measured with differential scanning calorimetry (HP DSC827e, Mettler-Toledo, USA). Prior to the measurements, the temperature and the heat flow were calibrated using certified indium and zinc samples. Samples were prepared in aluminum pans at room temperature. The samples were then hermetically sealed in aluminum pans to avoid any drying effects during measurements. Subsequently, masses of the particles were determined. 15.34 mg of dry particles, 16.72 mg of freshly (5 mins after the sample preparation, 42 wt%) prepared PMMA particles in CHB, and 16.22 mg of aged (7-8 days after the sample preparation, 42 wt%) PMMA particles were used for the measurements. Figure 3.1 shows differential scanning calorimetry data for 2.30 μm sized sterically stabilized PMMA particles heated at 10 °C/min. The decrease in heat capacity at T_g exhibits overshoot typical of aged glasses, followed by a small exothermic peak. The glass transition temperature was taken as the middle of the base line shift. The glass transition temperature of dry, freshly prepared PMMA particles in CHB, and aged PMMA particles in CHB were 144.5 °C, 142.5 °C, 137.8 °C respectively as seen in Figure 3.1.

Microscopy

After filling the cell with the colloidal suspension, we sealed it with UV-curing optical adhesive (Norland no.68), and we studied particle dynamics by means of confocal laser scanning microscopy (Leica TCS SP2). We recorded *xy* images of 512 $\times$ 512 and 1024 $\times$ 1024 pixels. We recorded 3D data, consisting of series of *xy* images at different depths (z). After drying the sample, structures that were made permanent by thermal annealing were imaged with a scanning electron microscopy (FEI, XL30FEG).

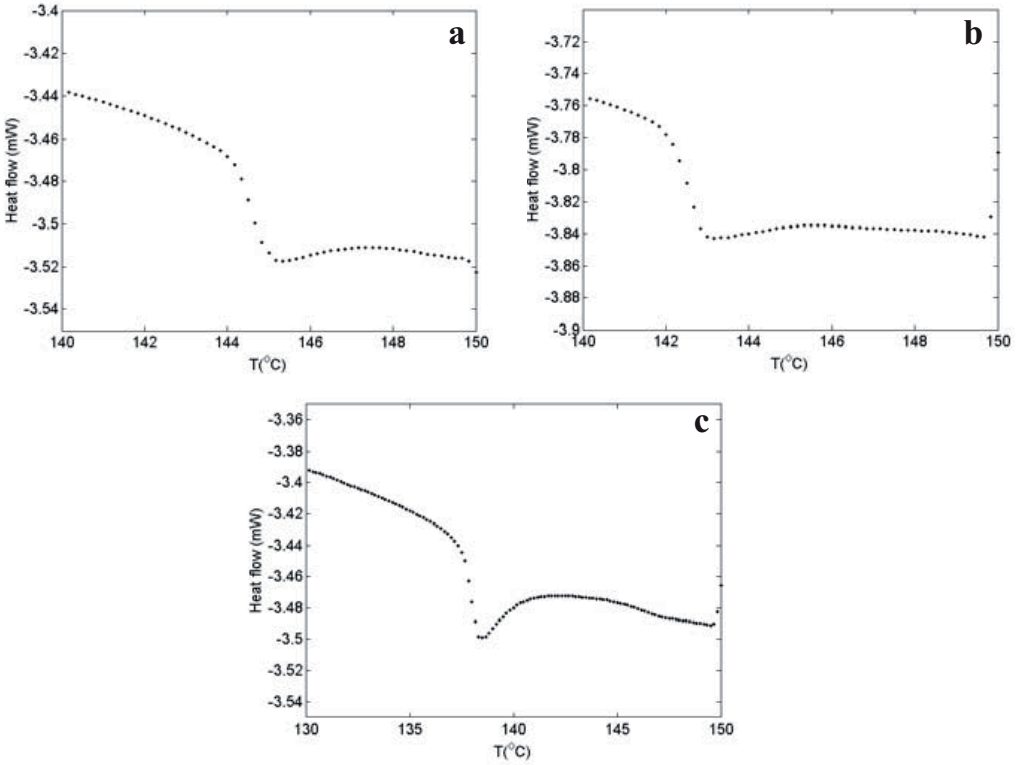

Figure 3.1: Differential scanning calorimetric diagrams of 2.30 μm sized sterically stabilized PMMA particles heated at 10 °C/min. **a**, Dry PMMA particles. **b-c**, PMMA particles in cyclohexyl bromide (CHB) after different waiting times. b, 5 mins after sample preparation. c, 7-8 days after sample preparation.

Electric cell

We used two types of sample cells for creating an uniaxial electric field: rectangular capillaries (VitroCom, UK) and home made sandwich ITO coated glass slides. The rectangular sample cells consisted of a 0.1 mm $\times$ 1.0 mm capillary with two 50 μm thickness nickel-alloy wires (Goodfellow) threaded along the side walls.

For creating biaxial electric fields, we used a sample cell with two mutually perpendicular pairs of semi-transparent electrodes by sputter coating the outer faces of a square borosilicate glass capillary (inner dimensions 0.2 mm $\times$ 0.2 mm and wall thickness 0.1mm, Vitrocom) with 3 nm chromium and 9 nm gold (Cressington). Using a razor blade, we then removed the unwanted contact at the four corners of the square tubing. For the electrical contacts with each of the plate electrodes, we used silver paint and thin thermocouple alloy wire (50 μm diameter) as shown in Figure 3.2. The cell was constructed on top of a standard microscopy slide, for extra support.

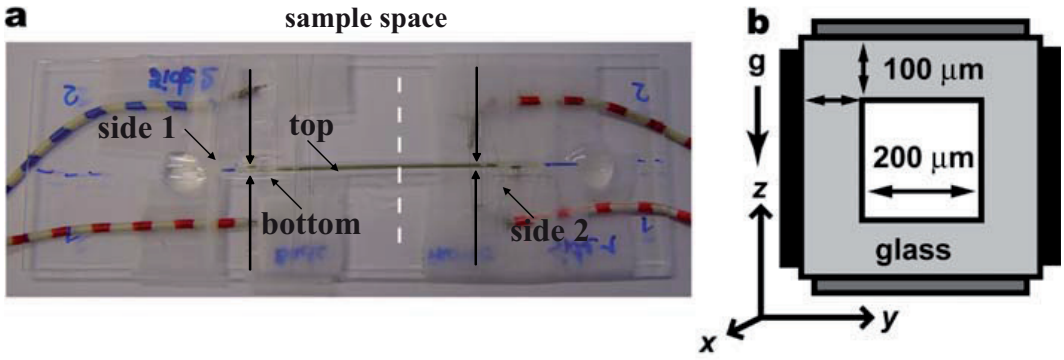

Figure 3.2: Biaxial electric field cell. **a**, Photograph of the $\sim 50\times0.4$ mm large sample cell, on top of a microscopy slide. Four wires provided independent contact each of the plate electrodes, here indicated with small arrows. The large arrows indicate the length and width of the actual sample space. The dashed line indicates the cross section that is depicted in (b). **b**, Schematic drawing of the cross section of the sample cell. Note that the plane of the electric field was parallel to the yz plane.

Electric-field setup

Uniaxial fields

We used a function generator (Agilent, Model 3312 OA) and a wide band voltage amplifier (Krohn-Hite, Model 7602M) to generate the uniaxial electric fields. The field strength and frequency were measured by an oscilloscope (Tektronix, Model TDS3052).

Biaxial electric fields

To circumvent the problem of angular momentum transfer to the particles, as was observed for granular systems [22, 23]. We did not use a truly rotating biaxial electric field but the equivalent of it, by applying a high-frequency 2D field vector with a randomly varying orientation [24]. To achieve this, we let an ordinary PC to generate a random sequence of angles for the field vector, together with the corresponding voltage differences for the two electrode pairs. Typically, this pattern consisted of 10^4 steps (we did not observe any change in suspension behavior in the range of 10 - 10^6 steps). A NI 6534 Digital I/O card (16 Mb memory) was used to generate a digital representation of the correct voltage for each of the electrode pairs, while continuously repeating the random sequence with a frequency of 1 MHz (pattern mode output). Its output was converted by two 12 bits digital-to-analog converters (one for each of the electrode pairs) and then amplified to

a maximum of 230 V_{pk-pk} with an inverting and a non-inverting amplifier. We connected the two output channels with an oscilloscope to check the balancing of the field in a Lissajous plot of the amplitude. The overall field strength in the sample cell was set by the total voltage difference of the two electrode pairs.

3.3 Fabrication and fixation of different colloidal structures

This section is divided into five subsections. Each subsection represents the fabrication of a colloidal assembly followed by its fixation into a permanent strucure.

3.3.1 Ionic colloidal crystals of oppositely charged particles with a CsCl morphology

Recently, it has been demonstrated that cesium-chloride-type (CsCl) crystals can be fabricated from a binary mixture of oppositely charged colloids in a density- and refractive index matched low-polar solvent mixture of cyclohexyl bromide (CHB) and cis-decahydronaphthalene (cis-decalin) by tuning the salt-concentration [16]. Instead of adding salt to the dispersion to induce opposite charges between the two particle species, we functionalized one of the particle species by incorporating the basic monomer 2-(dimethylamino)ethylmethacrylate during the synthesis. At sufficiently high volume fractions of the two different colloidal species, they acquired opposite charges after mixing them together. We were able to grow crystals (Figure 3.3a) consisting of oppositely charged particles with diameters of 1110 nm and 1050 nm respectively. The cesium-chloride structure consists of an equal number of cesium and chloride ions arranged alternatingly at the vertices of a body-centered cubic lattice, such that each particle has eight dislike neighbors. The maximum packing fraction for a CsCl crystal can be calculated using $\phi_{CsCl}(\gamma) = \sqrt{3}\pi(1+\gamma^3)/[(2+\gamma)^3]$, where γ is the size ratio [15]. For our binary system with a size ratio close to unity ($\gamma = 0.9545$) therefore the corresponding maximum volume fraction is 0.68. Although dense, the packing of the CsCl type structure is below that of the hcp and fcc structure, which achieve a packing fraction of 0.74. Because of their non-close packed nature, we observed that it was not feasible to preserve the CsCl structures simply by letting the solvent evaporate; due to the strong drying forces the regular structure was completely lost even after careful and slow drying for about 6-7 days at room temperature. However, we found that the assembled CsCl-type structures could be made to survive the drying step by a simple thermal annealing method.

To anneal the crystals, first a CsCl-type crystal was grown from oppositely charged particles. Typical suspensions consisted of NBD-labeled and RITC-labeled particles with a 1:1 particle number ratio had an overall volume fraction $\phi \approx 0.35$. The suspension was then transferred to a capillary cell of 0.1 mm $\times$ 1.0 mm cross

section with a desired length (4 - 5 cm). After 6 - 7 days, crystals of CsCl-type were observed in an upright positioned cell. The capillary was then immersed in a hot water bath (75 ^{o}C) for about 2 minutes. This was followed by cooling through contact with ambient air. After the heat treatment, all the particles were immobilized and we did not observe any Brownian motion at the single particle level within the structure, which still remained crystalline. Finally, we carefully opened the cell and then dried the crystalline structure for about 6-7 days at room temperature, similarly as was described above for the CsCl crystals that were not first heat treated. Confocal micrographs of CsCl-type crystals are shown before (Figure 3.3a) and after (Figure 3.3b) the heat treatment. Figure 3.3c-d are scanning electron micrographs of the dried CsCl-type crystals. Clearly the order was well preserved.

To probe the underlying mechanism of bonding between the physically touching neighboring particles we measured the glass transition temperature (T_g) of PMMA particles (σ = 2.30 μm) in both dry and wet states as shown in Figure 3.1. The glass transition temperature (T_g = 144.5 ^{o}C, Figure 3.1a) of dry PMMA particles was slightly higher than that of the particles in a wet state (T_g = 142.5 ^{o}C, Figure 3.1b). Note that the measurement was done 5 mins after the sample preparation (42 wt %). The glass transition temperature decreased further (T_g = 137.8 ^{o}C, Figure 3.1c) when the sample had been allowed to equilibrate for about 7-8 days. We suspect this effect was the result from a slight swelling of the PMMA particles in cyclohexyl bromide (CHB). Our bonding temperature was 70-75 ^{o}C which is still well below the glass transition temperature of PMMA particles in both dry and wet states. Therefore it is unlikely that viscous flow took place between the physically touching neighboring particles during the bonding step. We believe that an explanation for the bonding of particles may be found in the fact that at elevated temperatures, the steric PHSA-PMMA comb-graft-stabilizer that is present on the surface of the particles [21], redistributes so that the particles that are in contact bond (fuse) together permanently by the same van der Waals forces between the PMMA polymers that keep the uncrosslinked particles together. Once the dispersion was brought back to room temperature apparently the steric stabilizer rearranged to its original state, because the particle assemblies became stable again as we will show later in Section 3.4. Hence particle stability by steric stabilization was not lost after the bonding.

3.3.2 External electric field induced body-centered tetragonal (bct) crystal structure

External electric fields have been proven to be a versatile tool to direct colloidal self-assembly into strings (1D) [25, 26], sheets (2D) [24], and equilibrium 3D crystallites [18, 27]. The suspension of particles with a long-range screened Coulombic interaction and an induced dipolar interaction shows especially rich phase behaviour [17, 18, 28]. Non-close packed structures like body-centred-tetragonal (bct) and body-centred orthorhombic (bco) phases are among the pos-

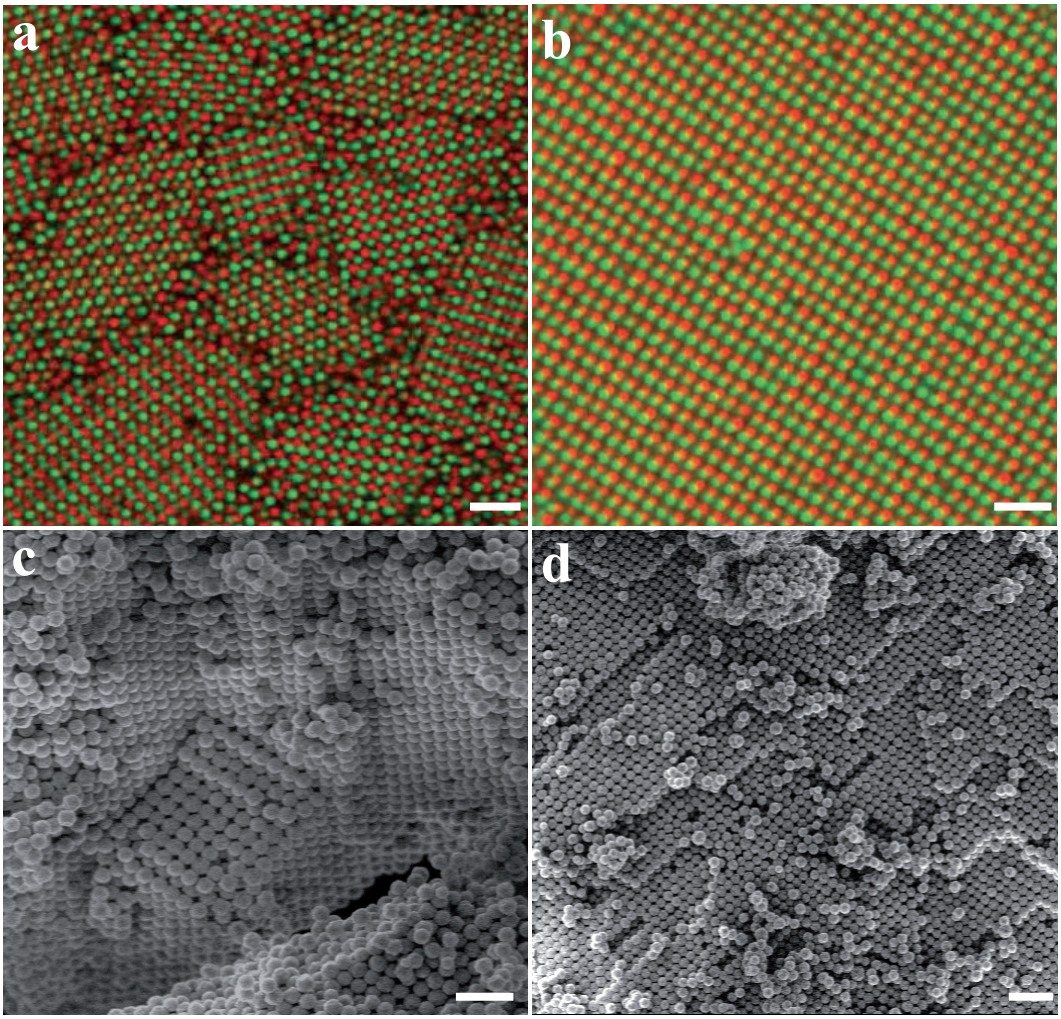

Figure 3.3: CsCl-type crystals. **a-b**, Confocal micrographs of 2D *xy* of positive (red, radius 555 nm) and negative (green, radius 525 nm) PMMA spheres, showing CsCl-like crystals with different orientations, before **a** and after **b** the heat treatment. Note that the images were not taken at the same spot in the sample. **c-d**, Scanning electron micrographs of dried CsCl-type crystals show that the CsCl structure was preserved. Scale bars are 5.0 μm.

sible crystal phases for these types of systems. An important feature of the field-induced crystals is their complete crystallinity. In contrast, colloidal sediments always contain a fluid layer on top therefore they are never completely crystalline [6, 29].

Our colloidal suspension consisted of positively charged 2.1 μm diameter PMMA particles ($\epsilon_p \approx 2.6$) in a nearly refractive-index matching organic solvent cyclohexyl bromide ($\epsilon \approx 7.9$). The particle volume fraction was $\phi = 0.25$. The suspension was then introduced into a thin indium tin oxide coated electric cell [17] and subsequently exposed to a strong AC field ($E_{rms} = 0.85$ Vμm^{-1}, f = 1 MHz, where E_{rms} is the root-mean-square electric field strength, and f is the

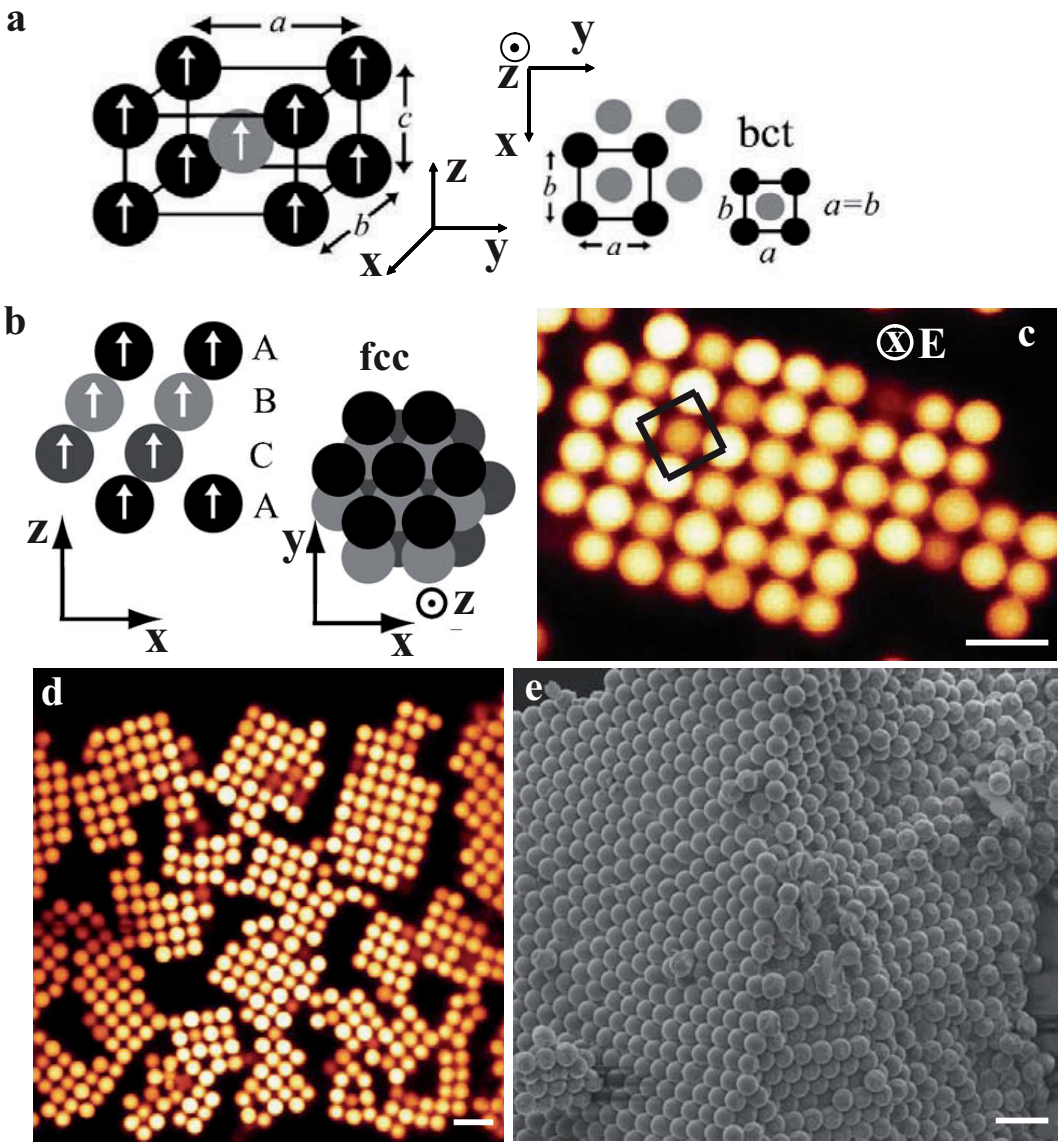

Figure 3.4: Large permanent bct crystallites were fabricated from 2.1 μm PMMA particles in cyclohexyl bromide. **a** Unit cell of the bct crystal. The white arrows indicate the direction of the field-induced dipole moments. The bct structure corresponds to a = b ≠ c. The top-view of the body-centered structure that can be constructed by placing strings of particles (with c inter particle distance in the strings) shifted by c/2 into two interpenetrating rectangular lattices. **b**, For comparison, the fcc structure is shown in side (*xz*) and top views (*xy*). **c**, A confocal micrograph clearly reveals the characteristic bct stacking: square arrangement of spheres perpendicular to the applied field (top layer was indicated with the square outline). **d**, Confocal microscopy image of an *xy* slice in the mid-plane of the sample, perpendicular to the applied field (in *z* direction). **e**, Scanning electron micrograph of dried bct structure. Scale bars are 5.0 μm.

frequency) [18]. After 5 - 6 hrs, large single-domain bct crystallites that do not have a layer of colloidal fluid on top were observed. Two things make it difficult

to preserve the bct structure by drying: i) the field and solvents that are required for it exist ii) it is metastable with respect (close-packed) fcc lattice, to which it deform under small perturbations [29]. To overcome these limitations, we first immobilized the "wet crystal" by our thermal treatment. The entire sample was heated to 70 - 75 ^{o}C for about 2 - 3 minutes using a stream of hot air that is much wider than the sample cell. We kept the field on for 8-10 minutes while the sample cell was allowed to cool down to room temperature. The assembled structures remained stable in the liquid even after the electric field was turned off (Figure 3.4d). Figures 3.4a-b clearly illustrate the difference between the bct and fcc structures. Figure 3.4e clearly shows that the bct order was also preserved in dried form.

3.3.3 Labyrinthine or maze-like structure induced by external electric fields

For particles interacting as magnetic or dielectric dipoles, labyrinthine patterns can be formed by particles that get stuck in one of the possible local minimum (metastable) energy states rather than being in the ground state as in the case for equilibrium structures [17, 28, 30]. The internal structure of the labyrinth is solely dependent on the rate at which the applied field was increased and on initial conditions, which is indicative of a configuration space that has a vast number of local energy minima [30–32]. However, eventually they slowly evolved to form three-dimensional crystals [17, 28].

At a moderate particle concentration (ϕ = 0.20, σ = 2.30 μm where ϕ is the volume fraction and σ is the particle diameter) and field strength (E_{rms} = 0.70 Vμm^{-1}, f = 1 MHz), a labyrinthine structure was observed when the field was increased from 0 to 0.70 V/μm in less than 30-45 secs (Figure 3.5a). The labyrinthine structures rely on the presence of an external electric field, i.e., particles disperse again when the field is switched off. After the structure had formed the entire sample was heated to 70 - 75 ^{o}C for about 2 - 3 minutes. Upon subsequent removal of the field, a confocal micrograph (Figure 3.5a) revealed that the structure was preserved. From a stack of 2D images, we reconstructed a 3D image that clearly revealing the three-dimensional network of the structure as seen in (Figure 3.5b).

3.3.4 Biaxial external electric fields induced hexagonal sheets

In contrast to the uniaxial electric field, the particles have a rotating induced dipole moment in the plane of the rotating field in biaxial electric fields. If the frequency of the rotating field is sufficiently high, the particles experience a time averaged dipolar interaction, leading to a net attraction in the plane of the biaxial field, and a repulsion perpendicular to the field. The time-averaged interaction that the particles experience in a biaxial field is exactly - 1/2 times the interaction potential generated by a uniaxial electric field (U_{bi} = - $\frac{1}{2}$ U_{uni}, see more details

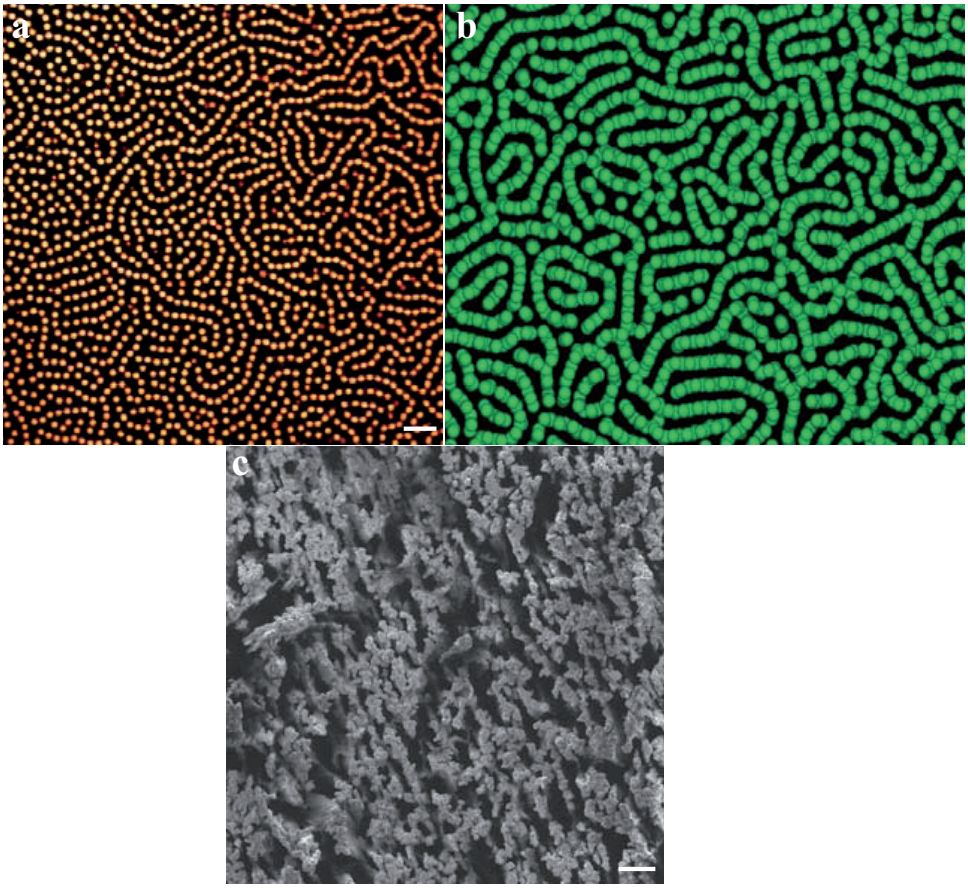

Figure 3.5: Labyrinth structure consisting of 2D particle sheets oriented in the direction of the applied field at a packing fraction of about 20 %. **a**, Confocal microscope image shows a cross section through a labyrinth pattern perpendicular to the applied field. **b**, Rendered particle coordinates revealing the three-dimensional network. **c**, Scanning electron micrograph of a labyrinth structure that has been immobilized by thermal annealing. Scale bars are 10.0 μm.

in the Chapter 2 for U_{uni}), and can be regarded as a negative or 'inverted' dipolar interaction. Computer simulations [33, 34] and experiments with magnetizable particles [22, 23] show that this modification of the sign of the dipolar interaction can lead to a macroscopically different suspension structure, with the particles separated into distinct layers.

Figure 3.6 shows the ordered particle arrangements that resulted when we applied a biaxial field to a suspension of 2.00 μm PMMA-particles in density-matched CHB-decalin mixture, with particle volume fraction $\phi = 0.20$. For moderate voltages (Δ V = 100-120 V), we observed only a slight structuring of the initially isotropic suspension into short chains of particles, but at a higher field (Δ V = 230 V) (Figure 3.6a-b) the particles assembled into sheet-like structures of one particle thick, parallel to the (*yz*) plane of the field. In the *xy* cross-sections of Figure 3.6a the sheets appear as stripes, while the *yz* image of Figure 3.6b show

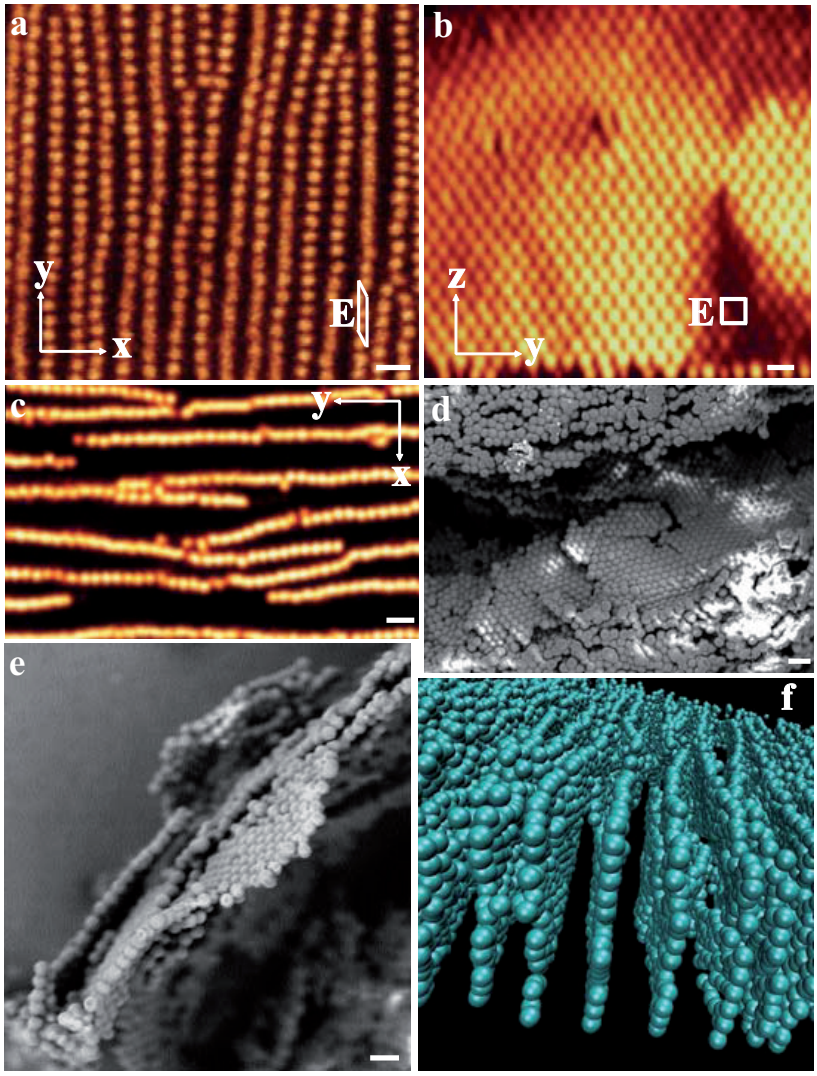

Figure 3.6: a-c, Confocal micrographs revealing the suspension structure in a biaxial electric field. **a**, *xy* image of the center of the sample cell, 11 mins after switching on Δ V = 230 V. The skewed white rectangle indicates the orientation of the plane of the biaxial field E, perpendicular to the image. **b**, *yz* image immediately above the bottom wall halfway the length of the sample cell (the white square indicates the orientation of the plane of the biaxial field, parallel to the image). **c**, Self-supported permanent sheet structures after thermal annealing in the absence of biaxial electric fields. **d-e**, Scanning electron micrographs of hexagonal sheets. The images were *xy* views of different parts of the sample and correspond to a top-bottom orientation of the long axis of the capillary that contained the suspension. **f**, Rendered particle co-ordinates revealing three dimensional structure of the permanent sheets. Scale bars are 5.0 μm.

their internal structure. Importantly, each sheet consisted of multiple, differently oriented hexagonal domains, as there was no preferred orientation in the plane of the field. A clear orientational preference was only found close to the bottom/top wall, with one of the hexagonal close-packed directions running parallel to the wall (Figure 3.6b). This likely was a packing effect, but image charge interactions could play a role too [17]. Although our statistics on individual domains is somewhat limited, the internal ordering seems to be good, with a 2D hexagonal bond order parameter $\Psi_6 \approx$ 0.8-0.9 for regions ranging in size from 45 to 70 μm on each side. After the structure had formed the entire sample was then heated to 70-75 °C for about 2-3 minutes, using a stream of hot air that is much wider than the sample cell. This is followed by cooling through contact with the ambient air. Upon subsequent removal of the biaxial field, the result is a suspension of free-standing thin membranes, which can be dried and extracted from the capillary. Also if left in suspension, the structures are stable over time as seen in Figure 3.6c. Finally, we carefully opened the cell and then dried the hexagonal sheets for about 6-7 days at room temperature. Figure 3.6d-e are scanning electron micrographs of the dried sheets.

3.3.5 Tuning the colloidal particle shape in close-packed crystals

Colloidal self-assembly by sedimentation is one of the most common and simple techniques for making colloidal crystals for a range of applications [2, 5, 6, 35]. Close-packed structures can be easily preserved simply by a controlled drying. Here, we present a new in situ method to permanently preserve the crystalline structure in a more robust way. A large random hexagonal closed-packed (rhcp) crystal (Figure 3.7a) was grown by sedimentation from a nearly refractive-index matched hard-sphere-like colloidal dispersion of 3.10 μm PMMA particles in cyclohexylbromide in a capillary cell of 0.1 mm $\times$ 2.0 mm. The capillary cell was then immersed into a hot water bath which had a temperature of 80 °C for about 2-3 minutes. Next, the cell was carefully opened and subsequently we dried the crystalline structure for about 6-7 days at room temperature (Figure 3.7b).

In an identical sample the close packed particles were heated for 15-20 mins. The surface tension forces between the particles and the solvent [36, 37] caused them to deform from a sphere to a rhombic dodecahedron (Figure 3.7c). It is well known that even for homogeneous polymer particles the glass transition temperature for the outer layer of the polymer can differ significantly (tens of degrees) from that of the interior [38–40]. This sintering process has been discussed in literature using a range of models arising from either a viscous flow process driven by surface tension effects or an elastic Hertzian deformation of elastic spheres under tension. Almost certainly the reality is some more complex visco-elastic intermediate form where the details depend mostly on particle and stabilizer properties [36, 37]. By varying the heating time we were able to tune the packing fraction within the crystalline structure, as was shown before for latex film formation [36, 37] and annealed inorganic colloidal crystals of silica particles

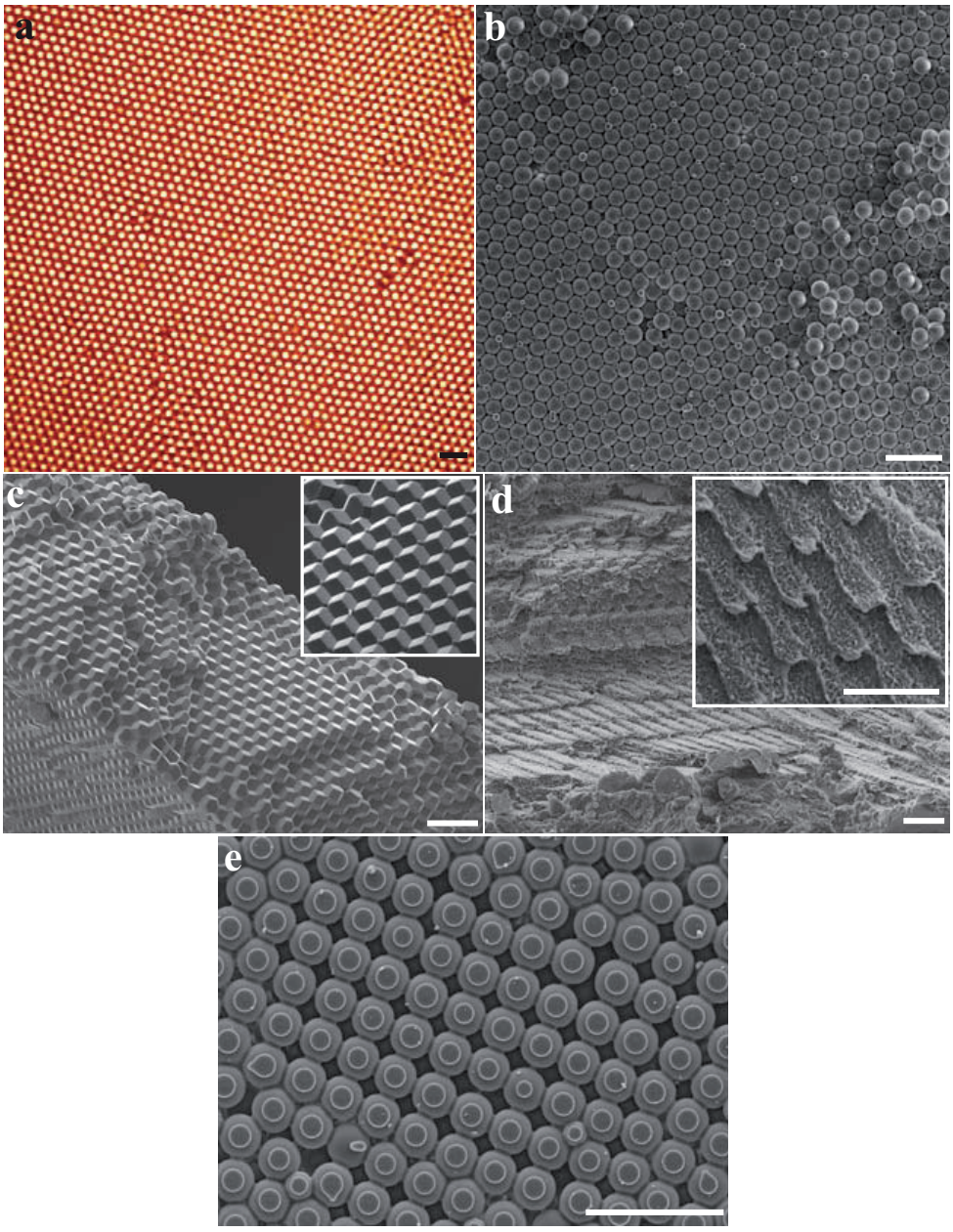

Figure 3.7: a-d, Close packed hard-sphere crystal. **a**, Confocal micrograph of the crystalline structure. **b-d**, Scanning electron micrographs of dried hard-sphere crystals that were annealed at different temperatures (T) and heating times (t_h): (**b**) T = 70 °C and t_h = 2-3 minutes, (**c**) T = 80 °C and t_h = 15-20 minutes, (**d**) T = 95 °C and t_h = 2.5 - 3 hrs (**c-d**, upper inset, a magnified view of the internal structure). **e**, Scanning electron microscopy image of a bct crystal, which shows square arrangement of spheres perpendicular to the applied field. Note that the particles that were in contact had bonded (soft - welded) permanently. A small part of sphere in a first layer flattened by the electrode wall. Scale bars are 10.0 μm.

at elevated temperatures [41, 42]. Moreover, tuning photonic bandgap properties in this way could also be possible.

Finally, we heated the sample cell at elevated temperatures (95 ^{o}C) for a longer period of time about 2.5 - 3.0 hrs. The space filling rhombic dodecahedron structures then transformed into thin films by polymer interdiffusion across the boundaries (Figure 3.7d). This inter diffusion process is also expect to increase the mechanical strength of the polymer film [43].

Moreover, this procedure can also easily be extended to different self-assemblies of the particles. For example, Figure 3.7 e illustrates that the start of particle deformation also in the films of bct crystals, here particles that were touching the electrode are shown.

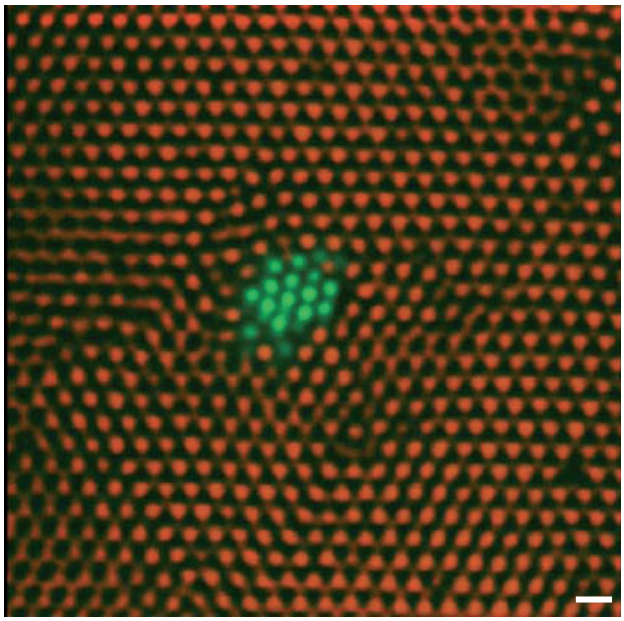

Figure 3.8: Colloidal stability of bonded structure. Confocal micrograph clearly reveals the permanently bonded particles (2.35 μm particles, green color) acted as an impurity in a dispersion of host particles (2.05 μm particles in CHB, red color) Scale bar is 5.0 μm.

3.4 Colloidal stability of bonded structures

Here, we demonstrate that the permanently bonded and dried structures could be used either as seeds for crystal nucleation [6, 44, 45] and growth studies or for a successive self-assembly process. Permanently bonded and dried close-packed structures were first cut into small pieces with a sharp razor blade. Subsequently, these pieces were dispersed into a suspension of host particles (18 % by volume of 2.05 μm particles in a salt saturated CHB). Note that the size of the host particles was chosen such that exactly one particle could fit in between neighboring seed

particles as can be seen in Figure 3.8. This dispersion was then transferred to a 0.1 mm $\times$ 2.0 mm capillary cell and was observed with confocal microscopy. After 2 - 3 hrs, colloidal crystals of the host-particles were observed around the permanently bonded seed-structures (Figure 3.8). We note that the orientation of host particles is different from the bonded seed-structure. This demonstrates that the permanently bonded structures can readily be redispersed and remain stable afterwards. Therefore this bonded structure acted as an impurity rather than a seed. However, we believe that by carefully tuning suspension parameters (e.g. particle diameter and Debye screening length) bonded structures can be used for nucleation and growth studies.

3.5 Conclusions & outlook

In summary, we demonstrated a simple and efficient thermal annealing method to bond colloids together permanently after an initial self assembly step without loss of colloidal stability. Subsequently, these structures can be used in a second self assembly step and/or in further processing steps such as drying and chemical depositions [1–4]. Additionally, our method will work with many (sterically stabilized) polymer colloids and could also easily be extended to more complex core-shell architectures in case the outer layer is a polymer layer. Moreover, the permanent Labyrinthine structures are interesting model systems to study diffusion of tracer particles in porous materials [46] and that they also useful for the fabrication of materials, which rely on strongly anisotropic arrangements of the particles, such as field-structured composites, for efficient and directed heat transfer [47]. In the previous chapter, we have already demonstrated on making 1D flexible chains of PVP stabilized particles. We believe that in a combination of biaxial electric fields and the PVP stabilized particles can be used for making 2D flexible sheets. Moreover, these sheets can be used as model systems for membranes.

Acknowledgements

We would like to thank Mirjam Leunissen for demonstrating the biaxial electric cell construction and useful discussions. Johan Stiefelhagen and Teun Vissers are acknowledged for synthesis of PMMA particles and CsCl-type crystals of oppositely charged colloids. We would also like to thank J. D. Meeldijk and Bo Peng for scanning electron microscope measurements, Rien van Zwienen and Arjen van de Glind for DSC measurements.

References

[1] C. Aguirre, E. Reguera, and A. Stein, *Tunable colors in opals and inverse opal photonic cystals*, Adva. Fun. Mat. **20**, 1033 (2010).

[2] A. Stein, F. Li, and N. R. Denny, *Morphological control in colloidal crystal templating of inverse opals, hierarchical structures, and shaped particles*, Chem. Mat. **20**, 649 (2008).

[3] F. Li, D. P. Josephson, and A. Stein, *Colloidal assembly: The road from particles to colloidal molecules and crystals*, Angew. Chemie. **50**, 360 (2011).

[4] J. Galisteo-López, M. Ibisate, R. Sapienza, L. S. Froufe-Perez, and C. López, *Self-assembled photonic structures*, Adva. Mat. **23**, 30 (2011).

[5] K. E. Davis, W. B. Russel, and W. J. Glantschnig, *Disorder-to-order transition in settling suspensions of colloidal silica- X - ray measurements*, Sceince **245**, 507 (1989).

[6] A. vanBlaaderen, R. Ruel, and P. P. Wiltzius, *Template-directed colloidal crystallization*, Nature **385**, 321 (1997).

[7] P. Jiang, J. F. Bertone, K. S. Hwang, and V. L. Colvin, *Single-crystal colloidal multilayers of controlled thickness*, Chem. Mat. **11**, 2312 (1999).

[8] B. J. Ackerson and P. N. Pusey, *Shear-induced order in suspensions of hard-spheres*, Phys. Rev. Lett. **61**, 1033 (1988).

[9] A. Imhof, A. Vanblaaderen, and J. K. G. Dhont, *Shear melting of colloidal crystals of charged spheres studied with rheology and polarizing microscopy*, Langmuir **10**, 3477 (1994).

[10] P. Jiang and M. M. J., *Large-scale fabrication of wafer-size colloidal crystals, macroporous polymers and nanocomposites by spin-Coating*, J. Ame. Chem. **112**, 13778 (2004).

[11] S. A. Asher, K. W. Kimble, and J. P. Walker, *Enabling Thermoreversible Physically Cross-Linked Polymerized Colloidal Array Photonic Crystals2008. 20(24): p. 7501-7509*, Chem. Mat. **20**, 7501 (2008).

[12] L. Liu, P. S. Li, and S. A. Asher, *Entropic trapping of macromolecules by mesoscopic periodic voids in a polymer hydrogel*, Nature **397**, 141 (1999).

[13] J. H. Holtz and S. A. Asher, *Polymerized colloidal crystal hydrogel films as intelligent chemical sensing materials*, Nature **389**, 829 (1997).

[14] R. Fenollosa and F. Meseguer, *Non-Close-Packed Artificial Opals*, Adva. Mat. **15**, 1282 (2003).

[15] P. Bartlett and A. I. Campbell, *Three-dimensional binary superlattices of oppositely charged colloids*, Phys. Rev. Lett. **95**, 128302 (2005).

[16] M. E. Leunissen, C. G. Christova, A. P. Hynninen, C. P. Royall, A. I. Campbell, A. Imhof, M. Dijkstra, R. van Roij, and A. van Blaaderen, *Ionic colloidal crystals of oppositely charged particles*, Nature **437**, 235 (2005).

[17] U. Dassanayake, S. Fraden, and A. van Blaaderen, *Structure of electrorheological fluids*, J. Chem. Phys. **112**, 3851 (2000).

[18] A. Yethiraj and A. van Blaaderen, *A colloidal model system with an interaction tunable from hard sphere to soft and dipolar*, Nature **421**, 513 (2003).

[19] M. Mittal and E. M. Furst, *Electric Field-Directed Convective Assembly of Ellipsoidal Colloidal Particles to Create Optically and Mechanically Anisotropic Thin Films*, Adv. Funct. Mater. **19**, 3271 (2009).

[20] A. Kuijk, A. van Blaaderen, and A. Imhof, *Synthesis of monodisperse, rodlike silica colloids with tunable aspect ratio*, J. Am. Chem. Soc. **133**, 2346 (2011).

[21] G. Bosma, C. Pathmamanoharan, E. H. A. de Hoog, W. K. Kegel, A. van Blaaderen, and H. N. W. Lekkerkerker, *Preparation of monodisperse, fluorescent pmma-latex colloids by dispersion polymerization*, J. Colloid Interf. Sci. **245**, 292 (2002).

[22] P. Carletto, G. Bosssis, and A. Cebers, *Structures in a magentic subjected to unidirectional and rotating field*, Int. J. Mod. Phys. B **16**, 2279 (2002).

[23] J. E. Martin, E. Venturini, J. Odinek, and R. A. Anderson, *Anisotropic magnetism in field-structured composites*, Phys. Rev. E **61**, 2818 (2000).

[24] M. E. Leunissen, H. R. Vutukuri, and A. van Blaaderen, *Directing colloidal self-assembly with*

biaxial electric fields, Adav. Mat. **21**, 3116 (2009).

[25] K. D. Hermanson, S. O. Lumsdon, J. P. Williams, E. W. Kaler, and O. D. Velev, *Dielectrophoretic assembly of Electrically functional microwires from nanoparticle suspensions*, Science **294**, 1082 (2001).

[26] H. R. Vutukuri, A. F. Demirors, P. Bo, P. D. J. van Oostrum, A. Imhof, and A. van Blaaderen, submitted.

[27] R. C. Hayward, D. A. Saville, and I. A. Aksay, *Electrophoretic assembly of colloidal crystals with optically tunable micropatterns*, Nature **404**, 56 (2000).

[28] A. P. Hynninen and M. Dijkstra, *SPhase diagram of dipolar hard and soft spheres: Manipulation of colloidal crystal structures by an external field*, Phys. Rev. Lett. **94**, 138303 (2005).

[29] A. A. Yethiraj, J. H. J. Thijssen, A. Wouterse, and A. van Blaaderen, *Large-area electric-field-induced colloidal single crystals for photonic applications*, Adva. Mat. **16**, 596 (2004).

[30] A. J. Dickstein, S. Erramilli, R. E. Goldstein, D. P. Jackson, and S. A. Langer, *Labyrinthine pattern-formation in magnetic fluids*, Science **261**, 1012 (1993).

[31] R. Rosensweig, M. Zahn, and R. Shumovich, *Labyrinthine instability in magnetic and dielectric fluids*, J. Magn. Mate **39**, 127 (1983).

[32] G. A. Flores, J. Liu, M. Mohebi, and N. Jamasbi, *Magnetic-field-induced nonequilibrium structures in a ferrofluid emulsion*, Phys. Rev. E. **59**, 751 (1999).

[33] J. E. M., A. A. Robert, and P. T. Chris, *Simulation of the athermal coarsening of composites structured by a biaxial field*, J. Chem. Phys. **108**, 7887 (1998).

[34] J. E. M., A. A. Robert, and P. T. Chris, *Thermal coarsening of uniaxial and biaxial field-structured composites*, J. Chem. Phys. **110**, 4584 (1999).

[35] P. N. Pusey and W. Vanmegen, *Phase-behavior of concentrated suspensions of nearly hard colloidal spheres*, Nature **320**, 340 (1986).

[36] S. Mazur, R. Beckerbauer, and J. Buckholz, *Particle size limits for sintering polymer colloids without viscous flow*, Langmuir **13**, 4287 (1997).

[37] A. F. Routh and W. B. Russel, *Deformation mechanisms during latex film formation: Experimental evidences*, Ind. Engg. Chem. Res. **40**, 4302 (2001).

[38] J. L. Keddie, R. A. L. Jones, and R. A. Cory, *Interface and surface effects on the glass-transition temperature in thin polymer films*, Faraday Discuss. **98**, 219 (1994).

[39] J. A. Forrest, K. Dalnoki-Veress, J. R. Stevens, and J. R. Dutcher, *Effect of free surfaces on the glass transition temperature of thin polymer films*, Phys. Rev. Lett. **77**, 4108 (1996).

[40] Z. Yang, Y. Fujii, F. K. Lee, C.-H. Lam, and K. C. Tsui, *Glass transition dynamics and surface layer mobility in unentangled polystyrene films*, Sceince **328**, 1676 (2010).

[41] H. Miguez, F. Meseguer, C. Lopez, A. Blanco, J. S. Moya, J. Requena, A. Mifsud, and V. Fornes, *Control of the photonic crystal properties of fcc-packed submicrometer SiO2 spheres by sintering*, Adva. Mat. **10**, 480 (1998).

[42] B. Gates, S. H. Park, and Y. N. Xia, *Tuning the photonic bandgap properties of crystalline arrays of polystyrene beads by annealing at elevated temperatures*, Adva. Mat. **12**, 653 (2000).

[43] S. Prager and M. Tirrell, *Healing-process at polymer-polymer interfaces*, J. Chem. Phys **74**, 5194 (1985).

[44] A. Cacciuto, S. Auer, and D. Frenkel, *Onset of heterogeneous crystal nucleation in colloidal suspensions*, Nature **428**, 404 (2004).

[45] V. W. A. de Villeneuve, D. R. P. A., E. Aarts, D. G. A. L. Groeneveld, J. H. Scherff, W. K. Kegel, and H. N. W. Lekkerkerker, *Colloidal hard-sphere crystal growth frustrated by large spherical impurities*, Science **309**, 1231 (2005).

[46] G. A. Flores, J. Liu, M. Mohebi, and N. Jamasbi, *Tracer dispersion in a percolation network with spatial correlations*, Phys. Rev. E. **61**, 583 (2000).

[47] J. E. Martin and G. Gulley, *Field-structured composites for efficient, directed heat transfer*, J. Appl. Phys. **106**, 084301 (2009).

4

A facile method for creating polyhedral colloidal latex particles

The demand for micron-sized colloidal particles with complex shapes is largely driven by applications in self-assembly, and also in advanced functional materials design. Here, we present a facile method for synthesizing polyhedral polymeric colloidal particles in large quantities. Our method consists of three simple steps: (i) the self-assembly of spherical polymeric particles into a 3D crystalline structure, (ii) the deformation of the spherical particles by thermal annealing in such a way that mass transport between the particles does not take place, and (iii) the detachment of the resulting deformed particles from the 3D superstructures into individual particles by sonication. The final shape of the particles is dictated by the symmetry and volume fraction of the initial 3D self-assembled structure comprised of spherical particles. The resulting polyhedral particles are less symmetric than spheres and still monodisperse. Because the method used is essentially a bulk method it can be scaled up easily. This makes it interesting for both fundamental, and applied studies utilizing these new polyhedral particle properties. The results we present are just preliminary results demonstrating a feasibility of the method; and more work has to be done to assess the right parameter space. We believe it quite likely that this method may be applicable to inorganic particles like silica as well.

4.1 Introduction

Particle shape is a critical parameter that can play an important role in colloidal self-assembly [1–4]. Building blocks consisting of non-spherical and anisotropic particles offer the possibility of structures with different symmetries, packing densities, and directionalities. Therefore, a vast variety of possible assembled structures is expected compared to structures that are build from spherical particles [1–4]. The last several years have been witness to an unprecedented revolution in control over the shape of nano particles. A variety of nano particles with well-defined shapes have been synthesized via photochemical [5, 6], thermal [7], electrochemical [8], and template-directed methods [9, 10].

In contrast, the list of micron-sized colloidal particles that have been synthesized with an anisotropic shape, especially in a combination with flat surfaces, i.e., particles with polygonal shapes, is significantly more limited. This can be attributed to the fact that, contrary to nanoparticles, the larger colloids only rarely consist of single crystals [1–4]. However, several synthesis routes have been reported to fabricate polymeric particles with non-spherical geometries. These approaches make use of self-assembly [11–13], photolithography [14], microfluidics [15], nonwetting template molding [16], stretching particle-embedded polymer films [17], thermal sintering of spherical particles at an oil-water interface [18], and seeded emulsion polymerization [19, 20]. Collectively, these methods have produced particles of several distinct shapes. However, of all these methods, only the seeded emulsion polymerization method [19, 20] is a truly '3D' method that allows for easy preparation of larger quantities, but the shapes that are possible with this method are limited.

A few computational and theoretical studies have predicted that the polyhedral colloidal particles show a rich phase behavior [3, 4], but experimental realization of those phases scarcely exists. Not only the phase behavior of polygonal particles is interesting, for instance, it has already been realized that the depletion force is much more effective between flat interfaces than it is between curved interfaces [14, 21]. Moreover, the rotational behavior of particles less symmetric than spheres is of fundamental interest as well [22]. In previous chapters, we have already demonstrated our thermal sintering method for creating permanently bonded 1D colloidal bead chains (Chapter 2), 2D sheets, and 3D structures (Chapter 3). In addition, we have shown that this method can be applied to make thin films by polymer inter-diffusion across the boundaries in between the neighboring particles (Chapter 3). In the present chapter, we describe that under certain conditions the sintering process can be carried out without significant exchange of material in between the neighboring particles, whist at the same time effecting the deformation of particles as influenced by their direct neighbors. Moreover, the deformed polygonally shaped particles can be redispersed as stable dispersion of single particles. We note that the sintering and particle deformation are part of the film formation process observed for latex particles, for example,

paints, paper coatings, textiles, and carpets [23–26]. In the following we first give a very brief overview of this literature with a focus on making regularly deformed individual latex spheres.

Herein, we describe how 3D assembled particles were deformed into a polygonal shape by heating in the presence of a liquid. Sintering phenomena which lead to particle deformation can also be observed in the intermediate stage of latex film formation, which is used in several industrial processes, e.g., paints, paper coatings, textiles, and carpets [23–26]. In film formation there are several processes and stages that are not relevant for the procedure that we describe in this chapter. For instance, in most cases the crystallization (and/or increase of density into a packed ordered or disordered state) of the system takes place under the influence of drying induced forces and effects. Some of the deformation of the particles once they are in close contact takes either place in a dry state (dry sintering) and/or in a wet state (wet sintering). Only the latter process is relevant to our procedure. Moreover, the exchange of material from one particle to its neighbors by polymer chain diffusion that occurs in the final stage of film formation would completely prohibit the ability to disperse the polymer particles individually by sonication and preserve their smooth surfaces. In wet sintering the driving force for particle deformation into a polygonal shape is driven by the free energy gain achieved lowering the exposed polymer surface area. It is well known that even for homogeneous polymer particles the glass transition temperature for the outer layer of the polymer can differ significantly (tens of degrees) from that of the interior [27–29]. This sintering process has been discussed in literature using a range of models as arising from either a viscous flow process driven by surface tension effects or an elastic Hertzian deformation of elastic spheres under tension. Almost certainly the reality is some more complex visco-elastic intermediate form where the details depend mostly on particle and stabilizer properties [23, 30].

The deformation of polymer particles that are part of a colloidal crystal into polygonal shapes is also used to tune the properties of photonic crystals. Xia and co-workers [31] have adopted a procedure first developed for silica particles by López *et al*. [32] to create the colloidal crystals with polyhedral polystyrene building blocks. However, they have limited their studies to optical properties of slightly deformed crystals such as photonic bandgap tuning. Their goal was never to try and see if the particles could be recovered as individual units. In this work we show that a combination of thermal sintering and sonication can be used to synthesize polyhedrally shape particles. Our method consists of three steps: (i) assembly of sterically stabilized pmma spheres into 3D arrays, (ii) deformation of the assembled structures by thermal annealing, and (iii) disassembly of these 3D structures into individual particles by sonication of the dispersion for about 10-15 minutes. We have found exact conditions that work for one batch of particles, but further research is required to determine the reproducibility of the method and under what range of conditions it functions.

This chapter is structured as follows. Experimental details are listed in Section

4.2, followed by a discussion of the results in Section 4.3. In Section 4.3.1 we present a general method for creating micron sized polyhedral particles. Finally, we give conclusions and an outlook for the future scope of work in Section 4.4.

4.2 Experimental details

Particle synthesis and suspensions

Polymethylmethacrylate (PMMA) particles were synthesized by dispersion polymerization [33]. The particles were covalently labelled with the fluorescent dye 7-nitrobenzo-2-oxa-1,3-diazol (NBD). They were sterically stabilized with poly(12-hydroxystearicacid), which was grafted on to a PMMA backbone forming a comb-graft steric stabilizer [33]. After the synthesis, particles were washed several times with hexane to remove the smaller particles and un-reacted species. We used suspensions of 3.1 μm diameter PMMA spheres. The particle size and polydispersity (4 %) were determined by static light scattering (SLS). The particles were dispersed in cyclohexyl bromide (CHB, Fluka), saturated with tetrabutylammonium bromide (TBAB, Sigma). In this dispersion, the particles were nearly refractive index-matched, and they behaved like hard-spheres [34]. All solvents were used as received without any further purification. We used rectangular capillaries of 0.1 mm $\times$ 1.0 mm and 0.1 mm $\times$ 2.0 mm (VitroCom, UK). After filling the cell with the colloidal suspension, we sealed both ends of the capillary with UV-curing optical adhesive (Norland no.68) and cured the glue with UV-light (λ = 350 nm, UVGL-58 UV lamp). We studied particle dynamics by means of confocal laser scanning microscopy. Finally, we used a sonicator of Branson, Model 8510.

Thermal sintering method

To anneal the crystals, first a random hexagonal closed packed crystal was grown by sedimentation from nearly refractive-index matched, hard-sphere-like colloidal suspension of NDB labelled PMMA particles in CHB. The initial volume fraction of the particles was $\phi = 0.15$. The suspension was then transferred to a capillary cell with a 0.1 mm $\times$ 2.0 mm cross section and of a desired length (6-7 cm). We let the sample sediment for 6-7 days. After 6-7 days, a large random hexagonal closed packed crystal was observed in an upright positioned capillary cell as shown in Figure 4.1a. The capillary cell was subsequently immersed into a hot water bath of 80 ^{o}C. This temperature well below the glass transition temperature (T_g = 140-145 ^{o}C) of PMMA. The water-bath heating step was followed by cooling through contact with ambient air. We carefully opened the cell and allowed the structure to dry for about 6-7 days at room temperature. After drying, the sample was examined by scanning electron microscopy.

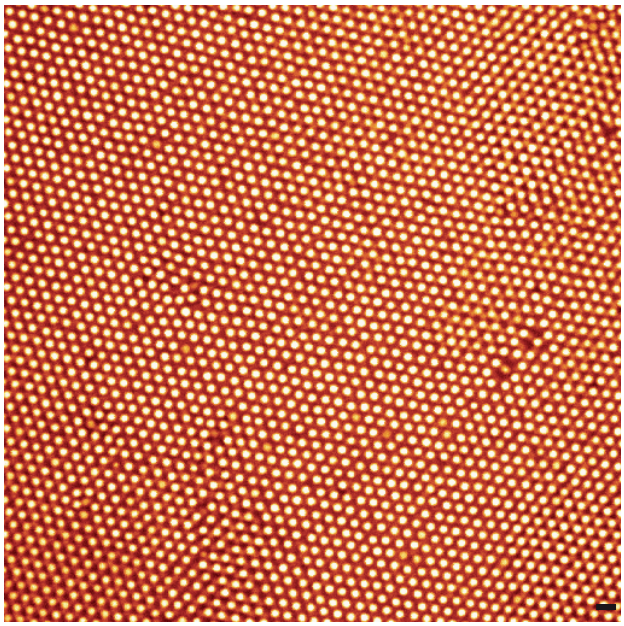

Figure 4.1: Hard-sphere like crystal formed under gravity. The image shows a confocal micrograph of random close packed PMMA particles in CHB. The crystal was grown from 3.10 μm sized PMMA particles in an index matching solvent (CHB) in an upright positioned capillary cell of 0.1 mm × 2.0 mm. Scale bar is 5 μm.

4.3 Results and discussion

4.3.1 Wet sintering

In wet sintering, the interfacial tension between the particles and the solvent is the dominant driving force. The deformation of the (almost) touching particles was performed in the presence of a solvent. Moreover, this liquid modifies not only the surface tension, but may also modify the glass transition temperature of the PMMA as it slightly swells the particles. During the initial stages of sintering, approximately 2-3 minutes after the start of heating, particles began to deform into polyhedral shapes due to the surface forces between the particle and the solvent. Such a sample was then cooled down to room temperature. Next, we carefully opened the cell and then dried the structure for about 6-7 days at room temperature. The sample was then examined by scanning electron microscopy. As shown in Figure 4.2a, it can clearly be seen that the crystal building blocks are now non-spherical particles and exhibit a hexagonal shape in the (111) plane.

Next, in an identical sample the close packed particles were heated for 15-20 mins. In this case the particles deformed further in order to obtain a completely uniform and void-free structure. Because each particle is surrounded by twelve neighboring particles, of which six are in the same layer and three are in each of the layers above and below. These particles all experienced a simultaneous flat-

tening of their interface surfaces and are deformed into rhombic dodecahedra. The resulting shape is determined by the reduction in free interface of the particles and the solvent [23–26, 30]. The structure of such a rhombic dodecahedron is clearly seen in Figure 4.2b. We observed that particles which are in contact with the wall obtained a different shape.

If the particles are ordered in a face-centered-cubic (fcc) array and regularly deformed, the resulting particles will be regular rhombic dodecahedra. We believe that simple cubic-packed particles should lead to simple cubic shape like, body centered cubic packed particles result in truncated octahedra, and hexagonal close packed particles transform to hexagonal prism shape particles. The final shape of the particle is dictated by the initial 3D assembled structure of the spherical particles. Although, it should first be determined how general the conditions are for being able to completely redisperse the particles with smooth interfaces.

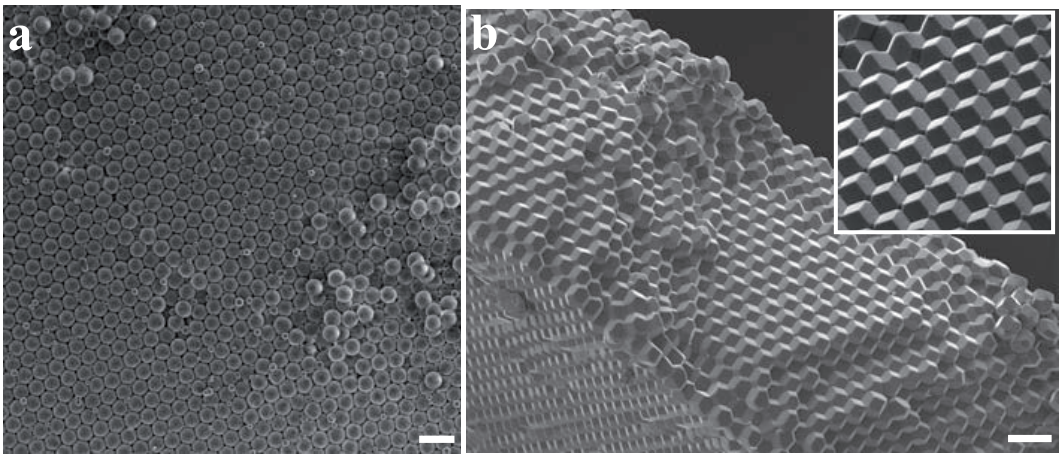

Figure 4.2: Deformed close packed crystals of PMMA spheres. **a-b**, Scanning electron micrographs of dried hard-sphere crystals that were annealed at different temperatures: (**a**) temperature = 70 °C and heating time = 2-3 minutes, (**b**) temperature = 80 °C and heating time = 15-20 minutes (upper-right inset, a magnified view of the internal structure). Scale bars are 5.0 μm.

4.3.2 Dispersible polyhedral particles

Even though the particles had completely deformed until the volume fraction reached to one, filling all interstitial space in the crystal, it turned out to be possibly to detach them from each other again. A bonded and dried 3D PMMA crystalline structure was transferred into CHB, and this 3D structure was then disassembled into individual particles by sonication of the dispersion for about 10-15 minutes at room temperature. A confocal laser microscope image (Figure 4.4) reveals that these particles are indeed dispersible in a nearly index matched apolar solvent (CHB). Apparently, the steric stabilizer remained present on the

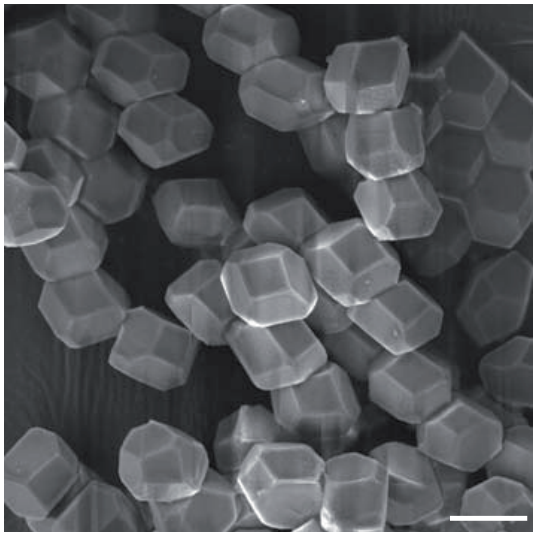

Figure 4.3: Rhombic dodecahedron shaped particles that were made by the combination of thermal annealing and sonication. Scanning electron micrograph clearly reveals the shape of such particles. Scale bar is 5.0 μm.

surface of the particles, separating the deformed particles in the crystal and no PMMA polymer had diffused yet to other particles. The resulted surfaces are remarkably smooth as seen in Figure 4.3. We observed the particle shape with confocal microscope for about 2-3 weeks to check whether particles had retained their non-spherical shape. This was indeed the case.

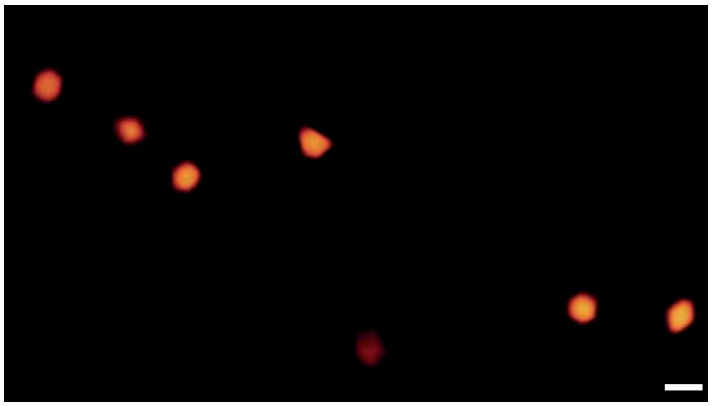

Figure 4.4: Dispersable rhombic dodecahedron like particles. Confocal microscopy image of rhombic dodecahedron type PMMA particles in CHB. Although it is difficult to observe the rhombic dodecahedron shape from the image it clearly shows that the particles are not spherical in shape. Scale bar is 5 μm.

4.4 Conclusions & outlook

In conclusion, we demonstrated the fabrication of polyhedral-shaped particles such as rhombic dodecahedral particles with flat interfaces. Our method is quite general since it relies on an initial 3D assembled structure that is comprised of spherical particles. Our method also enables us to tune the particle shape by varying the sintering time. However, the range of parameters for which it works still needs to be established, as it is for now only demonstrated with the one size of PMMA particles. We will further investigate if the method can be adopted to other polymeric particles and if it could also be used for inorganic amorphous particles such as silica. An added advantage is that our method should be easily scalable because it is a bulk method. As far as we know, the synthesis of micron-sized polyhedral shape particles with flat surfaces has not been reported before. We believe that our particles are interesting to examine out the effects of rotational degrees of freedom in self assembly studies, form new (liquid) crystalline phases and also give more opportunities to fine tune attractions between particles by using the depletion effect. Our systems can be both index and density matched, so that bulk measurements in real-space are possible. Escobedo *et al*. Recently, a simulation study has been reported on mesophase behavior of space-filling polyhedrons, namely, truncated octahedrons, rhombic dodecahedrons, hexagonal prisms, cubes, gyrobifastigiums and triangular prisms [4]. They predicted the formation of various new liquid-crystalline and plastic crystalline phases at intermediate volume fractions.

Acknowledgements

We thank Johan Stiefelhagen for the synthesis of PMMA spheres. Bo Peng and J. D. Meeldijk are acknowledged for scanning electron microscope measurements. Joost de Graaf is gratefully acknowledged for the critical reading of this chapter and for his useful comments.

References

[1] M. Grzalczak, J. Vermant, E. M. Furst, and M. Liz-Marzan, *Directed self-assembly of nanoparticles*, ACS Nano **4**, 3591 (2010).

[2] F. Li, D. P. Josephson, and A. Stein, *Colloidal assembly: The road from particles to colloidal molecules and crystals*, Angew. Chemie. **50**, 360 (2011).

[3] S. C. Glotzer and M. J. Solomon, *Anisotropy of building blocks and their assembly into complex structures*, Nat. Mate. **6**, 557 (2007).

[4] U. Agarwal and F. A. Escobedo, *Mesophase behaviour of polyhedral particles*, Nat. Mate. **10**, 230 (2011).

[5] J. Zhang, S. Li, J. Wu, G. C. Schatz, and C. A. Mirkin, *Plasmon-Mediated Synthesis of Silver Triangular Bipyramids*, Angew. Chem. **48**, 7787 (2009).

[6] R. C. Jin, Y. W. Cao, C. A. Mirkin, K. L. Kelly, G. C. Schatz, and J. G. Zheng, *Photoinduced conversion of silver nanospheres to nanoprisms*, Science **294**, 1901 (2009).

[7] Y. N. Xia, Y. J. Xiong, B. K. Lim, and S. E. Skrabalak, *Shape-Controlled Synthesis of Metal Nanocrystals: Simple Chemistry Meets Complex Physics?*, Angew. Chem **48**, 60 (2009).

[8] Y. Y. Yu, S. S. Chang, C. L. Lee, and C. R. C. J. Wang, *Gold Nanorods: Electrochemical Synthesis and Optical Properties*, The Journal of Physical Chemistry B **101**, 6661 (2001).

[9] C. R. Martin, *Nanomaterials: a membrane-based synthetic approach*, Science **266**, 1961 (1994).

[10] G. A. Somorjai and D. W. Blakely, *Mechanism of catalysis of hydrocarbon reactions by platinum surfaces*, Nature **258**, 5536 (1975).

[11] V. N. Manoharan, M. T. Elsesser, and D. J. Pine, *Anisotropy of building blocks and their assembly into complex structures*, Science **301**, 557 (2007).

[12] K. D. Hermanson, S. O. Lumsdon, J. P. Williams, E. W. Kaler, and O. D. Velev, *Dielectrophoretic assembly of Electrically functional microwires from nanoparticle suspensions*, Science **294**, 1082 (2001).

[13] H. R. Vutukuri, A. F. Demirors, P. Bo, P. D. J. van Oostrum, A. Imhof, and A. van Blaaderen, submitted.

[14] S. Badaire, C. Cottin-Bizonne, J. W. Woody, A. Yang, and A. D. Stroock, *Shape Selectivity in the Assembly of Lithographically Designed Colloidal Particles*, J. Ame. Chem. Soc. **129**, 40 (2007).

[15] D. Dendukuri, D. C. Pregibon, J. Collins, T. A. Hatton, and P. S. Doyle, *Continuous Flow Lithography for High-Throughput Microparticle Synthesis*, Nat. Mater **5**, 365 (2006).

[16] J. P. Rolland, B. W. Maynor, L. E. Euliss, A. E. Exner, G. M. Denison, and J. M. DeSimone, *Direct Fabrication and Harvesting of Monodisperse, Shape-Specific Nanobiomaterials*, J. Am. Chem. Soc. **127**, 10096 (2005).

[17] C. C. Ho, A. Keller, J. A. Odell, and R. H. Ottewill, *Preparation of monodisperse ellipsoidal polystyrene particles*, Colloid Poly. Sci. **271**, 469 (1993).

[18] B. J. Park and E. M. Furst, *Fabrication of Unusual Asymmetric Colloids at an Oil-Water Interface*, Langmuir **26**, 10406 (2010).

[19] M. Okubo, K. Kanaida, and T. Matsumoto, *Production of anomalously shaped carboxylated polymer particles by seeded emulsion polymerization*, Collod Poly. Sci. **265**, 876 (1987).

[20] M. Okubo, T. Fujiyashi, and A. Terada, *Synthesis of micron-sized, monodisperse polymer particles of disc-like and polyhedral shapes by seeded dispersion polymerization*, Collod Poly. Sci. **283**, 793 (2005).

[21] K. Zhao and T. G. Mason, *Directing Colloidal Self-Assembly through Roughness-Controlled Depletion Attractions*, Phys. Rev. Lett. **99**, 268301 (2007).

[22] M. T. Elsesser, A. D. Hollingsworth, K. V. Edmond, and D. J. Pine, *Large Core-Shell Poly(methyl methacrylate) Colloidal Clusters: Synthesis, Characterization, and Tracking*, Langmuir **27**, 917 (2011).

[23] A. F. Routh and W. B. Russel, *Deformation mechanisms during latex film formation: Experimental evidences*, Ind. Engg. Chem. Res. **40**, 4302 (2001).

[24] A. F. Routh and W. B. Zimmerman, *Distribution of particles during solvent evaporation from films*,

Chem. Engg. Sci. **59**, 2961 (2004).

[25] F. Dobler, T. Pith, M. Lambla, and Y. Holl, *Coalescence Mechanisms of Polymer Colloids*, Colloid Poly. Sci. **270**, 806 (1992).

[26] Y. Chevalier, C. Pichotl, J. Maquet, P. Lindner, and B. Cabane, *Film formation with latex particles*, Colloid Poly. Sci. **270**, 806 (1992).

[27] J. L. Keddie, R. A. L. Jones, and R. A. Cory, *Interface and surface effects on the glass-transition temperature in thin polymer films*, Faraday Discuss. **98**, 219 (1994).

[28] J. A. Forrest, K. Dalnoki-Veress, J. R. Stevens, and J. R. Dutcher, *Effect of free surfaces on the glass transition temperature of thin polymer films*, Phys. Rev. Lett. **77**, 4108 (1996).

[29] Z. Yang, Y. Fujii, F. K. Lee, C.-H. Lam, and K. C. Tsui, *Glass transition dynamics and surface layer mobility in unentangled polystyrene films*, Sceince **328**, 1676 (2010).

[30] S. Mazur, R. Beckerbauer, and J. Buckholz, *Particle size limits for sintering polymer colloids without viscous flow*, Langmuir **13**, 4287 (1997).

[31] B. Gates, S. H. Park, and Y. N. Xia, *Tuning the photonic bandgap properties of crystalline arrays of polystyrene beads by annealing at elevated temperatures*, Adva. Mat. **12**, 653 (2000).

[32] H. Miguez, F. Meseguer, C. Lopez, A. Blanco, J. S. Moya, J. Requena, A. Mifsud, and V. Fornes, *Control of the photonic crystal properties of fcc-packed submicrometer SiO2 spheres by sintering*, Adva. Mat. **10**, 480 (1998).

[33] G. Bosma, C. Pathmamanoharan, E. H. A. de Hoog, W. K. Kegel, A. van Blaaderen, and H. N. W. Lekkerkerker, *Preparation of monodisperse, fluorescent pmma-latex colloids by dispersion polymerization*, J. Colloid Interf. Sci. **245**, 292 (2002).

[34] A. Yethiraj and A. van Blaaderen, *A colloidal model system with an interaction tunable from hard sphere to soft and dipolar*, Nature **421**, 513 (2003).

5

Epitaxial growth of 3D colloidal structures in electric fields

Dielectrophoresis is the translational motion that polarizable objects exhibit as a result of their interaction with nonuniform electric fields. In systems where particles have a higher dielectric constant than the suspending medium, these particles experience a net force directing them towards the higher field region, and they are said to experience positive dielectrophoresis. Here, we exploited positive dielectrophoresis to achieve precise positional control of colloidal particles on a patterned electrode. We demonstrate that strings of micron-sized colloidal particles can be positioned with micrometer-scale precision by a combination of AC electric fields and patterned electrodes. Additionally, our preliminary results shows that the spacing between the strings of particles can be varied by changing the ionic strength of the dispersion and the particle size.

5.1 Introduction

The precise positioning of colloidal particles in two- and three-dimensional structures has attracted a great deal of attention for potential applications, such as optoelectronic devices [1–4], catalysts for chemical and biological processes [1–4], photonic band gap materials [1–5], and bio-chip devices and sensors [6, 7]. Several methods have been successfully used to direct the assembly of colloidal particles onto patterned surfaces, including flow-induced packing into cavities of controlled dimensions and shape to create highly ordered particle arrays with precise cluster sizes, assembly at air-water interface [8], and adsorption on self-assembled mono layers (SAMs) with specific interaction chemistries [9, 10] via microcontact printing (μCP) [11, 12]. However, most of these methods are limited to two dimensions. A combination of a structured electrode and electric or magnetic dipoles can be used to achieve precise control over the position of particles in 3D.

In an electric field colloidal particles, with a dielectric constant different from the surrounding medium, acquire an induced dipole moment. A suspension of particles, for which the inter-particle interactions are comprised of a long-range screened Coulombic interaction and an induced dipolar interaction, shows especially rich phase behavior [13–15]. The dispersion structure can be tuned to form strings (1D) [16, 17], which assemble into sheets (2D) [18], which eventually form equilibrium 3D crystallites [13, 19], by varying the dipolar field strength and the particle concentration. Which of these structures forms, depends on the electric field strength, the time (as some of the observed structures are metastable), and the particle concentration [13–15, 19]. Via these parameters there is control over the type of structures formed, but not over their orientation and placement. By using a structured wall with the symmetry and orientation of a desired crystal plane, crystallization in 3D can be manipulated in ways that are similar to epitaxial crystal growth [5, 20, 21]. This includes the growth of crystals that are out of equilibrium [5, 20, 21]. The use of a structured wall in the presence of external electric or magnetic interactions could induce the lateral positioning of strings of dipoles that form under the influence of the induced dipolar interaction between particles and surface features.

Manipulating the lateral position of colloidal particles in order to arrange particles in the solution above a pattern has been done for magnetic particles. Using polymer-on-polymer stamping Lyles *et al.* [22] made templates with micrometer precision. The magnetic particles were nicely localized on the pattern. The number of particles at each site of the template was, however, not fixed, i.e., in some cases several particles clustered together on one site of the template. Electro-hydrodynamic flows around particles close to an electrode surface have been used to induce crystallization caused by field induced attractions between the particles [23, 24]. Later this approach was extended by using light induced patterns of higher and lower conductivity on semiconductor electrodes, which al-

lowed for more control over where crystallization takes place [19]. However, this method is limited to only several crystal layers in the direction perpendicular to the electrode and also does not allow for control over the lattice spacing.

In this chapter, we describe experiments in which we control the position of micron-sized colloidal particles on patterned electrodes. By using a parallel plate capacitor of which one electrode contained a regular surface pattern we create a non-uniform electric field close to the electrode surface. Varying the electric field strength together with the ionic strength, controls the spacing of the strings of dipoles that form along the field lines, while the pattern on the electrodes influences the position perpendicular to the field lines. The frequency of the electric field is chosen to be high enough (1 MHz) that the ions in the double layer cannot follow the field thus limiting the dipolar interactions to the polarizability of the particles in the solvent. This chapter is organized as follows. Experimental details are listed in Section 5.2, followed by a discussion on fabrication of patterned templates in Section 5.2.2. Next, we show our first results on structure formation of colloidal PMMA particles in AC electric fields in Section 5.3. Finally, we give conclusions and an outlook on future work in Section 5.4.

5.1.1 Theory of dielectrophoresis

Dielectrophoresis is the motion of particles caused by electrical polarization effects in inhomogeneous electric fields. Particles whose dielectric constant (ϵ_p) is different from that of the solvent (ϵ_m), acquire a dipole moment parallel to an external electric field. Due to induced dipolar interactions the particles form strings along the applied field direction. There is no preference for the lateral position of the strings. The behavior is different in an inhomogeneous field. When there is a field gradient, colloidal particles experience a dielectrophoretic force $\mathbf{F}_{dep}$.

$$\mathbf{F}_{dep} = -\frac{1}{2}\nu_p \epsilon_{eff} \epsilon_\circ \nabla \mathbf{E}^2(r) \tag{5.1}$$

where $\epsilon_\circ$ is the permittivity of vacuum, ν_p is the volume of the particle, E is the local field strength, and ϵ_{eff} is the effective dielectric constant of the particle in the suspension. The effective particle dielectric constant is a function of the complex frequency-dependent dielectric constants of the particle and the solvent. Moreover, it is also depends on the overall particle concentration, because the induced dipole moments of surrounding particles alter the local field strength around a particle. At low particle concentrations and low field strengths, the effective dielectric constant can be expressed by the Claussius-Mossotti equation, $\epsilon_{eff} = 3\alpha\epsilon_m$. For the field frequencies used here, α is given by:

$$\alpha = \frac{(\epsilon_p - \epsilon_m)}{(\epsilon_p + 2\epsilon_m)} \tag{5.2}$$

where α is the real part of the Claussius-Mossotti factor.

Particles with a dielectric constant (ϵ_p) higher than that of the medium ($\epsilon_p > \epsilon_m$, 'positive' dielectrophoresis) are attracted towards the higher field strengths, whereas less polarizable particles ($\epsilon_p < \epsilon_m$, 'negative' dielectrophoresis) repelled from the areas with a higher electric fields.

5.2 Experimental details

5.2.1 Particle synthesis and suspensions

Polymethylmethacrylate (PMMA) particles were synthesized by dispersion polymerization [25]. The particles were covalently labelled with the fluorescent dye 7-nitrobenzo-2-oxa-1,3-diazol (NBD) and sterically stabilized with poly(12- hydroxystearic acid), which was grafted on to a PMMA backbone forming a comb-graft steric stabilizer [25]. After the synthesis, particles were washed several times with hexane to remove the smaller particles and un-reacted species. We used suspensions of 3.55 μm and 2.35 μm diameter PMMA spheres ($\epsilon_p \approx 2.6$ [26]) in *cis*-decahydronaphtalene (*cis*-decalin, $\epsilon_m \approx 2.17$ [27]) at volume fractions of $\phi = 0.01$ respectively. The particle size and polydispersity (4 %) were determined by static light scattering (SLS). Because our particles are positively charged [13], they tend to stick to the glass walls of the sample cell. Before using the cell we therefore coated the cell with the poly(12-hydroxystearicacid), (PHS)-PMMA comb-graft stabilizer, then allowed the stabilizer to adsorb to the walls, and let it dry. We flushed a 0.7 % by weight of (PHS)-PMMA comb-graft stabilizer in a mixture of ethyl acetate and butyl acetate (2:1 weight ratio) solution through the cell. After filling the cell with the colloidal suspension, we sealed it at both ends with UV-curing optical adhesive (Norland no.68), and studied particle dynamics by means of confocal laser scanning microscopy (Leica TCS SP2). We imaged the template (color coded, red) and the particles (color coded, green) in separate channels by using laser light with a wave length of λ = 543 nm, and 488 nm respectively.

5.2.2 Fabrication of patterned electrodes

Our fabrication process consists of three steps: (i) writing a polymethylmethacrylate (PMMA) master template by electron beam lithography, (ii) making a soft-lithography mold from the master template, and (iii) replicating the original master pattern using the soft-lithography mold.

Master patterns were prepared by electron beam lithography using PMMA coated indium tin oxide coated glass slides. First, the ITO slides (30-60 Ω/sq in, Diamond coatings limited, UK) were cleaned by sonication in an aceton bath for 5-10 minutes, after which they were rinsed with isopropyl alcohol. Then they were blown dry with nitrogen and subsequently dried in the oven for 10 min-

utes at 180 °C. The substrates were dried again at 180 °C for 1.5 min and a 550 nm thick PMMA-layer was deposited by spincoating a 4-8 % w/w solution of 950k PMMA in anisole at 3200 rpm for 40 seconds. The thickness of the coating was not precisely known, but on the order of 400-500 nm. After spincoating, the PMMA was baked at 180°C for 1 hour. The patterns were written in the PMMA-layer using an electron beam lithography system (Raith e-LiNE). Doses of 100, 200 and 400 $\mu C/cm^2$ were used, of which the 200 $\mu C/cm^2$ dose resulted in patterns with the intended dimensions as shown in Figure 5.1. After electron beam writing the PMMA-coated templates were immersed in a 1:3 mixture of methyl isobutyl ketone and isopropanol for about 1-2 minutes. The dissolution reaction was stopped by rapidly transferring the substrate to pure isopropanol.

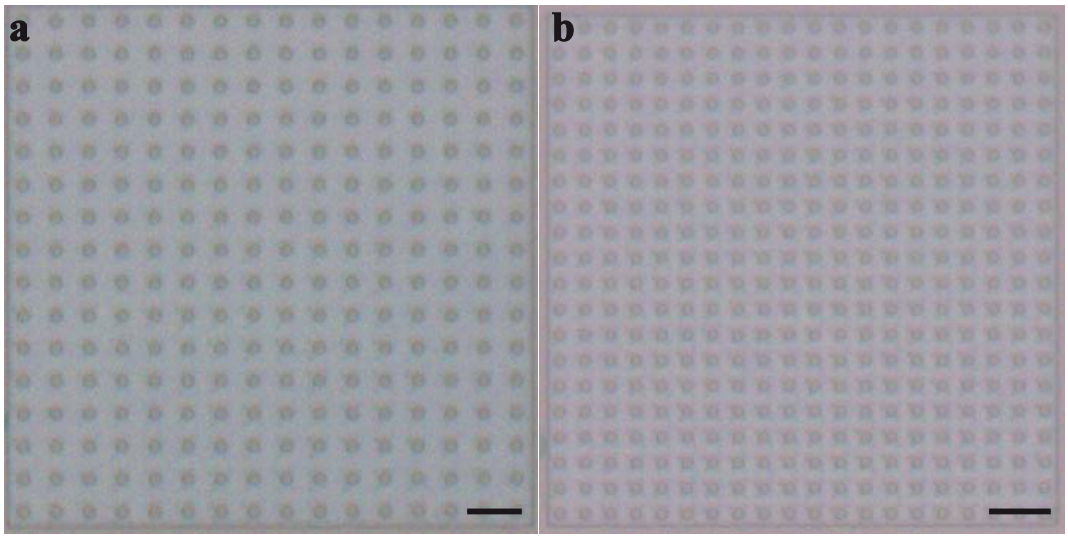

Figure 5.1: Optical micrographs of PMMA-patterned substrates. Patterns were written directly in the PMMA-layer using an electron-beam pattern generator. **a**, PMMA pattern with a lattice spacing of 4.05 μm. The width and height of the pillars are about 1.90 μm and 500 nm respectively. **b**, A template with a lattice spacing of 3.10 μm, width of 2.05 μm and height of 500 nm. Scale bars are 10 μm.

Soft lithography [28] was used to transfer the pattern of the master template to a new ITO coated cover slide in two steps. First the negative of the pattern was stamped into a soft mold. Second, the soft mold was transferred to the final material, leaving a copy of the original pattern. Soft molds were made from poly(dimethyl siloxane) (PDMS). The PDMS precursor and curing agent (Dow Corning Sylgard 184) were mixed in a 10:1 weight ratio, after which bubbles were removed by short centrifugation (10 seconds at 2000 rpm). A drop of the PDMS precursor mixture was placed on the pattern and left to cure at room temperature for about 2-3 days. The PDMS was then peeled from the template and post-cured in an oven at 100 °C for about 1 hour.

The final template was created by pressing the PDMS-mold firmly in a small drop of UV glue (Norland Optical Adhesive 68) on an ITO coated glass cover

slide (Menzel no. 1). The glue was then exposed to long wavelength UV light (~ 350 nm) through the mold for at least 2-3 hrs to cure. After 2-3 hrs, the PDMS-mold was carefully removed. The dimensions of the resulting templates are seen in Figure 5.2.

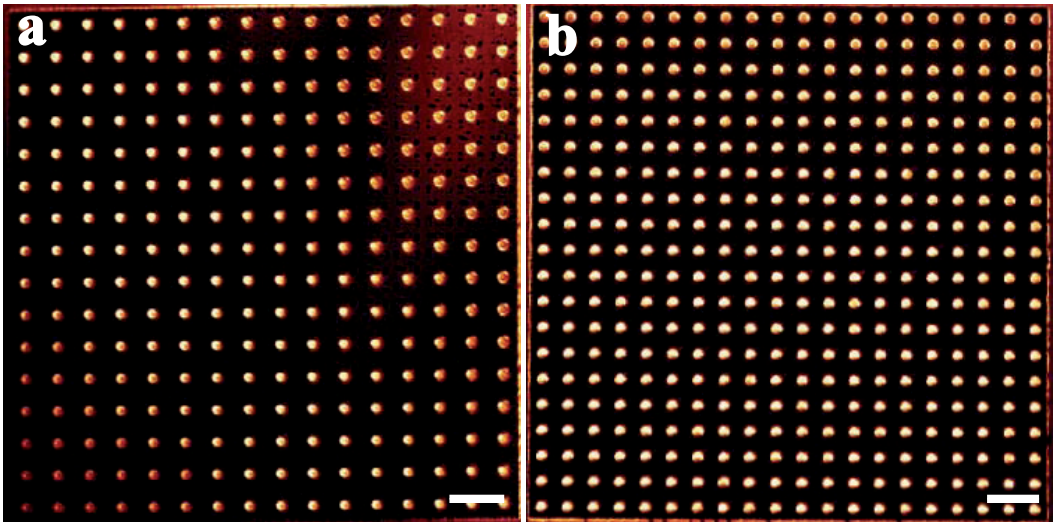

Figure 5.2: Confocal micrographs show the square arrangement of pillars of UV glue (Norland Optical Adhesive 68) on ITO coated cover slide made via soft-lithography. **a**, UV template with a lattice spacing of 4.05 μm and height of about 500 nm. **b**, A template with a lattice spacing of 3.10 μm and height of about 500 nm. Scale bars are 10 μm.

5.2.3 Electric-field setup

Templates made on ITO coated glass cover slips were now ready for making the electric field cell. Sandwich ITO coated glass cells were constructed by gluing the bottom patterned electrode (patterned side up) onto a glass microscopy slide. Two 80 - 120 μm thick spacers were placed on top of the of the electrode such that the area of pattern was in between the spacers. The top electrode was then placed on top of the spacers (conducting side down) and glued with no. 71 UV-curing optical adhesive (Norland) in a way that left an opening on two sides of the sample cell. Typically, the height of the sample space, enclosed by the cover slips, was 150 - 200 μm, with an area of ~ 1 cm^2. The conductive ITO layer of the top electrode was in contact with the suspension, whereas ITO layer of the bottom electrode was also in contact but with a glue layer on top it as shown in Figure 5.3. The sample cell was filled by placing a drop of colloidal suspension on one of the open ends. For the electrical contacts with the ITO electrodes we used silver paint (Jeol) and thin thermocouple alloy wire (diameter 50 μm, Goodfellow), which was then wrapped around standard electronic wire. We used a function generator (Agilent, Model 3312 OA) and a wide band voltage amplifier (Krohn-Hite, Model 7602M) to generate the electric fields. The field strength and the frequency were

measured with an oscilloscope (Tektronix, Model TDS3052).

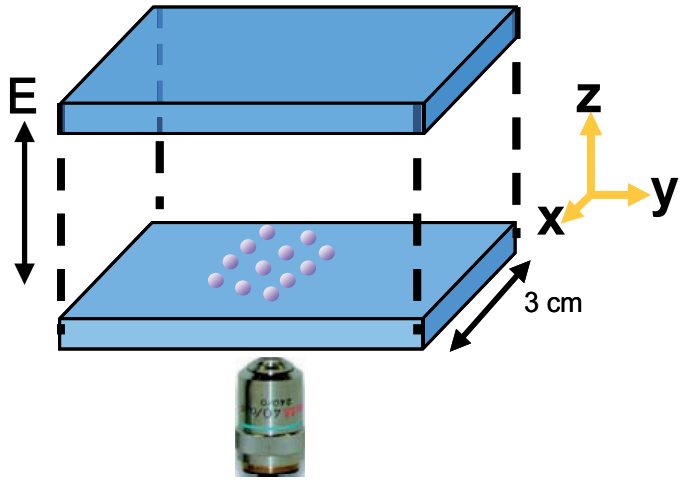

Figure 5.3: Schematic representation of the electric cell. The conducting sides were kept in contact with the suspension.

5.3 Results and discussion

5.3.1 Directing the strings of dipolar particles on a patterned template

Our suspensions consisted of 3.55 μm sized PMMA particles in *cis*-decalin. We used a high frequency (1 MHz) electric field to minimize the polarization of the electric double layer around particles. Before the 3.55 μm sized PMMA particles had sedimented onto the bottom in the *cis*-decalin the electric field was ramped up to $E_{rms} = 0.40$ Vμm^{-1}. The bottom electrode contained a regular pattern of pillars (Figure 5.2a) of UV-curing optical adhesive positioned 4.03 μm apart. Therefore, the electric field strength is higher at places where close to pillars are present. The induced dipole moment in each particle favored the assembly of the particles into strings of one particle thick, aligned in the field direction in a head-to-tail arrangement. PMMA has a higher dielectric constant ($\epsilon_p \approx 2.6$ [26]) than the medium (*cis*-decalin, $\epsilon_m \approx 2.17$ [27]); in a nonuniform electric field the positive dielectric force therefore pushes the particles towards the pillars of the template. As expected the strings of particles formed right on top of the pillars making up square template as shown in Figure 5.4a. Note that the positions of particles outside the template are irregular as seen in Figure 5.4a. Confocal image (Figure 5.4b) and rendered particle coordinates (Figure 5.4c) show the 3-4 particles long strings on the template in *xz* plane.

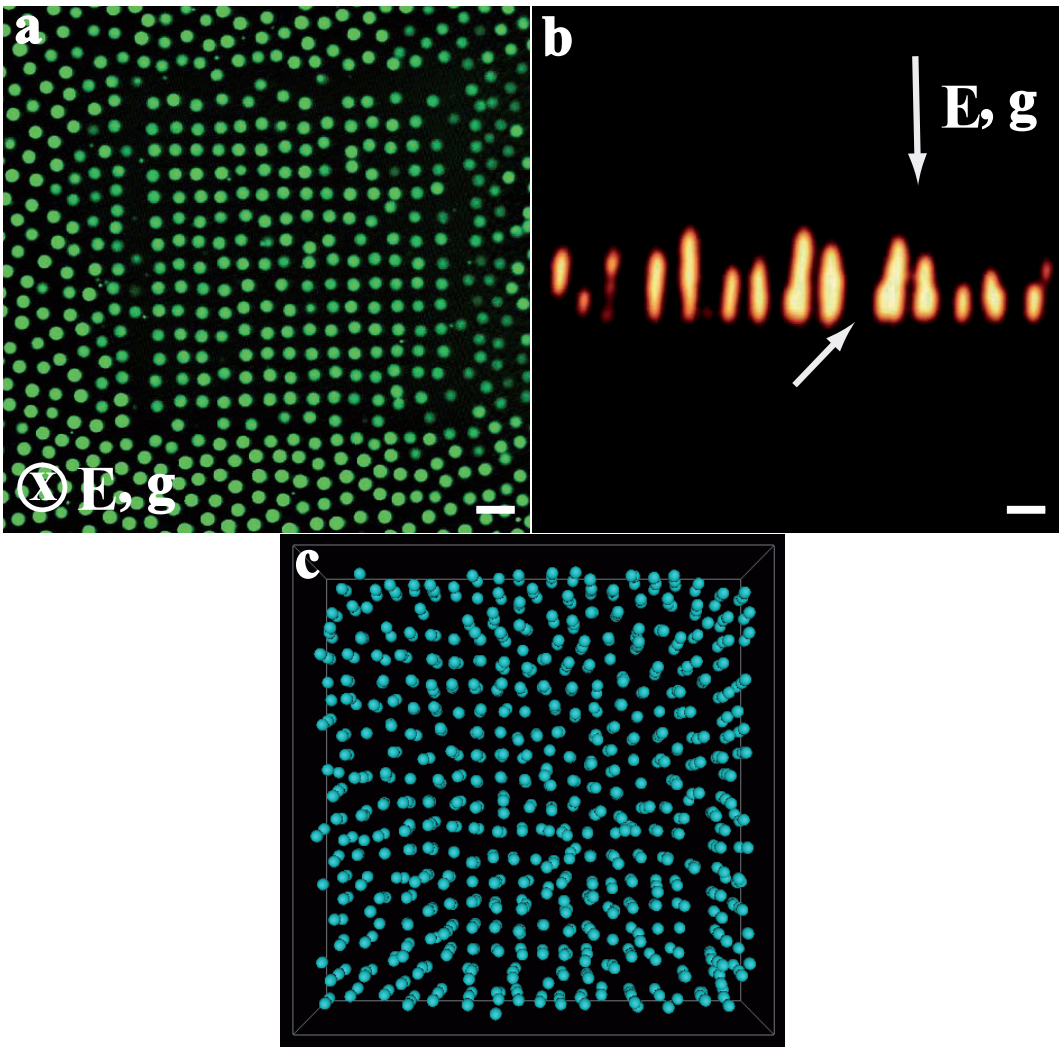

Figure 5.4: Confocal micrographs of 3.55 μm diameter PMMA particles in *cis*-decalin at a volume fraction $\phi = 0.01$. Due to induced dipolar attractions between the particles, strings formed in an AC field ($E_{rms} = 0.40\ V\mu m^{-1}$). The bottom electrode contained a template of 16 × 16 pillars which are 4.03 μm (Figure 5.2a) apart. **a**, *xy*-confocal microscopy image shows the first layer of the particles on the template. **b**, Strings of the particles on the template in *xz* plane. The arrow points at the only site in this plane on top of which no string formed. **a-b**, The direction of the applied electric field and the direction of gravity are indicated by an arrow in the lower-left corner, and upper-right corner respectively. **c**, Rendered particle coordinates revealing that the strings of particles spanned over 3-4 layers on the template. Scale bars are 10 μm.

We demonstrated that we are able to exploit the positive dielectrophoresis effect to achieve precise positioning of the particles with micrometer-scale precision using a patterned electrode. When the field was turned off, the particles started to diffuse away from the pillars of the template. The size of particles (3.55 μm) was greater than the size of pillars (≈ 1.90 μm). We let the particles to diffuse, driven solely by the thermal energy (k_BT), for about 15-20 mins. Figure 5.5b clearly

shows that the particles randomly ordered on the template. When the field was turned on (E_{rms} = 0.40 Vμm^{-1}), the particles (color coded, green) immediately (3-5 secs) migrated onto the pillars (color coded, red) of the template as seen in Figure 5.5c. Although more than one particle clustered at some places of the template, it clearly demonstrates that the position of the particles can be controlled with sub-micrometer-scale precision. Next, we switched off the field for 5 secs, after which the field was turned on again. We repeated this procedure 5-6 times. The particles occupancy and ordering increased by comparing Figure 5.5c & d.

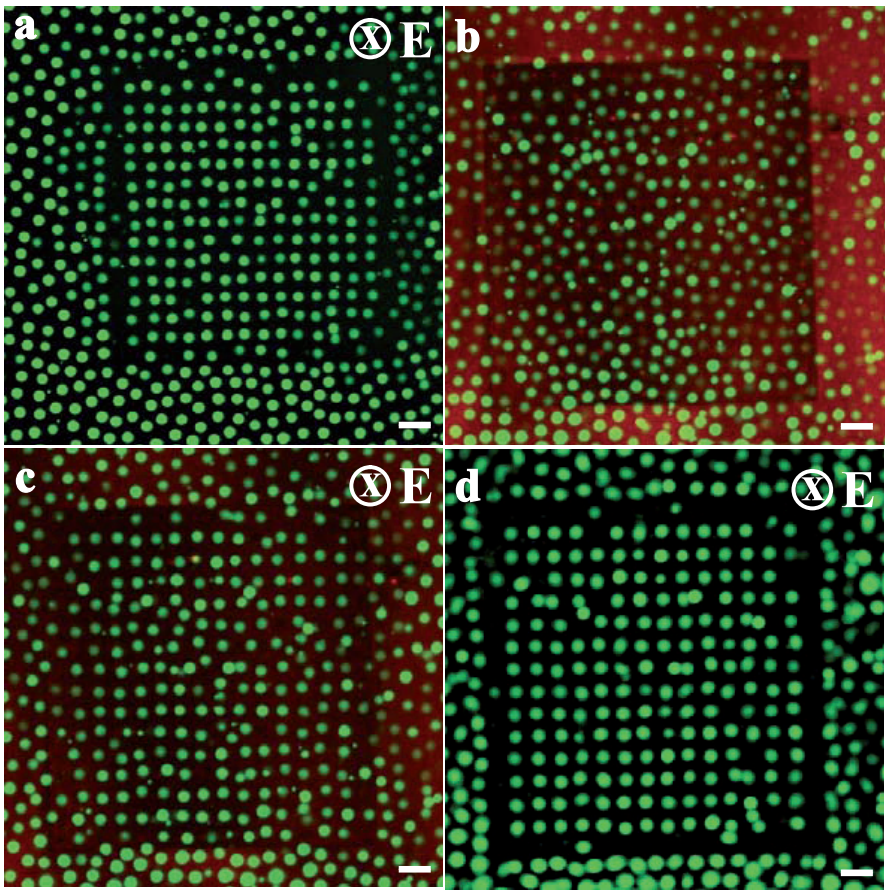

Figure 5.5: Confocal *xy* micrographs of 3.55 μm diameter PMMA particles in *cis*-decalin at a volume fraction $\phi = 0.01$. **a**, The first layer of the particles on the template. **b**, After turning off the field, particles randomly dispersed on the template. **c**, At a field strength (E_{rms} = 0.40 Vμm^{-1}), particles were again positioned on the template. **d**, After repeating the procedures **b & c** 5-6 times. **a, b-d**, The direction of the applied electric field is indicated in the upper-right corner. Scale bars are 10 μm.

The lattice spacing between the pillars of the template, the size of the particle, and the electric double layer around the particle play an important role. For instance, the 3.55 μm sized particles perfectly sit (Figure 5.6a) on the pillars of template when the pillars are separated by a 4.03 μm distance, whereas the particles did not order (Figure 5.6b) on the template with a 3.07 μm lattice space.

By varying either the ionic strength or the particle size, the spacing (lattice space) between strings of particles can be controlled.

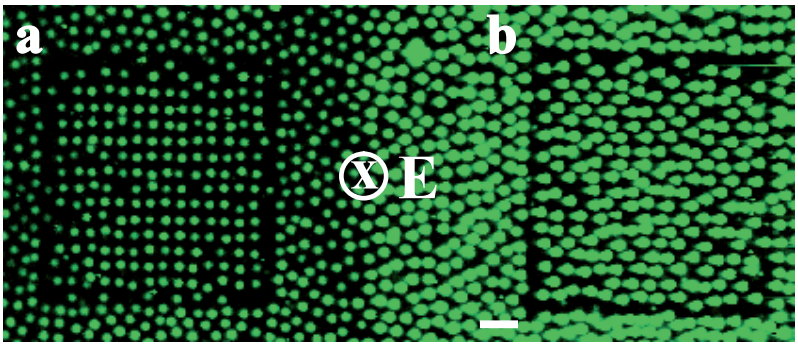

Figure 5.6: Confocal *xy* micrographs of 3.55 μm diameter PMMA particles in *cis*-decalin at a volume fraction $\phi = 0.01$. The first layer of the particles on the template with different lattice spacings (s) in an electric field ($E_{rms} = 0.40\ V\mu m^{-1}$). **a**, $s = 4.03$ μm. **b**, $s = 3.07$ μm. Due to a prolonged exposure to the laser light, the particles were bleached in the left hand side of the figure. The scale bar is 15 μm.

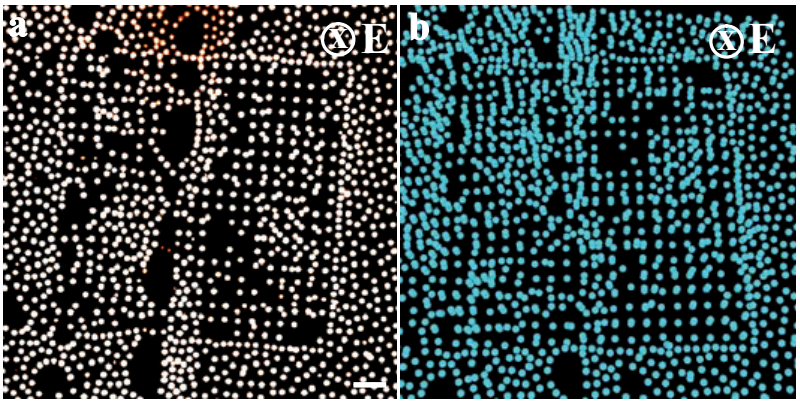

Figure 5.7: 2.35 μm diameter PMMA particles in *cis*-decalin at a volume fraction $\phi = 0.01$. **a**, Confocal *xy* micrograph shows the first layer of the particles on the template with a lattice spacing of $s = 3.07$ μm in an electric field ($E_{rms} = 0.60\ V\mu m^{-1}$). Note that the strings of particles positioned on the right side of the template only. **b**, Rendered particle coordinates revealing that the strings of particles spanned over 2-3 layers on the template. The scale bar is 15 μm.

Next, we chose the 2.35 μm sized particles, such that the particles would fit on a template with a lattice spacing of 3.07 μm. Upon application of an AC external electric field ($E_{rms} = 0.60\ V\mu m^{-1}$), the induced dipole moment in each particle led the particles to assemble into strings, aligned in the field direction in a head-to-tail arrangement. Due to the patterned bottom electrode, strings of particles were directed to the pillars. The way in which the particles were positioned on the template can be seen in Figure 5.7a. Note that the particles on left side of the template were not well ordered compared to the right side of the template. We suspect this effect might be a result from a possible contamination in caused

by transfer of the negative PDMS template to the UV glue by pressing the PDMS stamp on UV glue too hard.

5.4 Conclusions & outlook

In inhomogeneous electric fields, particles that are more polarizable than the medium, for instance, PMMA particles in *cis*-decalin, are pulled along the field gradient into areas of highest field intensity. This can be used to direct particles toward surface corrugations. We demonstrated precise micrometer-scale positional control of strings of PMMA particles with a combination of patterned electrodes and AC electric fields. Our preliminary results suggest that this method can be used to fabricate 3D structures with a desired lattice spacing by simply varying the ionic strength and the particle size. In this manner non-close packed assemblies can be achieved. Additionally, these structures could be made permanent by using our simple in-situ thermal annealing method as we described in the previous chapters.

We believe that this method can likely also be implemented to achieve precise positional control of significantly smaller particles by using the giant electrorheological effect [29]. By choosing a two-component colloidal system in which one particle type has a higher and another has a lower dielectric constant than that of the solvent, the strings of particles it may be possible to arranged alternatingly. Thus fabricating a crystal of less and more polarizable particles on the template by exploiting the positive and negative dielectrophoresis together.

Acknowledgements

I would like to thank Judith Wijnhoven for the preparation of the master template. Yu Ling Wu and Anke Kuijk are thanked for useful discussions.

References

[1] C. I. Aguirre, E. Reguera, and A. Stein, *Tunable colors in opals and inverse opal photonic cystals*, Adva. Fun. Mat. **20**, 1033 (2010).

[2] A. Stein, F. Li, and N. R. Denny, *Morphological control in colloidal crystal templating of inverse opals, hierarchical structures, and shaped particles*, Chem. Mat. **20**, 649 (2008).

[3] F. Li, D. P. Josephson, and A. Stein, *Colloidal assembly: The road from particles to colloidal molecules and crystals*, Angew. Chemie. **50**, 360 (2011).

[4] J. Galisteo-López, M. Ibisate, R. Sapienza, L. S. Froufe-Perez, and C. López, *Self-assembled photonic structures*, Adva. Mat. **23**, 30 (2011).

[5] A. vanBlaaderen, R. Ruel, and P. P. Wiltzius, *Template-directed colloidal crystallization*, Nature **385**, 321 (1997).

[6] O. D. Velev and E. W. Kaler, *In situ assembly of colloidal particles into miniaturized biosensors*, Langmuir **15**, 3693 (1999).

[7] H. Gau, S. Herminghaus, P. Lenz, and R. Lipowsky, *Liquid morphologies on structured surfaces: from microchannels to microchips*, Science **283**, 46 (1999).

[8] J. Liu, T. Lee, D. B. Janes, B. L. Walsh, M. R. Melloch, J. M. Woodall, R. Reifenberger, and R. P. Andres, *Guided self-assembly of Au nanocluster arrays electronically coupled to semiconductor device layers*, App. Phys. Lett. **77**, 373 (2000).

[9] J. Tien, A. Terfort, and G. M. Whitesides, *Microfabrication through electrostatic self-assembly*, Langmuir **13**, 5349 (1997).

[10] J. Aizenberg, P. V. Braun, and P. Wiltzius, *Patterned Colloidal deposition controlled by electrostatic and capillary forces*, Phys. Rev. Lett. **84**, 2997 (2000).

[11] B. D. Gates, Q. Xu, M. Stewart, D. Ryan, C. G. Willson, and G. M. Whitesides, *New approaches to nanofabrication: molding, printing, and other techniques*, Chem. Rev. **105**, 1171 (2005).

[12] H. Zheng, M. F. Rubner, and P. T. Hammond, *Particle assembly on patterned plus/minus polyelectrolyte surfaces via polymer-on-polymer stamping*, Langmuir **18**, 4505 (2002).

[13] A. Yethiraj and A. van Blaaderen, *A colloidal model system with an interaction tunable from hard sphere to soft and dipolar*, Nature **421**, 513 (2003).

[14] A. P. Hynninen and M. Dijkstra, *SPhase diagram of dipolar hard and soft spheres: Manipulation of colloidal crystal structures by an external field*, Phys. Rev. Lett. **94**, 138303 (2005).

[15] U. Dassanayake, S. Fraden, and A. van Blaaderen, *Structure of electrorheological fluids*, J. Chem. Phys. **112**, 3851 (2000).

[16] H. R. Vutukuri, A. F. Demirors, P. Bo, P. D. J. van Oostrum, A. Imhof, and A. van Blaaderen, submitted.

[17] K. D. Hermanson, S. O. Lumsdon, J. P. Williams, E. W. Kaler, and O. D. Velev, *Dielectrophoretic assembly of Electrically functional microwires from nanoparticle suspensions*, Science **294**, 1082 (2001).

[18] M. E. Leunissen, H. R. Vutukuri, and A. van Blaaderen, *Directing colloidal self-assembly with biaxial electric fields*, Adav. Mat. **21**, 3116 (2009).

[19] R. C. Hayward, D. A. Saville, and I. A. Aksay, *Electrophoretic assembly of colloidal crystals with optically tunable micropatterns*, Nature **404**, 56 (2000).

[20] J. P. Hoogenboom, A. Yethiraj, A. K. van Langen-Suurling, J. Romijn, and A. van Blaaderen, *Epitaxial crystal growth of charged colloids*, Phys. Rev. Lett. **89**, 256104 (2002).

[21] J. P. Hoogenboom, A. K. van Langen-Suurling, J. Romijn, and A. van Blaaderen, *Hard-sphere crystals with hcp and non-close-packed structure grown by colloidal epitaxy*, Phys. Rev. Lett. **90**, 138301 (2003).

[22] B. F. Lyles, S. T. Terrot, P. T. Hammond, and A. P. Gast, *Directed patterned adsorption of magnetic beads on polyelectrolyte multilayers on glass*, Langmuir **20**, 3028 (2004).

[23] M. Trau, D. A. Saville, and I. A. Aksay, *Field-induced layering of colloidal crystals*, Science **272**, 706 (1996).

[24] M. Baohmer, *In situ observation of 2-dimensional clustering during electrophoretic deposition*,

Langmuir **12**, 5747 (1996).

[25] G. Bosma, C. Pathmamanoharan, E. H. A. de Hoog, W. K. Kegel, A. van Blaaderen, and H. N. W. Lekkerkerker, *Preparation of monodisperse, fluorescent pmma-latex colloids by dispersion polymerization*, J. Colloid Interf. Sci. **245**, 292 (2002).

[26] Mikhailov. and Borisova., *Polymer Science*, USSR **2**, 387 (1961).

[27] P. Staudhammer and W. F. Seyer, *The dielectric constant of cis- and trans- decahydronaphtalene and cyclohexane as a function of temerature and frequency*, J. Ame. Chem. Soc. **80**, 6491 (1958).

[28] Y. Xia and G. M. Whitesides, *Soft lithography*, Annu. Rev. Mater. Sci. **28**, 153 (1998).

[29] W. J. Wen, X. X. Huang, S. H. Yang, K. Q. Lu, and P. Sheng, *The giant electrorheological effect in suspensions of nanoparticles*, Nature Materials **2**, 730 (2003).

6

Directed self-assembly of highly anisotropic gold platelets in an electric field

In this chapter, we investigated the response of gold platelets, which are about 1 μm wide and 16 nm thick, to an external AC field as a function of salt concentration. At moderate salt concentrations (0.8 - 2.0 mM), these platelets assembled into reversible worm-like columns due to the secondary minimum of the potential energy between two particles. The length of the columns and spacing between the platelets depended on the depth of the secondary minimum and also on the concentration. The particles in the columns were individually in Brownian motion, and the entire column also showed active Brownian motion. We found that the response of the gold platelets strongly depends on the ionic strength of suspension in an electric field, just as the phase behavior. In the absence of salt, the particles were aligned with their longest axis in the field direction in a head-to-tail arrangement. However, in the presence of enough salt the worm-like chains were aligned perpendicular to the applied field direction. Moreover, we obtained directed self-assembly of these columns into a 2D-columnar-like phase with an electric field.

6.1 Introduction

A variety of metallic particles with well-defined shapes have been synthesized via photochemical [1, 2], thermal [3], electrochemical [4], and template-directed methods [5, 6]. Chemical and physical properties of noble-metal nanostructures can be controlled not only by varying material composition, but also by tailoring their size and shape [2, 7, 8]. In recent years, self-assembly of nanoparticles has attracted a great deal of attention due to the potential applications in optics, electronics, and catalysis [7–9]. Self-assembly of these particles strongly depends on inter-particle interactions, particle-size distributions, and particle shape. However, in order to successfully exploit nanoparticle self-assembly in technological applications and to ensure efficient scale-up, a high-level of direction and control is required.

In the past few years there has been a remarkable increase in control over directed self-assembly [7, 8, 10, 11]. Directed assembly is a case where the self-assembly is directed by external forces such as a structured-template, external fields e.g., magnetic, electric, and even flow, but also the modification of inter-particle interactions such as with polymers or supra-molecular chemistry. For instance, DNA-controlled isotropic [12, 13] and also anisotropic [14] gold nanoparticle self-assembly was pioneered by Mirkin and his group using this supramolecular methodology. Subsequent studies were successful in fabricating ionic colloidal crystals of oppositely charged particles by tuning the range and strength of electrostatic interactions between the particles [10, 11]. Velev and co-workers fabricated microwires of micrometer diameter from a solution of gold spheres with diameters between 30-40 nm [15]. This assembly was based on strong dielectrophoresis and dipolar interactions between the particles and the strings caused by alternating electric fields. AC electric fields were also used to align much smaller gold nano-rods leading to the possibility of selectively exciting their longitudinal or transverse plasmon modes [16].

Here, we used an external electric field to direct the self-assembly of gold platelets. The platelets had a large aspect ratio with diameters in the micron size regime and thicknesses in the nano regime, in addition they were of a single crystalline nature. A key strength of external electric field directed assembly is the reversibility of the interactions, which leads to a rapid return to the disordered state when the field is removed, as long as the particles are sufficiently stabilized when the field is on to not aggregate in their primary minimum. Such effects are useful in obtaining reconfigurable and switchable assemblies, but could also be exploited to quickly anneal defects in structures by rapidly cycling the field on and off.

This chapter is organized as follows. Experimental details are listed in Section 6.2, followed by a discussion of the results in Section 6.4. In Section 6.4.2 we present a method for measuring the inter-platelet distance in the presence of salt. In Section 6.4.3 we compare the response of the particles with and without the

salt in an external AC field. Finally, we give conclusions and an outlook on future work in Section 6.5.

6.2 Experimental details

Particle synthesis and suspensions

We synthesized gold platelets by a modified procedure of Hachisu *et al*. [17]. An important disadvantage of the original method of Hachisu *et al*. [17] was that the dispersions suffered from a low yield (less than 10 % of particles, by number, are platelets in a typical synthesis), and a high degree of polydispersity both in size and shape as seen in Figure 6.1. We used silver platelets as seeds to overcome this limitation. Ag nano-platelets were synthesized in two steps by the method of Liz-Marzán *et al*. [18]. We first synthesized small Ag nano particles as follows. In a closed 200 ml glass vial, 1 mL of 0.3 mM trisodium citrate (Sigma) was added to 100 ml of 0.1 mM silver nitrate (99 %, Aldrich) solution. Next, 1 ml of 0.5 mM of sodium borohydrate (AldrichSigma) was added under gentle stirring, and immediately followed by the addition 1 ml of a 5 wt % polyvinylpyrrolidone (Fluka, 15K) solution. Stirring was gradually stopped when the solution had turned to yellow color. We used these Ag nano particles as seeds to synthesize silver nano platelets [18]. This step simply consists of placing the suspension of silver seeds in 40 ml glass vials at a distance of about 3-4 cm from the light source in a photo reactor. The temperature inside the reactor was maintained at 40 °C. After 24 hrs, silver plates resulted as shown in Figure 6.2. These particles were subsequently used as seeds for the gold platelets synthesis [18]. Platelets with a width of 1.0 μm and a thickness of ~16 nm were prepared as follows. In a room that is not bright, 500 μl Ag nano-platelets was added to the 25 ml of de-ionized water (18.2 MΩ-cm, Millipore). Next the suspension was mixed by shaking the vial for about 3-4 secs and followed by the addition of 5 ml of 10 mM an aqueous chloroauric acid, and 1.5 ml of filtered saturated salicylic acid solution. The solution was maintained in a thermostat water bath at 60 °C for 18 hr. After the synthesis, the particle suspension was washed several times with de-ionized water (18.2 MΩ-cm, Millipore) to remove smaller particles and also un-reacted species. Hexagonal and triangular shape particles thus synthesized were shown in Figure 6.3a. The gold platelets suspension to be stable with time, but the sample was kept in a dark place. The yield of the synthesis was about 70-80%. The surface potential of the particles was -38 mV measured by the zetasizer (Marven, Zetasizer).

The gold particles were dispersed in de-ionized water. All samples were confined to glass capillaries with inner dimensions (cross section) of 0.1 mm × 1.0 mm or 0.1 mm × 2.0 mm (Vitrocom). The capillaries were tailor-made for each experiment with a desired length. After filling the cell with the colloidal suspension, we sealed it with UV-curing optical adhesive (Norland no.68), and we studied particle dynamics by means of optical microscopy.

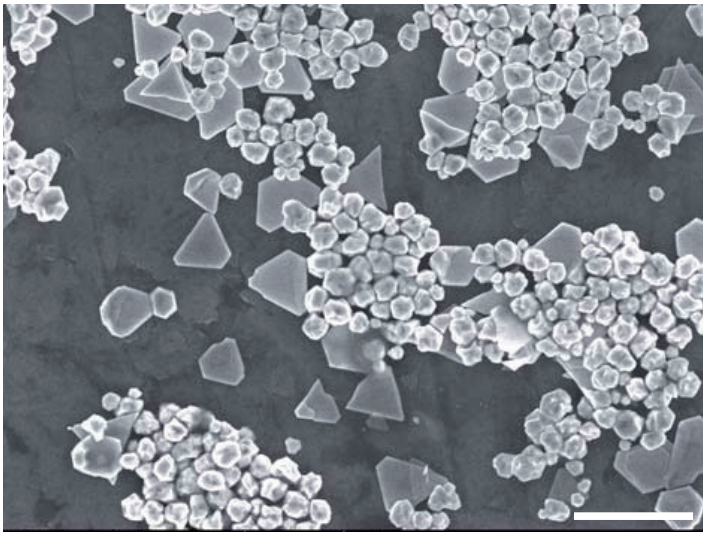

Figure 6.1: Thin gold platelets were synthesized by Hachisu *et al*. method. Scanning electron micrograph of typical synthesis. Scale bar is 2 μm.

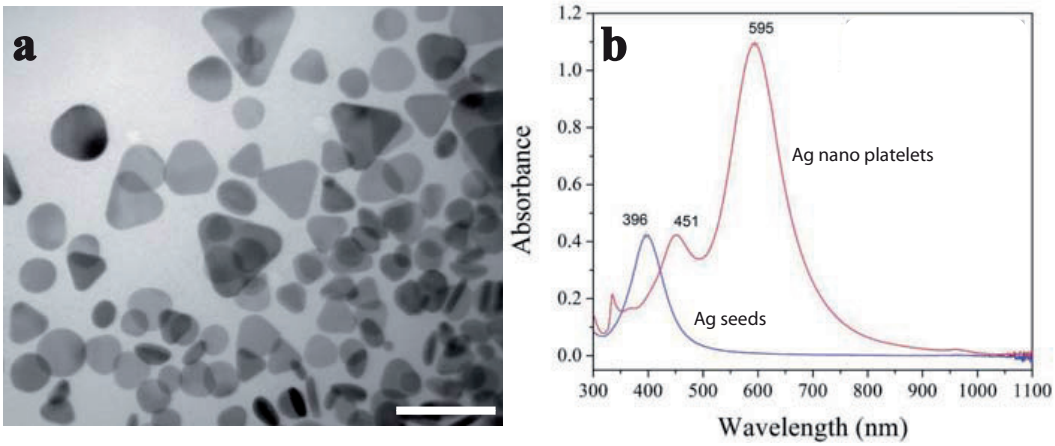

Figure 6.2: a, TEM image of Ag nano platelets were prepared by illumination of Ag seeds with the light bulbs. **b**, UV-vis-NIR spectra of dispersions of Ag seeds, and nano platelets in water, respectively. Scale bar is 100 nm.

Electric-field setup

We used different sizes of rectangular glass capillaries. The electric cell consisted of a 0.1 mm × 1.0 mm or 0.1 mm × 2.0 mm cross section capillary with two 50 μm thickness nickel-alloy wires (Goodfellow) threaded along the side walls. We used a function generator (Agilent, Model 3312 OA) and a wide band voltage amplifier (Krohn-Hite, Model 7602M) to generate the electric fields. The field strength and frequency were measured by an oscilloscope (Tektronix, Model TDS3052).

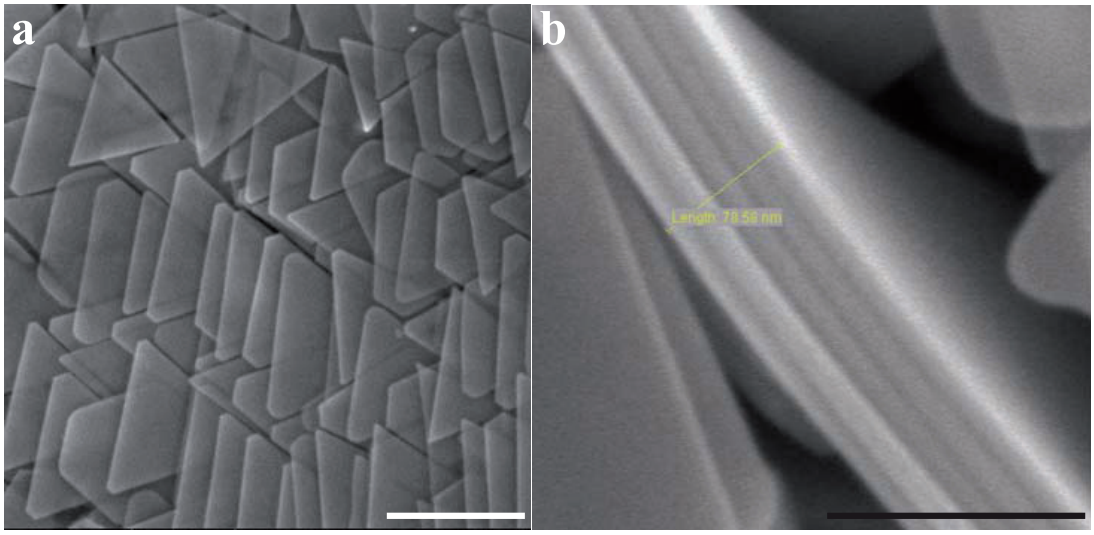

Figure 6.3: Thin gold platelets that are about 1 μm long and 16 nm thick. **a**, Scanning electron micrograph of such gold platelets. **b**, Scanning electron micrograph reveals that the total thickness of a stack of 5 platelets is 78.53 nm therefore thickness of a single gold platelet is about 16 nm. Scale bars are 1 μm, and 100 nm, respectively.

(cryo-) Focused ion beam - scanning electron microscopy

Prior to the measurement, we mixed the gold suspension with 30 wt % of glycerol. Glycerol was used to preventing crystallization of water and thus affecting colloidal structures. We plunged a sample which was prepared on a TEM grid in a pool of cryo-coolant (liquid nitrogen) thereby freezing the stacks. Subsequently, these stacks were transferred to the SEM chamber which was maintained at cryo-temperatures. The transfer from the bath of cryo-coolant to the cryo-preparation chamber and from the cryo-preparation chamber to the SEM chamber was performed by a cryo-shuttle. We used a combination of focused ion beam (FIB, Nova Nanolab 600, FEI, Netherlands) and cryo-SEM (XL FEG 30, Philips) for 3D sectioning and imaging of the worm-like columns. Sectioning conditions used were 30 kV, and 0.3 nA.

6.3 Particle interactions

The stability of many charge stabilized colloidal dispersions can be described in terms of a screened electrostatic repulsive potential and an attractive van der Waals potential between the particles using the DLVO (Deryaguin-Landau-Verwey-Overbeek) theory [19–21]. For semi-infinite plates of area S, separated by a distance d, and assumed to be at constant surface potential $\psi_\circ$; the repulsive potential can be approximated as

$$\frac{V_R}{S} = \frac{64\pi n k_B T}{\kappa}\gamma^2 \exp(-\kappa d) \tag{6.1}$$

where

$$\gamma = \frac{\exp(\frac{e\psi_0}{2k_B T}) - 1}{\exp(\frac{e\psi_0}{2k_B T}) + 1} \tag{6.2}$$

where d is the distance between the platelets, n is the ion concentration, k_B is Boltzman's constant, T the absolute temperature, e is the elementary charge, and κ is the inverse Debye screening length. The Debye screening length κ^{-1} is a measure for the range of electrostatic repulsion that depends on the ion concentration (assumed to be monovalent), n, according to

$$\kappa^{-1} = n^{-\frac{1}{2}} \left(\frac{e^2}{\varepsilon \varepsilon_0 k_B T} \right)^{-\frac{1}{2}} \tag{6.3}$$

The van der Waals attractive potential between two half spaces is given by

$$\frac{V_A}{S} = -\frac{H_{eff}(d)}{12\pi\ d^2} \tag{6.4}$$

where the Hamaker function H_{eff} is estimated by the Lifshitz theory.

$$H_{eff} = -\frac{3}{2} k_B T \sum_{n=0}^{\infty}{}' \int_{r_n}^{\infty} x \{\ln[1 - \Delta_{pm}^2 e^{-x}] + \ln[1 - \bar{\Delta}_{pm}^2 e^{-x}]\} dx \tag{6.5}$$

where $\Delta_{jk} = \left(\epsilon_j S_k - \epsilon_k S_j\right) / \left(\epsilon_j S_k + \epsilon_k S_j\right)$, $\bar{\Delta}_{jk} = \left(S_k - S_j\right) / \left(S_k + S_j\right)$, p, m denotes the particle and medium respectively, $S_k^2 = x^2 + \left(2\xi_n d c^{-1}\right)^2 (\epsilon_k - \epsilon_m)$, $r_n = (2d\xi_n \sqrt{\epsilon_m})/c$, $\xi_n = (2\pi n k_B T)/\hbar$, $\epsilon_k = \epsilon_k(i\xi_n)$, here $i = \sqrt{-1}$, h is Planck's constant, c is the speed of light in vacuum, and $\epsilon_k(\omega)$ is the dielectric constant of material k at frequency ω. The prime ($'$) next to the summation indicates that the first term (n = 0) is multiplied by (1/2) (1 + 2κd) exp(-2κd). The factor of 1/2 avoids double accounting while the remainder of this factor accounts for the screening of the zero frequency contribution. Note that the physical properties of the materials enter through the function $\epsilon_k(i\xi)$.
The total potential is sum of the screened electrostatic repulsive potential and the van der Waals attractions

$$V_{DLVO} = V_R + V_A \tag{6.6}$$

From these equations, the stability of the suspension can be determined.

6.4 Results and discussion

6.4.1 Phase behavior of the gold platelets as a function of salt concentration

In the absence of salt, the repulsion overwhelms the attraction at all separations, and the particles remain isotropically dispersed as shown in Figure 6.5a. These particles sediment quickly to the bottom due to their high density (19.3 g/cc). Moreover, no interaction between the particles was observed even when the particle concentration increased by sedimentation. Apparently, the effective aspect ratio of our samples was so much reduced by the electric double layer around the particle therefore we did not observe a nematic phase.

Here, we present the phase behavior of the gold particles as a function of salt concentration. The ionic strength of the suspension was varied by changing the salt (KCl) concentration. We calculated the interaction potential between two gold platelets in water as a function of the inter-platelet distance for different salt concentrations as shown in Figure 6.4. Figure 6.4 clearly shows that the potential energy has a secondary minimum at an inter-particle distances between 50 nm to 200 nm for $\geq$ 0.2 mM dispersions, whereas at lower salt concentrations this minimum is about -2 k_BT which is comparable to the thermal energy (see also the inset of the Figure 6.4).

At a salt concentration of 0.8 mM of KCl, the potential energy calculations showed these particles experience an attractive potential of about -6 k_BT at an inter particle distance around 130 nm. We believe that such an attractive potential is sufficient to lead the formation of worm-like columns. The following mechanism is proposed for the formation of the worm-like structures, when the Brownian motion causes the particles to approach each other they experience the minimum in the interaction potential and thus they form strings as shown in Figure 6.5b. The particles in the columns were individually in Brownian motion, and the columns themselves also showed active Brownian motion. Occasionally columns would break or reconnect and individual particles were also seen to attach and detach indicating that the system could still attain equilibrium. Furthermore, the structures formed in this way could hardly be separated into individual ones by the Brownian motion. These columns could however easily be dispersed into individual ones by sonication.

In the following we estimate the effects of gravity for particles orientated as in Figure 6.6a as compared to those oriented as in Figure 6.6b. The gravitational height of an individual particle is 0.025 μm. For a single particle, a competition can be expected to occur between joining the columns and lying flat on the surface. Here, we approximated the particles with a circle of 1.0 μm diameter and thickness of 16 nm. The difference in gravitational potential between a gold particle lying parallel to the bottom surface and one standing vertical is about 1.0 k_BT (Figure 6.6). On the other hand, the potential difference between an isolated par-

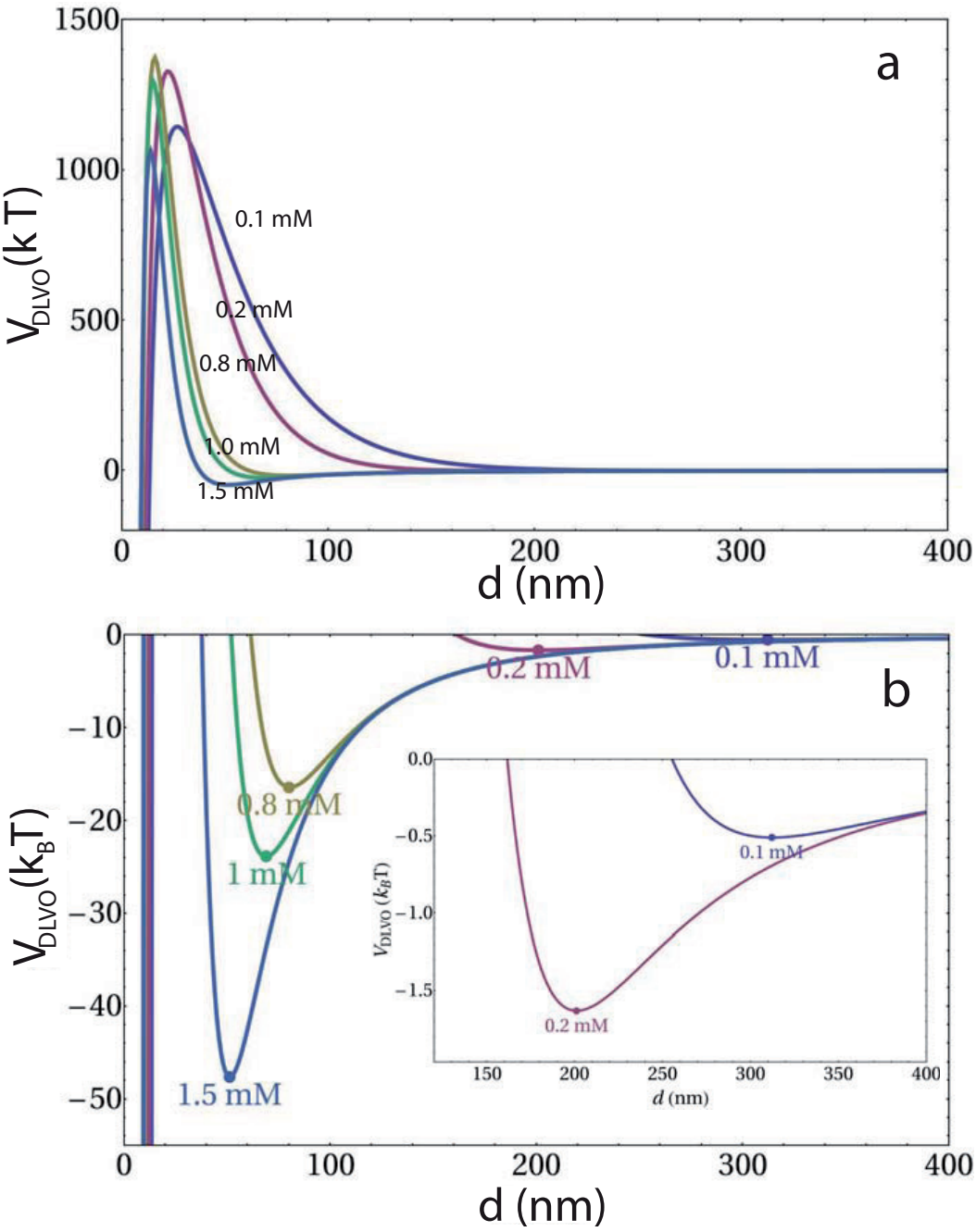

Figure 6.4: DLVO potential between two gold platelets. Interaction potentials were calculated as a function of the inter-platelet distance *d* for different salt concentrations. **a**, DLVO potential. **b**, The secondary minimum of the DLVO potential.

ticle which is lying by itself flat and one trapped in the secondary minimum of another is about -6 k_BT. Therefore, a gold particle joining the column is more stable than a single one lying on the bottom. When the salt concentration was

within the range of 0.80 mM to 2.0 mM, both ends of these columns continuously caught particles or small columns moving around them, thus growing into a longer columns as shown in Figure 6.5c-d. Additionally, making a columnar phase in this way is still limited due to the severe effects of gravity making it unlikely that the equilibrium columns would survive if many stacks of particles would be compressed by gravity. However, this limit was not yet investigated as the scale of the particle synthesis performed was kept low.

At higher salt concentrations ($\geq$ 2.0 mM), the particles aggregated irregularly (Figure 6.5e) and we did not observe Brownian motion of individual particles.

6.4.2 *Inter-platelet distance measurements*

Three things make it difficult to measure the inter platelet distance within a column by presently available microscopy techniques: (i) the small thickness of the particles (16 nm), (ii) active Brownian motion of the columns, and (iii) strong absorption of light by the platelets. To overcome these limitations, we used cryo electron microscopy technique in which we froze the solvent fast enough on the diffusion time scale of the particles that essentially the structures were a snapshot in time. The frozen samples were gradually sectioned with a focused ion beam, and subsequently imaged by cryo-SEM as shown in Figure 6.7a. Figure 6.7b shows that the inter-plate distance was about 64 nm in the 1.0 mM suspension, in good agreement with the calculated distance as shown in Figure 6.4.

6.4.3 *Directed self-assembly of nano gold platelets with an electric field*

Absence of salt

External electric fields have proven to be a robust tool to direct colloidal self-assembly into strings (1D) [15, 22], sheets (2D) [23], and equilibrium 3D crystallites [24, 25]. Here, we used a high frequency (1 MHz) field to prevent polarization of the double layer. For a thin gold platelet, the polarizability is different between the two directions. The energetically most favorable state is that of particles in strings with their major axis along the field. Our colloidal suspensions consisted of 0.1 % by weight of gold platelets in water. At low field strengths (E_{rms} = 0.05 Vμm^{-1}, f = 1 MHz, where E_{rms} is the root-mean-square electric field strength, and f is the frequency), the induced dipole moment in each particle led the platelets to assemble into one particle thick strings that were aligned with their largest length oriented in the field direction in a head-to-tail arrangement as seen in Figure 6.8. In absence of salt, the response of a very thin gold platelets is thus similar to spheres. The time scale for chain formation was on the order of a few seconds. However, alignment induced by the electric fields is reversible, so that the particles redisperse when ever the field is switched off. Note that the particles (Figure 6.1) were used in this experiment had been synthesized

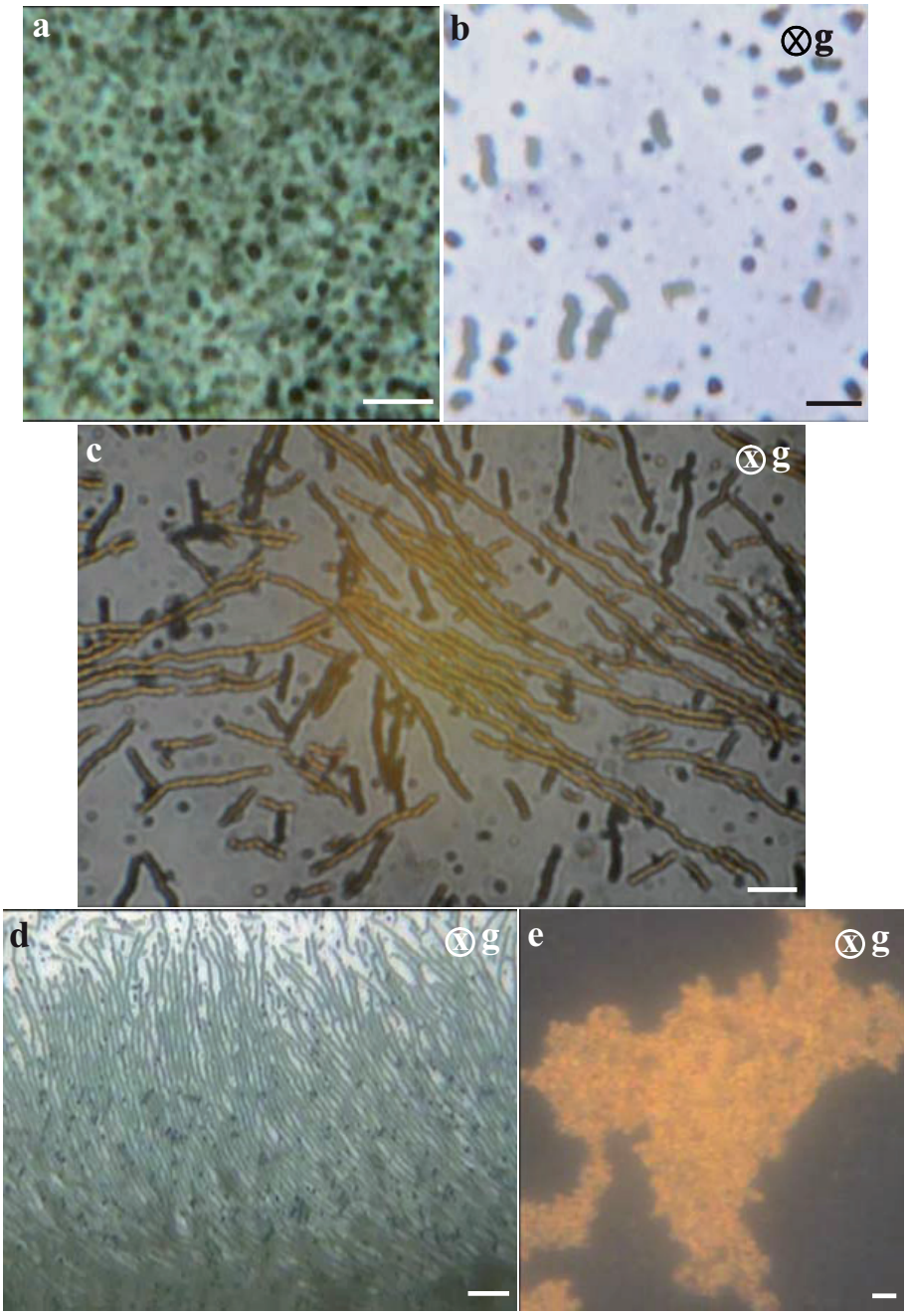

Figure 6.5: Optical micrographs showing the phase behavior of the gold platelets as a function of salt concentration. **a**, The particles isotropically dispersed in water at zero salt concentration. **b**, After 3 mins of waiting time at 0.8 mM of KCl. **c**, After 30 mins of waiting time at 0.8 mM of KCl. **d**, After 30 mins of waiting time at 1.5 mM of KCl. **e**, At higher salt concentrations $\geq$ 2.0 mM of KCl, particles aggregated irregularly and irreversibly. **b-e**, The direction of gravity is indicated in the upper-right corner. Scale bars are 15 μm.

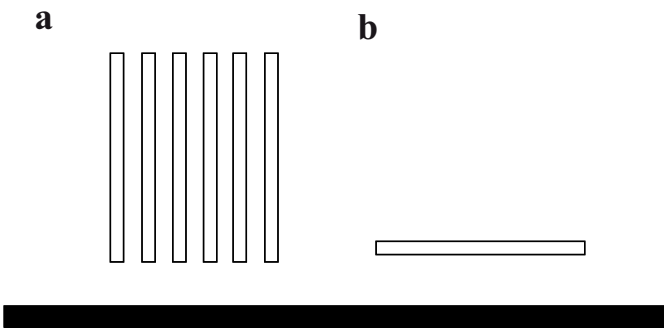

Figure 6.6: Illustration of interaction potential between the particles. State **a**, a gold particle interacts with an other one and joins the row. State **b**, a particle does not interact and lays down on the surface.

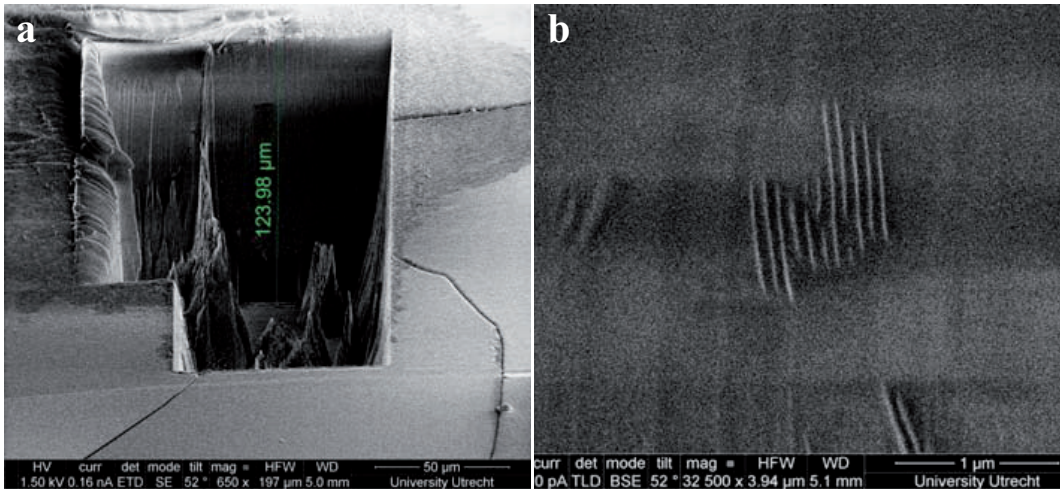

Figure 6.7: Cryo-scanning electron micrographs. **a**, A well-frozen sample was sectioned with a Focused Ion Beam and subsequently it was imaged with a cryo-SEM. **b**, A cross-sectional view of a stack of gold plates. The inter-platelet distance within a columns is uniform and is about 64 nm in 1.0 mM suspension.

by the original procedure of Hachisu *et al*. [17].

Presence of salt

Here, we investigated the response of gold platelets for two different salt concentrations (0.8 mM & 1.5 mM) in an AC electric field. As we discussed in Section 6.4.1, we observed short worm-like columns (Figure 6.5b) at a salt concentration of 0.8 mM. When such a dispersion was exposed to an external electric field (E_{rms} = 0.015 Vμm^{-1}, f = 200 KHz), these columns started to align perpendicular to the applied field direction. However, the major axis of individual particles within a column were still in the field direction. Figure 6.9a shows large columns of particles that formed within seconds after applying a relatively small field strength (E_{rms} = 0.015 Vμm^{-1}, f = 200 KHz). These structures are more dynamic than the

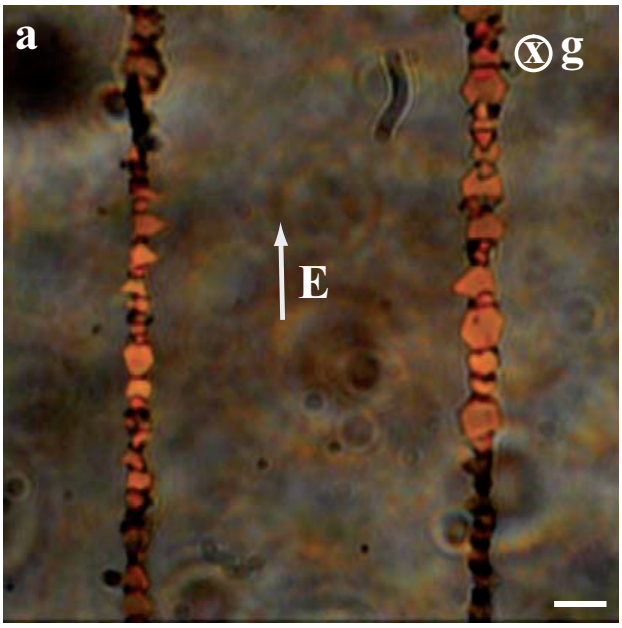

Figure 6.8: Gold platelets in an external electric field (E_{rms} = 0.05 Vμm^{-1}). Optical micrograph of strings of gold platelets in water. The particles became aligned with their longest axis along the field direction. The direction of the applied electric field and the direction of gravity are indicated in the figure. Scale bar is 2 μm.

columns in the absence of the field. This is indicated by new small columns continuously coming to join both ends, thereby forming longer columns. Moreover, induced dipolar attractions between columns forced them to arrange sidewise because the major axis of the individual particles in a column was in the field direction. Although we were not able to follow the alignment of particles between the columns on a single particle level, we believe that this arrangement is the most energetically favorable state.

When the salt concentration was increased to 1.5 mM, within about 1 - 1.5 hrs time, most of the dispersion transformed into long columns (Figure 6.5c). Even at very low field strength (E_{rms} = 0.015 Vμm^{-1}, f = 200 KHz), all these columns became aligned perpendicular to the field direction and then transformed into a defect-rich 2D columnar phase. A few minutes later, all the defects annealed out by further merging the columns together. These columns then transformed into a well ordered structures (2D columnar phase) as shown in 6.9b. We exploit this opportunity to characterize the optical properties of the platelets as a function of their orientation.

In this section, we demonstrate on how stacks of columns can be used as a light filter with a combination of polarized optical microscopy and an external electric field. In order to interpret the polarized light micrographs one has to realize the following. When light passes through an ordered phase in crossed polarized microscopy, the orientation of the director is not parallel to one of the

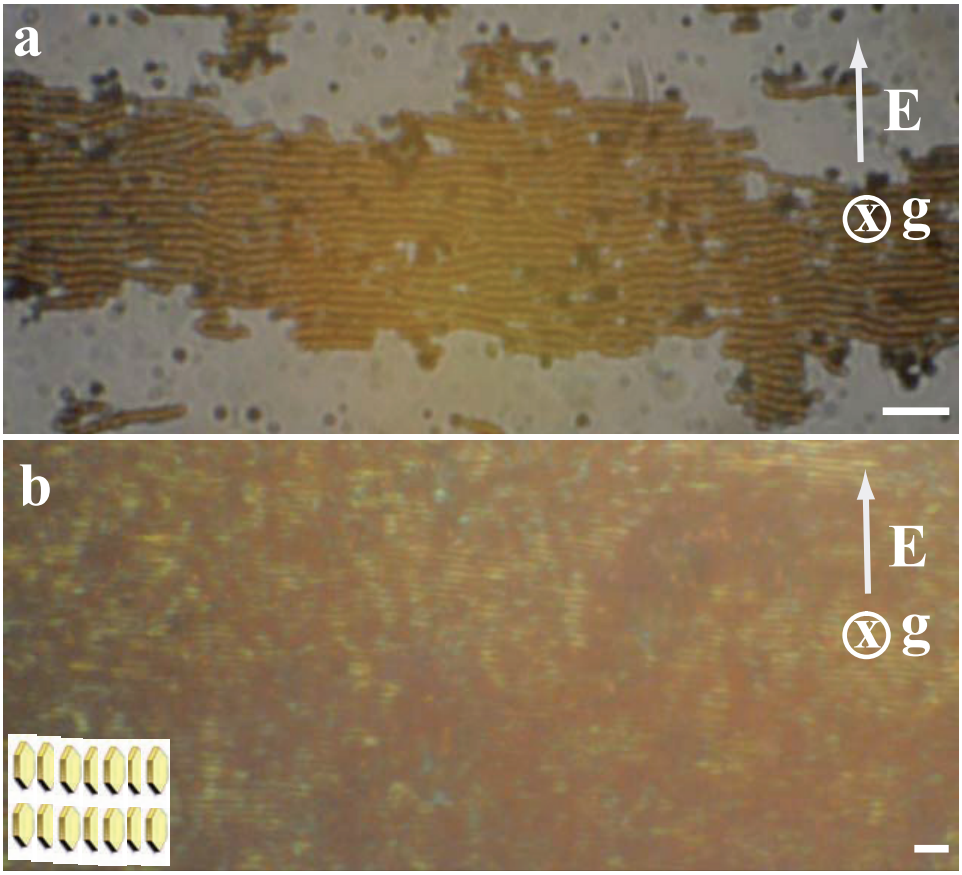

Figure 6.9: Worm-like columns in an external electric field. Optical micrographs of the directed columnar phase at different salt concentrations in an AC field. **a**, A defect-rich columnar phase was observed at 0.8 mM of KCl. **b**, A defect-free 2D columnar phase was observed at 1.5 mM of KCl. Lower inset, schematic illustrates the orientation of particles between the columns. Note that the same field (E_{rms} = 0.015 Vμm^{-1}, f = 200 KHz). The direction of the applied electric field and the direction of gravity are indicated in the upper-right corner. Scale bars are 15 μm.

polarizers. While an ordered phase is dark when the director parallel to either of the polarizers. Disordered (isotropic) phases are always dark irrespective of the orientation of the polarizers because the scattering by these phases does not change the polarization of the light. Here, a two dimensional directed columnar phase of 1.5 mM dispersion was observed with the polarized light microscopy. In fact we just used a bright-field microscopy equipped with an adjustable polarizer. Note that the dashed arrows indicate the orientation of the polarizers (Figures 6.10a-b). Figure 6.10a shows that the two dimensional columnar phase blocked

the entire light when one of the polarizers had maintained parallel to the orientation of the columnar phase. Moreover, when both polarizers were rotated about 45 ° subsequently light passed through the phase as seen in Figure 6.10b. We note that individual platelets appeared as dark spots in Figure 6.10b.

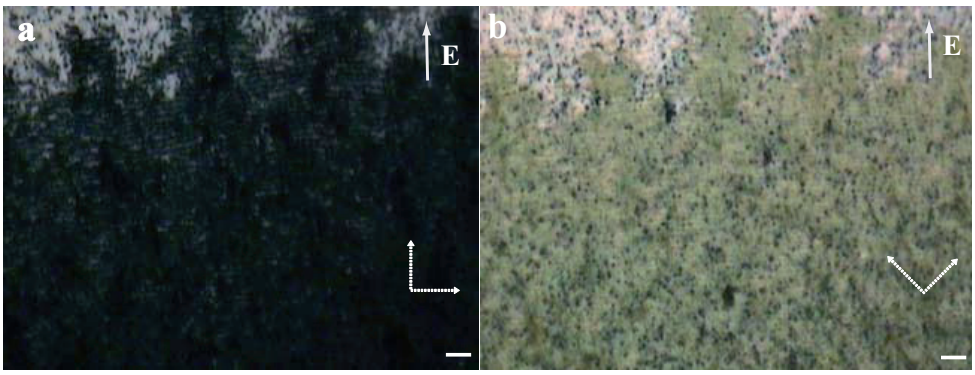

Figure 6.10: Polarization light micrographs of worm-like columns of 1.5 mM dispersion in an electric field. The orientation of the polarizers and the applied electric field are indicated by arrows in the lower-right corner, and upper-right corner respectively. **a**, The orientation of the director parallel to one of the polarizers. **b**, The polarizers were orientated at about 45° to the applied field direction. Scale bars are 15 μm.

Electrohydrodynamic instability

Upon increasing the field strength ($E_{rms} > 0.04$ Vμm^{-1}, f = 200 KHz), the columns that were initially aligned perpendicular to the applied field direction started to rotate slowly, thereby forming bands at nearly 45° relative to the applied field direction, as shown in Figure 6.11. The speed and direction of the rotation depends on the relative position of the columns with respect to the external electric field. Within a band, the columns were dynamically unstable, circulating in a counter-clockwise fashion, if the band tilted to the right relative to the applied field, and circulating clockwise, if the band tilted to the left. There were isolated bands, and also bands tilted in opposite directions joined together at the ends (Figure 6.11c-d). The speed of columns circulation increased when the strength of the applied field was increased, and the circulation was also sensitive to the frequency of the field. Although we could not able follow the dynamics on a single particles level, we did see the rotation of columns at low field strengths (E_{rms} = 0.06 Vμm^{-1}, f = 200 KHz). After 2-3 mins the field was turned off, and it was observed that the circulations immediately stopped. Many shorter columns formed, which resulted from breakage of longer ones due to a strong rotational motion. Here, we demonstrate on how the field can be exploited to grow longer columns from smaller ones. The same dispersion was exposed to a lower field strength E_{rms} = 0.015 Vμm^{-1}, which was well below the critical field strength for the onset of instability, the small columns then started to join together again and forming longer columns thereby moving towards the 2D columnar phase as shown

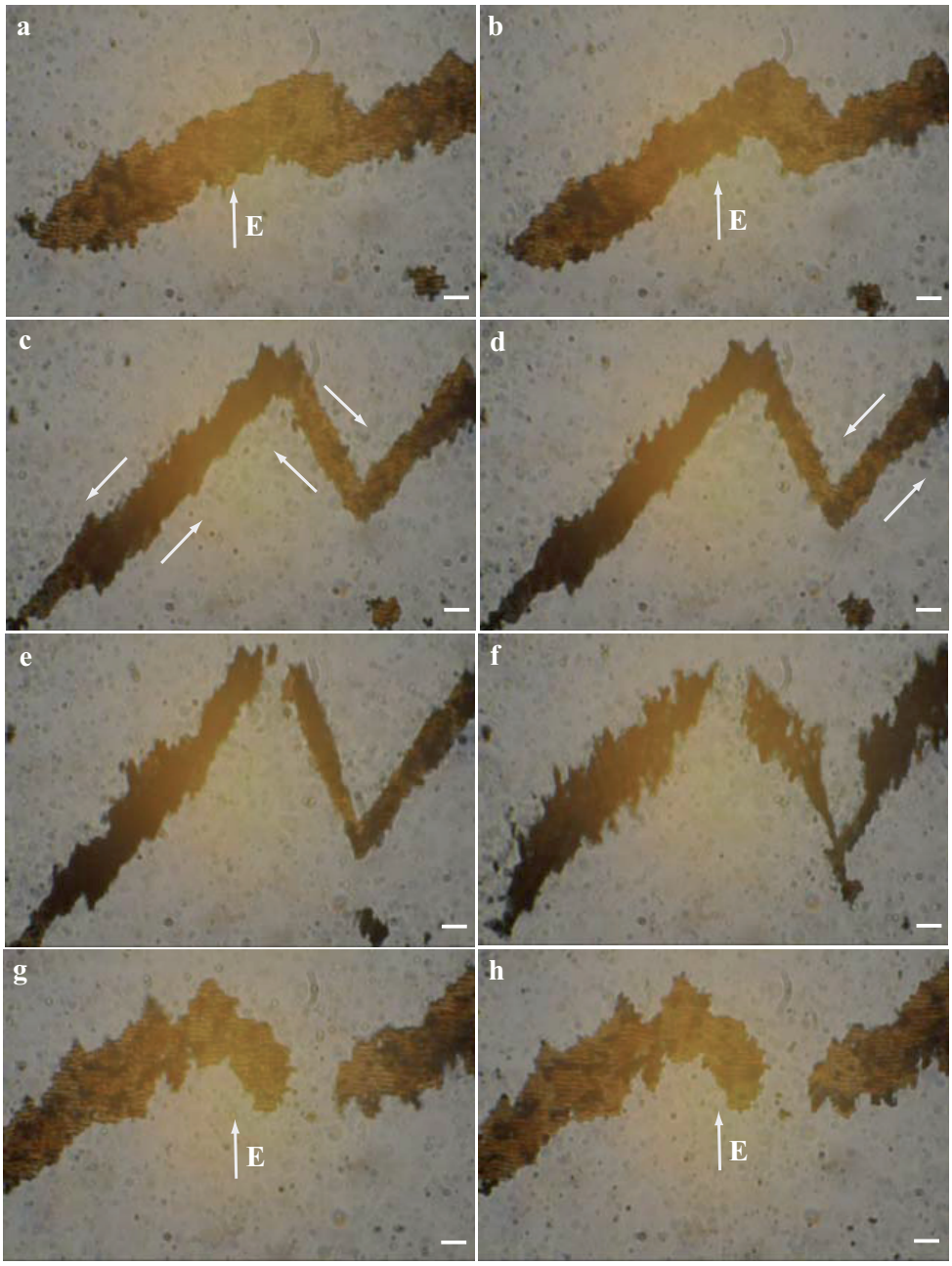

Figure 6.11: Electrohydrodynamic instability. **a-f**, Optical micrographs showing the formation of diagonal bands that consists of worm-like columns when the field was increased to $E_{rms} > 0.04\ V\mu m^{-1}$, f = 200 KHz. Arrows indicate the direction of the circulation. The time lapse between the frames is 30 secs. The field was turned off after 2-3 mins. As a result of strong circulations smaller columns were resulted. **g-h**, These columns were then exposed to a field of $0.015\ V\mu m^{-1}$ which was below the critical field strength for onset of instabilities. Scale bars are 10 μm.

in Figures 6.11g-h. These phenomena clearly demonstrated that the presence of the field altered the distribution of column lengths. It is not clear at present if this

was simply due to changes of local concentrations of the columns (by the aligning effect of the field) or if there were also additional attractive components between the column ends and/or sides induced by the electric fields.

Since our system is complex so we restricted ourself to a more qualitative interpretation. In the following, we adapt a simple time scale argument that is already reported in literature [28–30] for spherical particles, bringing our observations in line with others already described in literature. It is instructive to compare two time scales: i) the time required for the counter-ions to diffuse over the distance of ($\delta + \kappa^{-1}$), and ii) the oscillation period (τ_p) of the alternating field

$$\tau_D = \frac{(\delta + 2\kappa^{-1})^2}{2D} \tag{6.7}$$

where τ_D is the counterions diffusive time, δ is the thickness of the plate, and κ^{-1} is the Debye screening length.

The counterions diffusivity is on the order of 10^{-9} m^2/s, Debye screening length is about 8 nm for a 1.50 mM suspension, the thickness of the particle δ is about 16 nm. Here we used a 200 KHz frequency field therefore an oscillation period of the applied field is $\tau_p = 1/2\pi f$. When the the oscillation period of the applied field $\tau_p(O(10^{-4})) >$ diffusion time of the counterions $\tau_D(O(10^{-7}))$ a phase lag develops between the induced dipole moment of the double layer and the applied electric field. Due to this phase shift, the time-averaged torque on each particle is non-zero. Therefore, when the two particles are not aligned parallel or perpendicular to the direction of the applied field, they will spin. The torque has a maximum amplitude at $\theta = 45^\circ$ [28, 30], which induces a strong flows and instabilities. We believe that these circulations have electrohydrodynamic origin as was reported for the spherical particles [28–30].

6.5 Conclusions & outlook

We demonstrated that reversible stacks of sheet-like particles with a large aspect ratio, which consist of very thin (<20 nm) single crystalline gold platelets, can be realized at a specific range (0.8 - 2.0 mM) of salt concentrations. Moreover, the length distribution could be controlled by varying the salt concentration and also the spacing between the sheets is a strong function of salt concentration as is clear from approximate calculations of the interaction potential between the particles. The stacks of the platelets formed because of the secondary minimum in the interaction potential between two parallel plates. At low concentrations of salt the secondary minimum was not deep enough therefore stacks did not form. We studied the dielectric response of the gold platelets in the absence and presence of salt. Different behavior was observed in both cases. Platelets at low salt concentrations that in bulk did not form stacks, were aligned with their longest axis in the field direction in a head-to-tail arrangement. While particles were at

salt concentrations that did form stacks were seen to align in the same direction. However, the stacks still formed, meaning that these stacks were oriented perpendicular to the field. In addition, stacks were also seen to form 2D regular patterns. As far as we know, such a control has not been demonstrated previously. These 2D regular patterns (columnar phase) were able to strongly polarize light as was demonstrated experimentally. It is not clear of these patterns were 2D crystalline or liquid crystalline. Our system enable us to vary the inter-plate distance within a column by tuning the salt concentration such that a plasmon resonance shift could be achieved.

Acknowledgements

First of all, we would like to thank Stéphane Badaire for particle synthesis and Cryo-scanning electron microscope measurements. It was a great pleasure working with you. We thank Matthijs de Winter, Chris Schneijdenberg, and Jan Andries Post for FIB measurements. Bas Kwaadgras was thanked for useful assistance in the DLVO potential calculations.

References

[1] J. Zhang, S. Li, J. Wu, G. C. Schatz, and C. A. Mirkin, *Plasmon-Mediated Synthesis of Silver Triangular Bipyramids*, Angew. Chem. **48**, 7787 (2009).

[2] R. C. Jin, Y. W. Cao, C. A. Mirkin, K. L. Kelly, G. C. Schatz, and J. G. Zheng, *Photoinduced conversion of silver nanospheres to nanoprisms*, Science **294**, 1901 (2009).

[3] Y. N. Xia, Y. J. Xiong, B. K. Lim, and S. E. Skrabalak, *Shape-Controlled Synthesis of Metal Nanocrystals: Simple Chemistry Meets Complex Physics?*, Angew. Chem **48**, 60 (2009).

[4] Y. Y. Yu, S. S. Chang, C. L. Lee, and C. R. C. J. Wang, *Gold Nanorods: Electrochemical Synthesis and Optical Properties*, The Journal of Physical Chemistry B **101**, 6661 (2001).

[5] C. R. Martin, *Nanomaterials: a membrane-based synthetic approach*, Science **266**, 1961 (1994).

[6] G. A. Somorjai and D. W. Blakely, *Mechanism of catalysis of hydrocarbon reactions by platinum surfaces*, Nature **258**, 5536 (1975).

[7] M. Grzalczak, J. Vermant, E. M. Furst, and M. Liz-Marzan, *Directed self-assembly of nanoparticles*, ACS Nano **4**, 3591 (2010).

[8] D. A. Walker, B. Kowalczyk, M. Olvera de la Cruz, and B. A. Grzybowski, *Electrostatics at the nanoscale*, Nanoscale **3**, 1316 (2011).

[9] S. C. Glotzer and M. J. Solomon, *Anisotropy of building blocks and their assembly into complex structures*, Nat. Mate. **6**, 557 (2007).

[10] E. V. Shevchenko, D. V. Talapin, N. A. Kotov, O. Brien, and C. B. Murray, *Structural diversity in binary nanoparticle superlattices*, Nature **439**, 55 (2006).

[11] M. E. Leunissen, C. G. Christova, A. P. Hynninen, C. P. Royall, A. I. Campbell, A. Imhof, M. Dijkstra, R. van Roij, and A. van Blaaderen, *Ionic colloidal crystals of oppositely charged particles*, Nature **437**, 235 (2005).

[12] C. A. Mirkin, R. L. Letsinger, R. C. Mucic, and J. Storhoff, *A DNA-based method for rationally assembling nanoparticles into macroscopic materials*, Nature **382**, 607 (1996).

[13] S. Y. Sung Yong Park, K. R. Lytton-Jean, B. Lee, S. Weigand, G. C. Schatz, and C. A. Mirkin, *DNA-programmable nanoparticle crystallization*, Nature **451**, 553 (1996).

[14] M. R. Jones, R. J. Macfarlane, B. Lee, J. Zhang, K. L. Young, A. J. Senesi, and C. A. Mirkin, *DNA-nanoparticle superlattices formed from anisotropic building blocks*, Nat. Mate. **9**, 913 (2010).

[15] K. D. Hermanson, S. O. Lumsdon, J. P. Williams, E. W. Kaler, and O. D. Velev, *Dielectrophoretic assembly of Electrically functional microwires from nanoparticle suspensions*, Science **294**, 1082 (2001).

[16] B. M. I. van der Zande, B. M. I., G. J. M. Koper, and H. N. W. Lekkerkerker, *Alignment of Rod-Shaped Gold Particles by Electric Fields*, Langmuir **103**, 5754 (1999).

[17] S. Okamoto and S. Hachisu, *Onthe long-range attraction force between plate-like gold particles*, J. Colloid and Inter. Sci **43**, 30 (1972).

[18] V. Bastys, I. Pastoriza-Santos, B. Rodríguez-González, R. Vaisnoras, and L. Liz-Marzán, *Formation of Silver Nanoprisms with Surface Plasmons at Communication Wavelengths*, Adv. Funct. Mater. **16**, 766 (2006).

[19] B. W. Derjaguin and L. Landau, *Theory of the stability of strongly charged lyophobic sols and of the adhesion of strongly charged particles in solutions of electrolytes*, Acta Physicochim. URRS **14**, 633 (1941).

[20] E. J. Verwey and J. T. Overbeek, *Theory of the Stability of Lyophobic Colloids*, Elsevier, New York, 1948.

[21] R. J. Hunter, *Zeta Potential in Colloid Science*, Academic Press, London, 1981.

[22] H. R. Vutukuri, A. F. Demirors, P. Bo, P. D. J. van Oostrum, A. Imhof, and A. van Blaaderen, submitted.

[23] M. E. Leunissen, H. R. Vutukuri, and A. van Blaaderen, *Directing Colloidal Self-Assembly with Biaxial Electric Fields*, Adav. Mat. **21**, 3116 (2009).

[24] R. C. Hayward, D. A. Saville, and I. A. Aksay, *Electrophoretic assembly of colloidal crystals with optically tunable micropatterns*, Nature **404**, 56 (2000).

[25] A. Yethiraj and A. van Blaaderen, *A colloidal model system with an interaction tunable from hard sphere to soft and dipolar*, Nature **421**, 513 (2003).

[26] H. Kramer, M. Deggelmann, C. Graf, M. Hagenbuechle, C. Johner, and R. Weber, *Electric birefringence measurements in aqueous fd virus solutions*, Macromolecules **25**, 4325 (1992).

[27] X. Schlagberger and R. R. Netz, *Anomalous birefringence and polarizability saturation of charged elastic rods: Field-strength, salt and finite-concentration effects*, Europhys. Let. **83**, 36003 (2008).

[28] Y. Hu, J. L. Glass, A. E. Griffith, and S. Fraden, *Observation and simulation of electrohydrodynamic instabilities in aqueous colloidal suspensions*, J. Chem. Phy **100**, 4674 (1994).

[29] H. Isambert, A. Ajdari, V. J. L., and J. Prost, *Electrohydrodynamic Patterns in Charged Colloidal Solutions*, Phy. Lett **78**, 971 (1997).

[30] A. S. Negi, K. Sengupta, and A. K. Sood, *Frequency-Dependent Shape Changes of Colloidal Clusters under Transverse Electric Field*, Langmuir **25**, 11623 (2005).

7

Colloidal cubes in an external electric field

In previous chapters, we have already demonstrated that external electric fields can be used to take systems out of equilibrium in a controlled way. In the present chapter, we study the effect of external electric fields on the phase behavior of sharp-edged colloidal cubes using optical microscopy and Monte Carlo simulations. Contrary to most anisotropic particles, the orientation of a single cube with homogeneous properties is not affected by external electric fields: the symmetry of the particle causes its potential energy to be independent of its orientation. As a result, colloidal cubes can rotate freely in the electric field. This was experimentally demonstrated with micron-sized cubes of single crystalline neighborite ($NaMgF_3$) in a MHz electric field. However, the dipolar attractions induced by the external electric field between particles can lead to alignment when two or more particles are in close proximity. In addition to string fluid and indications for the formation of an orientationally ordered body-centered tetragonal (BCT) phase and a columnar phase consisting of hexagonally ordered strings of rotationally disordered cubes. Moreover, we compare our experimental observations with the predicted phase diagram using Monte Carlo simulations in the NPT ensemble.

7.1 Introduction

Nowadays, particles with a wide variety of shapes, compositions, and functionalities are being synthesized in the nano to micrometer size regime with an ensuing self assembly step in mind [1–4]. Materials that result from such a self assembly process form new amorphous or (liquid) crystalline materials with new properties of interest to applications and and devices with great technological potential. Compared to standard fabrication methods based on top-down approaches, such as optical lithography, colloidal self-assembly offers the potential for easier and thus cheaper fabrication and manipulation of nano- and microstructures, especially in three dimensions. Additionally, introducing directional, anisotropic interactions using magnetic or electric dipoles is a practical strategy to impart anisotropy into self-assembled morphologies even for the most symmetric building blocks: colloidal spheres [2, 3, 5–11].

Non-spherical particles often exhibit more complex phase behavior than spheres, including smectic, nematic, columnar, and cubatic liquid crystals. Recently, methods to synthesize cubes on the micrometer [12, 13] and nanometer scale [14, 15] have become available and thus regained interest, because of the peculiar phase behavior of cube-shaped particles. Several simulation studies have investigated the phase behavior of cubic and other anisotropic particles, resulting in phase diagrams for tetragonal parallelepipeds [16] and colloidal superballs [17], as well as for a range of polyhedral shapes with varying degrees of anisotropy [18]. A study on cubes with dipole moments that are fixed with respect to the particle shape, as expected in nanoparticles, showed that these can self-assemble into wires, sheets or ring-like structures depending on the orientations of the dipoles [19]. Rossi *et al*. [13] have recently experimentally observed depletion driven simple close-packed cubic crystals of micron-sized hollow silica cubes. An important conclusion that arose from this work is that even a slight softening of the cube shape around the edges can result in significant difference in the symmetry of the phases formed by the depletion effect.

The cubatic liquid crystalline phase is a most extraordinary state of matter. Unlike other liquid-crystalline phases, the cubatic phase is characterized by orientational ordering in three mutually perpendicular directions while the particles retain translational mobility. This phase is closely related to a bi-axial nematic phase that was recently observed for board shaped colloidal particles by Vroege *et al*. [20]. A biaxial phase results from a combination of the tendencies of either flat or rods to form nematic phases in one particle systems. Flat particles like to align in a nematic phase with the director of the particles perpendicular to the flat face and rods form nematic phases with the particle director in the direction of the rod. Particles which combine both tendencies can order with nematic alignment in perpendicular directions. Because of its higher symmetry cubes could potentially form bi-axial nematic phases where also the third direction obtains automatically long-range orientational order as well. Such unusual ordering may

lead to novel optical, and rheological properties. This phase has been predicted in the simulations of sharp-edged cubes [16, 18], and truncated hard spheres [21]. However, an experimental realization of a cubatic phase does not yet exist for a colloidal system as far as we are aware of. Here, we used an external electric field to direct the self-assembly of sharp-edged colloidal cubes and present our first preliminary results on this system. A key strength of external electric or magnetic field directed assembly is the reversibility of the interactions, which can lead to a rapid return to a disordered state when the field is removed. Such effects are useful in obtaining reconfigurable and switchable assemblies, for instance, electronic ink or other applications in optics, but could also be exploited to anneal defects in structures by cycling the field on and off at an optimal frequency.

In this chapter, we investigate the effect of external electric fields on the phase behavior of sharp-edged colloidal cubes. Subsequently, we compare our preliminary experimental observations with the predicted phase diagram by Monte Carlo simulations. This chapter is organized as follows. All experimental and simulation methods details are listed in Section 7.2, followed by a discussion of the results in Section 7.3. In Section 7.3.1 we present experimental observations. In Section 7.3.2 we present simulation results. Finally, we give conclusions and also an outlook on future work in Section 7.4.

7.2 Methods

Particle synthesis and suspensions

We synthesized cube-shaped particles of sodium magnesium fluoride (neighborite, $NaMgF_3$) by the method of Sevonkaev *et al*. [12]. Crystalline structure of neighborite is orthorhombic [22]. Sharp-edged cubic colloidal particles of 1.10 μm size were prepared as follows: 10 ml of an 0.2 M aqueous magnesium chloride ($MgCl_2$) and 100 ml of an 0.2 M aqueous sodium fluoride (NaF) solutions were mixed in a 500 ml laboratory flask. The flask was then immersed in a silicon oil bath, maintained at 80 °C and stirred at 100 rpm. The dispersion was maintained at the same temperature and the reaction was allowed to proceed for three hours. After the synthesis, the reaction mixture was washed 3-4 times with de-ionized water (18.2 MΩ-cm, Millipore) to remove smaller particles and also un-reacted species. Next, the supernatant was removed and the particles in the sediment were redispersed in de-ionized water. Scanning and transmission electron micrographs of thus synthesized particles after the cleaning are shown in Figure 7.1. The average size and standard deviation were measured using iTEM imaging software. The polydispersity is defined as p = standard deviation/average length. For each sample 80 to 100 particles were measured. The size and the polydispersity of the particles were 1.10 μm and 8 % respectively. The density, and refractive index of the particles are 3.05 g/cc and 1.364 respectively [12]. The dielectric constant of the particles is 4.50 [22].

Our suspensions consisted of positively charged $NaMgF_3$ cubic particles in water. Because our particles are positively charged, they tend to stick to the negatively charged glass walls of the sample cell. Before using the cell we coated the cell with a cationic polyelectrolyte (polyethyleneimine, PEI ($M_w = 750$ kg/mole). We flushed a 0.5 % by weight PEI aqueous solution through the cell. After filling the cell with the colloidal suspension, we sealed it with UV-curing optical adhesive (Norland no.68). Particle dynamics were followed by bright field microscopy using a charged coupled device (CCD) camera (UNIQ, UP-600).

Electric-field setup

We used two types of sample cells: rectangular capillaries (VitroCom, UK) and home made sandwich indium-tin oxide (ITO) coated glass cells. The rectangular sample cells consisted of a 0.1 mm $\times$ 1.0 mm capillary with two 50 μm thick nickel-alloy wires (Goodfellow, UK) threaded along the side walls. Our sandwich ITO coated glass cell consisted of two parallel no. 1 glass cover slips (130 - 160 μm thick, Menzel), which were completely coated with a conductive, semi-transparent layer of indiumtinoxide (ITO, Diamond coatings limited, UK). They were kept apart by a pair of glass spacers, which were cut out of no. 1 or no. 0 (80 - 120 μm thick) slides, and which were placed at opposite sides of the sample space. Typically, the height of the sample space, enclosed by the cover slips, was 100 - 200 μm, with an area of ~ 1 cm^2. The conductive ITO layer was in contact with the suspension. The cell was constructed on top of a 1.0 mm thick microscopy slide, for extra support and easy mounting on the stage of the microscope. We glued everything together with no. 71 UV-curing optical adhesive (Norland). For the electrical contacts with the ITO electrodes we used silver paint (Jeol) and thin thermocouple alloy wire (diameter 50 μm, Goodfellow), which was then wrapped around standard electronic wire. We used a function generator (Agilent, Model 3312 OA) and a wide band voltage amplifier (Krohn-Hite, Model 7602M) to generate the electric fields. The field strength and the frequency were measured using an oscilloscope (Tektronix, Model TDS3052).

Monte Carlo Simulations

We modeled the colloidal cube-shaped particles as perfect hard cubes with edge length σ and one or more point dipoles inside each particle. The interactions thus consisted of a dipolar interaction between the cubes and a hard-core repulsion that prevents particles from overlapping. In the case where each particle contains a single dipole, the dipolar interaction potential between two particles i and j is given by:

$$\beta u_{dip}(r_{ij}, \theta_{ij}) = \frac{\gamma}{2}\left(\frac{\sigma}{r_{ij}}\right)^3 (1 - 3\cos^2\theta_{ij}), \tag{7.1}$$

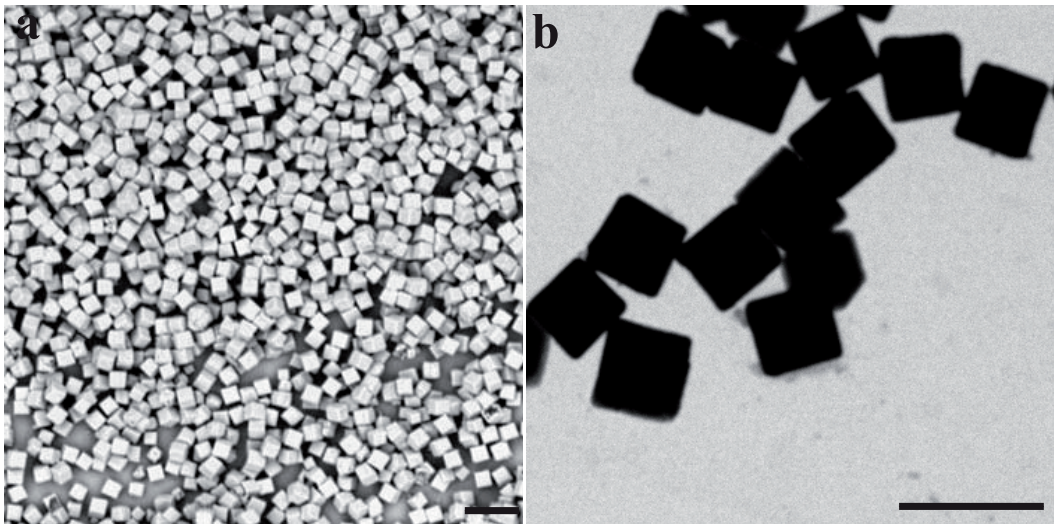

Figure 7.1: Neighborite ($NaMgF_3$) sharp-edged colloidal cubes. **a**, Scanning electron micrograph reveals that the particles are sharp-edged. **b**, Transmission electron micrograph of the particles. Scale bars are 2 μm.

where r_{ij} denotes the distance between the two particles, and θ_{ij} the angle between the distance vector between the particles and the direction of the field. As is mentioned in the Chapter 2, the strength of the dipole interaction is given by the field strength $\gamma = \pi\alpha^2\epsilon_0\epsilon_m\sigma^3E_{loc}^2/8k_BT$ where $\mathbf{E}_{loc}$ is the dipole moment induced in the particle by the local electric field, where $\mathbf{E}_{loc} = \mathbf{E} + \mathbf{E}_{dip}$. Here, $\mathbf{E}$ is the external electric field and $\mathbf{E}_{dip}$ is the field induced by the other dipoles. Note that we neglected the effect of neighboring dipoles on the polarization of their neighbors. Finally, the polarizability of the particles in the medium is determined by $\alpha = (\epsilon_p - \epsilon_m)/(\epsilon_p + 2\epsilon_m)$ where ϵ_p and ϵ_m are particle and medium dielectric constants. Experimental γ values were estimated using Eq. 7.1. Moreover, our particles are charge stabilized therefore in our calculations we allowed 10 % of the size of the particles in addition to the inter-particle distance between neighboring particles in a string.

The long-range interactions were handled using Ewald summations [23, 24]. To detect overlaps between two cubes, we used a triangle tesselation scheme [25]. While a cube-specific algorithm based on the separating axis theorem would likely be more efficient, the difference is negligible compared to the computational cost of the Ewald summations used to calculate the potential energy.

In the simplest approximation, the dipole interactions were modeled by a single point dipole in the middle of each cube. In this model, rotations do not affect the dipolar pair interaction between two cubes, and rotational order can only emerge due to the hard-core interactions. However, it is not clear that the interaction between two cubes can be approximated with two point dipoles: due to the external field, the full volume of each colloidal cube will be polarized, resulting

in a more complex interaction. While at large distances the interaction between two particles should behave as a simple dipole-dipole interaction, there will be short-range deviations from this behavior. To investigate this, we also studied cubes containing multiple dipoles arranged in a simple cubic lattice aligned with the orientation of the particle. Thus, if a particle at position $\mathbf{r}$ contains n^3 point dipoles, the positions of these dipoles are given by:

$$\mathbf{r}_{ijk} = \mathbf{r} + (2i + 1 - n)\mathbf{a} + (2j + 1 - n)\mathbf{b} + (2k + 1 - n)\mathbf{c}, \tag{7.2}$$

where $\mathbf{a}, \mathbf{b}$ and $\mathbf{c}$ denote the three (mutually perpendicular) edge directions of the particle, and $1 \leq i, j, k \leq n$. Each point dipole interacts with all others via Equation 7.1, with the interaction strength γ lowered by a factor n^3 to ensure that the interactions between particles at large distances are unchanged. Even with multiple point dipoles in each particle, the potential energy of a single particle was found to be orientation independent. However, the particle pair interaction is now a function of both the relative position of the two particles and their individual orientations.

We investigated the phase behavior of this system by performing Monte Carlo simulations in the NPT ensemble, at a fixed number of particles $N = 512$, pressure P and temperature T. Simulations were performed in a series where the pressure was either increased or reduced slowly, leading to compression or expansion of the system. During the compression runs, the simulations started from an initial configuration in the fluid phase, and the pressure was increased in small steps, up to pressures well past the expected coexistence pressure. Expansion runs started from an initial configuration in one of the crystal phases likely to be stable for the field strength γ used in the simulations. Where needed, additional compression and decompression runs were performed using a different structure as the initial configuration. From the phase transitions observed in both runs, we determined the approximate phase boundaries of the system.

As the strings in the string fluid at high field strengths span the simulation box, it is likely that the phase behavior of the system in this regime is affected by finite size effects. To investigate this, the simulations for high field strengths ($\gamma \geq 12.5$) and low pressures ($P\sigma^3/k_BT < 1$) were performed in a system of $N = 1024$ particles as well. No significant shift in the phase behavior was observed.

To determine the transition from a simple cubic (sc) to a body-centered tetragonal (BCT) crystal structure, we performed simulations at constant pressure for a range of field strengths γ, starting from either of the two phases. Since the system can easily switch between these structures, no clear hysteresis was visible in these simulations, and determining the approximate phase boundary was straightforward.

7.3 Results and discussion

7.3.1 Experimental Results

Our experimental system consisted of positively charged cube-shaped sodium magnesium fluoride (neighborite) particles in water (Figure 7.2a). The particles sediment quickly to the bottom due to their high density (3.05 g/cc), thereby increasing the volume fraction. On the single-particle level the gravitational length (l_g) is 0.15 μm, which characterizes at what heights gravity will start to play an important role in the equilibrium phase behavior. However, induced dipolar attractions between the particles are strong enough to overcome gravitational effects when the field is also applied in same direction [26]. Due to fast sedimentation of the particles it is difficult to follow the dynamics in bulk. Moreover, it is difficult to follow behavior of a single particle as a function of time in concentrated systems, because the particles are not labeled with a fluorescent dye. Neither was the solvent labeled with a dye nor the index of the suspension well matched, thus making the use of confocal microscopy impossible. Therefore, we restricted our studies to essentially 2D, although particles that are not in focus also contribute to the image. By using two types of cell we were able to observe the structures in two mutually perpendicular planes. We used a high frequency (1 MHz) field to prevent polarization of the electric double layer around particles. Upon application of an electric field (E_{rms} = 0.015 Vμm^{-1}, γ = 6.16) these particles acquire an induced dipole moment due to the difference in dielectric constant between the particles and the solvent. In contrast with most anisotropic particles, the potential energy of a single cube in an electric field is independent of its orientation [27]. As a result, colloidal cubes can rotate freely in the electric field as shown with the arrow in Figures 7.2b-f. From series of optical micrographs (Figures 7.2b-f), it is clear that a single cube (e.g., as seen with the arrow in Figures 7.2b-f) does not show a strong preferential orientation, whereas the hard-core interactions between particles can lead to alignment when two or more particles are in close proximity as seen in Figures 7.2b-f, due to the dipolar attractions induced by the external field in combination with the relatively short-ranged particle repulsions caused by the thin double layer around the particle. Kwaadgras *et al*. [27] have theoretically predicted that a single cube is equally polarizable in all directions, and thus has no preferred orientation in an external electric field. We note that our experimental observations are in a good agreement with their predictions.

When the volume fraction of the particles was increased, the induced dipole moment in each particle led the particles to assemble into one particle thick strings that were aligned with the applied field direction in a head-to-toe fashion. The volume fraction of the particles was $\eta \approx 0.60$. As a result of induced dipolar interactions between the particles, strings of particles formed (Figure 7.3b) within seconds after applying a low field strength of E_{rms} = 0.03 Vμm^{-1} (γ = 24.6). Moreover, the particles were oriented along the direction of the applied electric field. Some strings were shifted along the field direction with respect to its near-

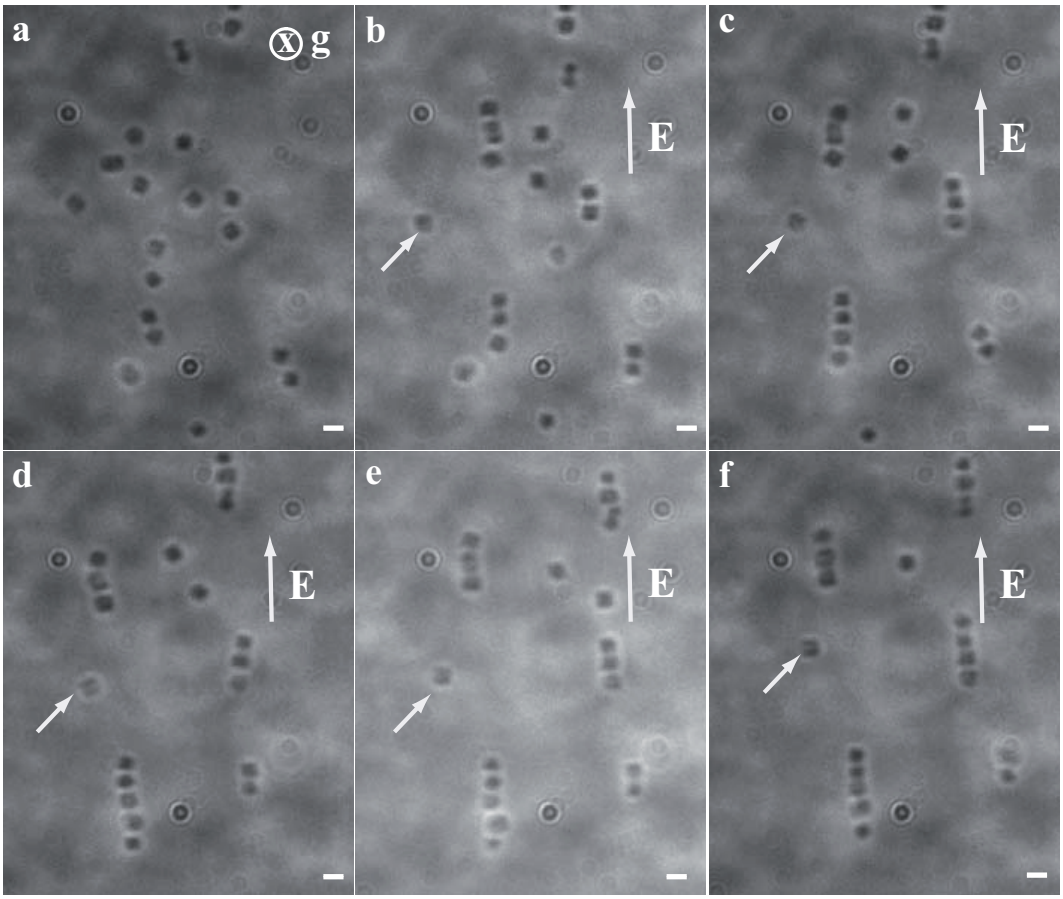

Figure 7.2: Time-lapse optical microscopy images of sharp-edged cubic particles in an electric field. **a**, Isotropically dispersed particles at zero field strength. **b-f**, At a low field strength (E_{rms} = 0.02 $V\mu m^{-1}$, f = 1 MHz), particles were aligned in the field direction in a head-to-tail fashion, while a single cube does not show any preferential orientation. The arrow indicates the different orientations of the single cube. The time lapse between the frames is 2 sec. Scale bars are 2 μm.

est strings by a distance equal to one half of the particle size. Although rotations along the field axis do not influence the potential energy of the system, we did not observe rotation of cubes within a string. Moreover, neighboring cubes in a string were aligned such that the touching faces of the two cubes were approximately parallel. As a result, all faces of the cubes aligned within a single string as shown in an inset of Figure 7.3b. Hard-core interactions with neighboring strings and also the bottom flat wall could caused the particles to align in all three directions. It can also be seen in the snapshot (Figure 7.3b) that the particles were orientationally ordered along the direction of the applied field. However, we were not able to follow the alignment of particles in the z-direction. We believe that the strings possess orientational order in that direction as well due to sedimentation of the strings on a flat wall. Additionally, the particles possess long range positional order within a string along the applied field direction while no positional

correlations between neighboring strings. Therefore, this phase is can be seen as a string fluid phase.

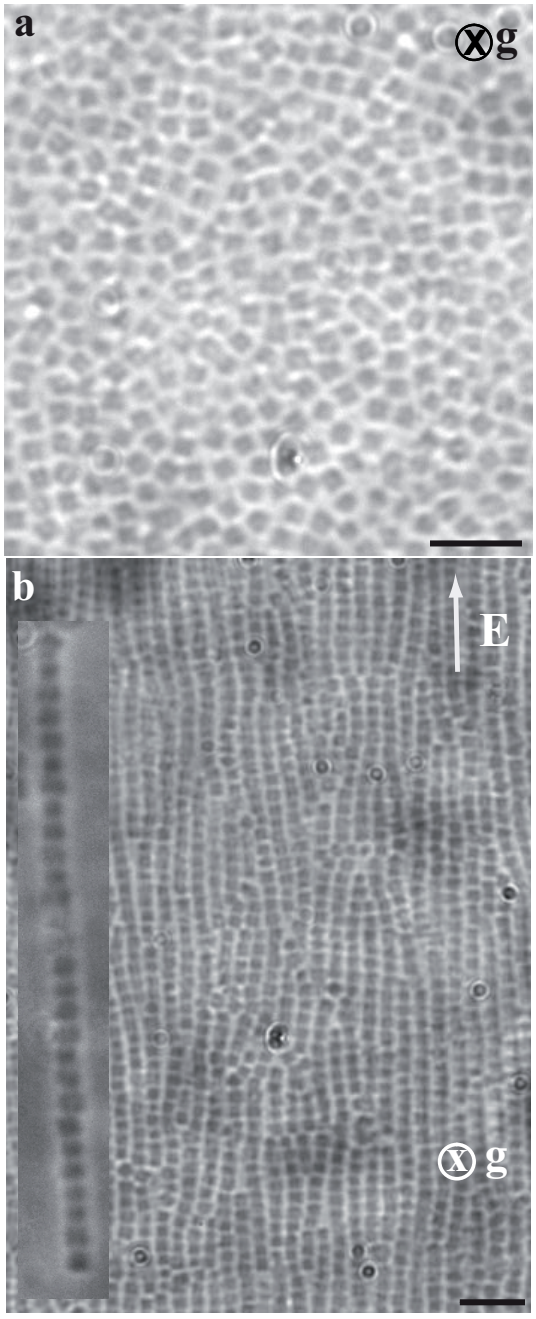

Figure 7.3: Optical micrographs of cube-shaped neighborite ($NaMgF_3$) particles in an external electric field. **a**, Isotropically dispersed particles at zero field strength. **b**, Particles were aligned in the applied field direction at a low field strength (E_{rms} = 0.04 $V\mu m^{-1}$, f = 1 MHz). Left inset, a magnified view of a single string. We note that images were recorded close the glass wall at the bottom of the capillary. Scale bars are 5 μm.

To observe order in a plane perpendicular to the field, we used a sandwich ITO coated cell. At intermediate field strengths (E_{rms} = 0.06 - 0.10 $V\mu m^{-1}$, γ = 100 - 280) and a particle concentration of $\eta \approx 0.60$, the particles formed a hexagonal arrangement of strings which are rotationally disordered around the applied field direction as shown in Figure 7.4. Although we were unable to follow rotations of the particles on a single particle level, we could see that the particles were rotationally disordered as seen in Figures 7.4b-e. Moreover, multiple hexagonal domains with different orientations were observed. We observed this structural change within 25 - 30 mins. We followed the structure over a period of 2 days, we did not observe any long range hexagonal positional order in the system. In addition, we did not see any structural changes at higher field strengths ($E_{rms} \geq$ 0.20 $V\mu m^{-1}$, $\gamma \geq 1000$). We suspect that the system might be out of equilibrium. When we switched off the field, the suspension returned to the fluid state, indicating that this structure was indeed stabilized by induced dipolar interactions.

Next, we found indications of the body-centered tetragonal phase. The initial volume fraction of the dispersion was $\eta \approx 0.45$. We let the sample sediment for about 40-45 mins to obtain volume fraction of $\eta \approx 0.85$ close to the bottom. Subsequently, the dispersion was exposed to higher field strengths ($E_{rms} \geq$ 0.20 $V\mu m^{-1}$, $\gamma \geq 1000$). After 1-1.5 hrs, the particles slowly transformed from a fluid to a square like arrangement due to strong induced dipolar interactions. Unfortunately, our particles are non-fluorescent therefore we could not able follow the particles in z- direction. As a result, it is hard say whether a string in the same plane with respect to neighboring strings or shifted along the field direction by a distance equal to half of the lattice spacing. The characteristic feature of the bct structure is that each string is shifted along the field direction with respect its four neighboring strings by a distance equal to half of the lattice spacing. Optical micrographs (Figure 7.5) clearly show the square arrangement of particles perpendicular to the applied field. The maximum volume fraction that can be achieved with sharp-edged cubes in a BCT lattice is $\eta = 1$, whereas spheres result in non-close packed structures. Possible reasons of the observed discrepancies between the experimental γ values and the simulations are polydispersity of the system, and porous nature of the particles (the effective dielectric constant of the particle is close to the solvent).

7.3.2 Computer simulations

An approximate phase diagram for colloidal hard cubes in an electric field is shown in Figure 7.6 as a function of the field strength γ and the packing fraction η. For this phase diagram, the dipole interactions were modeled by a single point dipole in the middle of each particle. The phase behavior bears close resemblance to that of dipolar hard spheres [28], with the main difference being the hexagonal string phase. In addition, the FCC crystal structure that is stable at low field strengths for spheres is replaced by a simple cubic (SC) crystal in the case of cube-shaped particles. As the simple cubic and BCT structures pack equally well

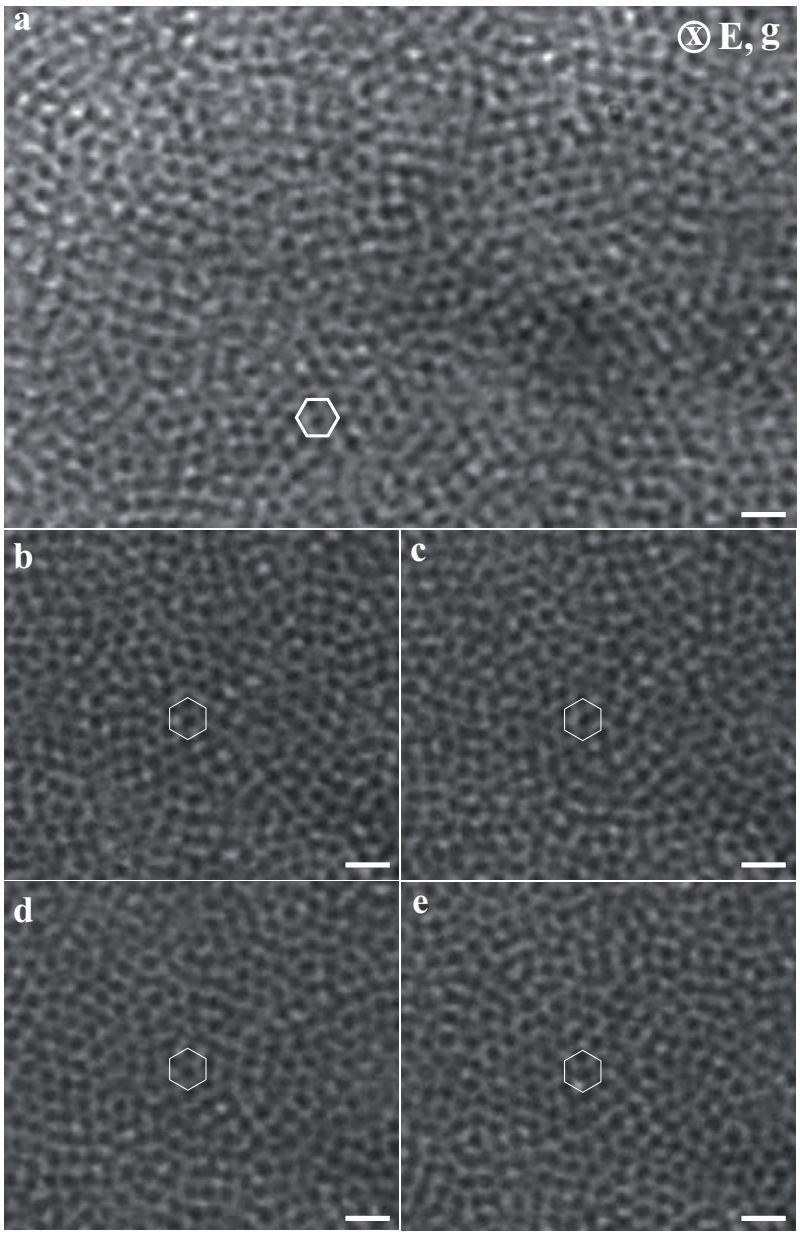

Figure 7.4: Optical micrographs of hexagonally ordered strings of rotationally disordered cubes at $\eta = 0.60$. **a**, 2D snapshot reveals the hexagonal arrangement of strings at intermediate field strengths (E_{rms} = 0.06 - 0.10 $V\mu m^{-1}$). The skewed white hexagon indicates the arrangement of the cubes. **b-e**, Series of xy images showing the change in orientation of the individual cubes in an electric field. Time lapse between the frames is 2 secs. Scale bars are 3 μm.

for cubes ($\eta_{max} = 1$), the simple cubic structure only appears for a sufficiently low field strength.

As in the case of hard spheres in an external field, a string fluid appears for low field strengths and low packing fractions as seen in the experiment (Figure

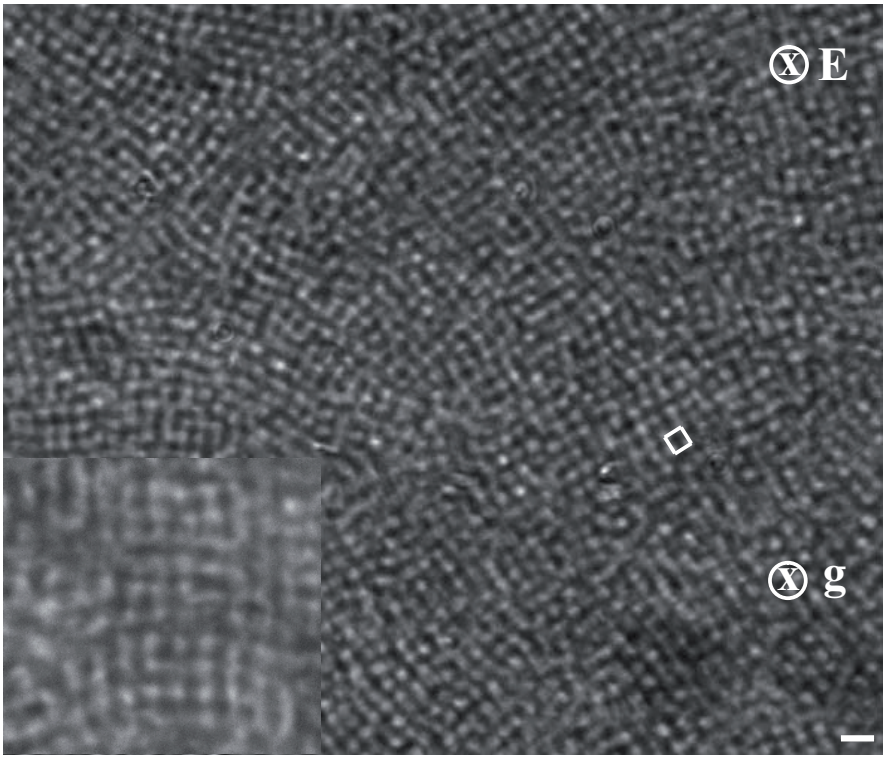

Figure 7.5: Optical micrograph of square-like arrangement of strings of particles. The image (xy) clearly shows indications of the characteristic bct stacking: square arrangement of cubes perpendicular to the applied field ($E_{rms} = 0.13\ V\mu m^{-1}$). The white square shows square like arrangement. Left inset, a magnified view of the square-like arrangement. Scale bars are 4 μm.

7.2). Neighboring cubes in a string are aligned such that the touching faces of the two cubes are approximately parallel, as this allows the point dipoles to approach each other more closely. Because aligning the cubes along this direction carries an entropic cost, the field strengths required to form strings are slightly higher than those seen in the case of spheres. However, it should also be noted that the dipole moment induced by an external field in cube-shaped particles will be stronger than that of a sphere with diameter σ, due to its larger volume, provided the material of the particle is the same. Therefore, the same value of γ for spheres and cubes does not correspond to the same external field strength. Since the cubes only contain a single point dipole, rotations around the field axis do not influence the potential energy of the system. As a result, the cubes do not align all faces within a single string: there is only alignment in one direction. Hard-core interactions with neighboring strings or a wall could cause the particles to align in all three directions, but this was only observed in the body-centered-tetragonal crystal phase that appears at high packing fractions.

The maximum packing fraction for sharp cubes is $\eta = 1$. At this packing fraction, all cubes are aligned along the same three axes, but a limited amount of freedom remains for the positions of the particles. At $\eta = 1$, the lowest energy

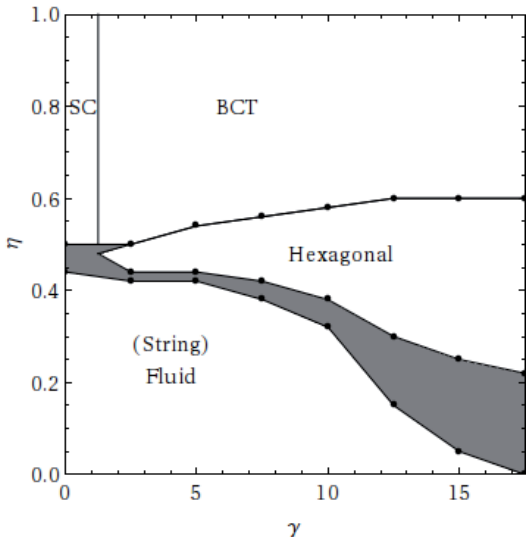

Figure 7.6: Approximate phase diagram for colloidal hard cubes in an external electric or magnetic field, as a function of the field strength γ and the packing fraction η. The black points indicate where phase boundaries were determined based on the phases found in MC simulations at constant pressure. The labels SC and BCT denote a simple cubic and body-centered tetragonal phase, respectively, while the hexagonal phase consists of strings of particles arranged on a hexagonal lattice.

state is a body-centered tetragonal (BCT) structure. This structure can be seen as a further aggregation of strings of cubes onto a square lattice, with all the particles aligned. Each string is shifted along the field direction with respect to its four neighboring strings by a distance equal to half of the lattice spacing. A typical snapshot of this structure is shown in Figure 7.7a and agrees with the experimental structure observed in Figure 7.5. This structure is readily seen to form at high field strengths, regardless of the starting configuration. However, for lower field strengths, the same starting configuration can also lead to a hexagonal ordering of strings, without alignment with respect to rotation along the field axis. In this case, the lowest energy state would likely have three of the six neighbors of each string shifted up by a third of the inter-particle distance in a string, and the other three shifted down by the same amount, but this order is not clearly visible in the simulations so far. For an example, see Figure 7.7b. The hexagonally ordered strings of rotationally disordered cubes were observed experimentally (Figure 7.4). This configuration maximizes the distance between strings, allowing for larger orientational entropy at the cost of a lower potential energy. It might be interesting to note that an added Yukawa repulsion as in the experiment would likely further stabilize this phase, as this would increase the distance between the strings. In the limit of high field strengths, the hexagonal columnar phase is expected to vanish eventually: the BCT phase has a lower potential energy, and will coexist with a dilute gas at sufficiently high interaction strengths.

When the field strength $\gamma = 0$, the stable crystal phase is a simple cubic crystal (SC). At low but finite fields, this structure remains stable, but becomes slightly

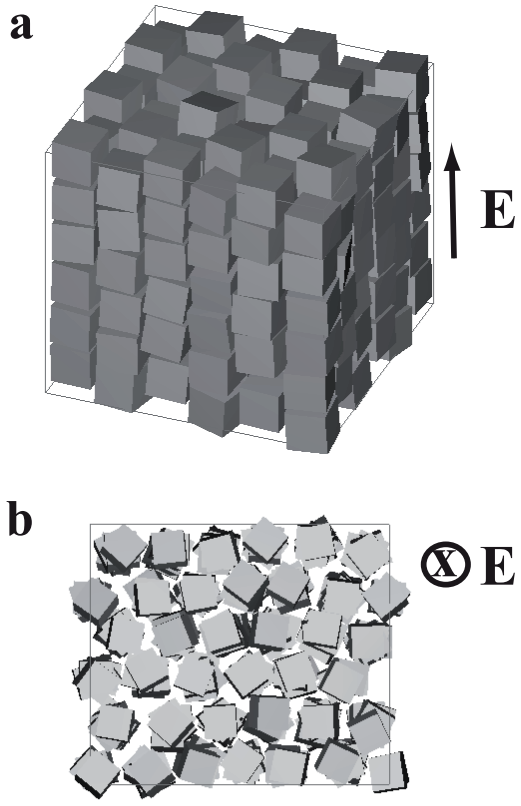

Figure 7.7: a, Snapshot of the BCT phase, at $\gamma = 15$ and pressure $\beta P\sigma^3 = 4$ ($\eta = 0.64$). The external field points along the vertical direction. **b**, Snapshot of the hexagonal phase, at $\gamma = 15$ and $\beta P\sigma^3 = 1$ ($\eta = 0.43$). The field direction is perpendicular to the plane of view.

distorted: the lattice is compressed along the field direction, actually leading to a simple tetragonal lattice. As the distortions are small, this crystal is still labeled SC in Figure 7.6.

In simulations of the string fluid, cubic particles in strings show orientational disorder: while the top and bottom faces of neighboring particles are aligned in order to minimize the distance between them, particles are free to rotate around the field axis. This can be understood from the way the interactions are modeled: since the potential in Eq. 7.1 only depends on the positions of the centers of the particles, there is no way for it to align the particles orientationally. In experiments performed on a dilute string fluid of cube-shaped particles in an external electric field, particles within the same string were seen to mostly align orientationally only at high field strengths. This suggest that weak aligning forces may exist as a result of the way cube-shape particles are polarized in the external field.

To investigate possible effects of different dipole moment distributions, we

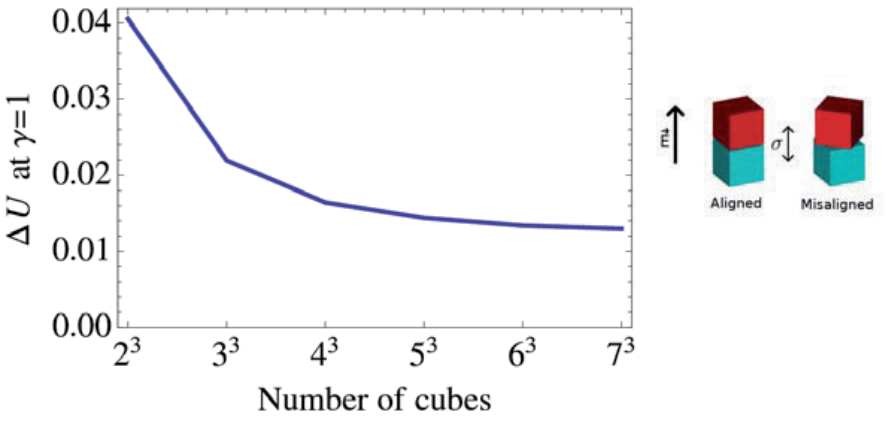

Figure 7.8: Energy difference ΔU between the most favorable (aligned) and least favorable (misaligned) orientations of two particles at distance σ along the z-axis, for different numbers of point dipoles per particle. A cartoon depicting the aligned and misaligned orientations is also shown

approximated the polarization of the cube with multiple dipoles evenly spread through the particle. To do this, we divided each cube into n^3 smaller cubes, and place a weaker dipole in the middle of each smaller cube, resulting in a simple cubic lattice. As the total number of dipoles quickly becomes hard to simulate directly, we only performed simulations for the case where each cube contains $n^3 = 2^3 = 8$ point dipoles, but performed energy calculations for cubes containing up to $n^3 = 7^3$ point dipoles.

It is interesting to note that even with multiple dipoles, a single particle in an external electric field still has a potential energy that is independent of the orientation. Thus, particles will not align in the electric field purely due to their polarization with this distribution of dipoles. Note that this is not true for all possible dipole distributions in the cube. Note that in these calculations we did not allow the dipole moment of one dipole to be influence by the field of others.

Secondly, if two cubes are placed on top of each other (as if they were in a string), the potential energy difference between different orientations turns out to be small, but still an order of magnitude larger than that of the difference at freezing between hard spheres in an fcc compared to an hcp configuration. For 8 dipoles in each cube, the difference between perfect alignment and the maximum misalignment (45^o) is only around $0.04\gamma k_B T$. While this difference will induce alignment at very high field strengths, the effect will be small below $\gamma \simeq 25$. Moreover, for particles containing more than 8 point dipoles, the effect of rotations on the potential energy decreases with the number of dipoles (see Figure 7.8). The energy difference appears to level off around $0.01 k_B T$, which would indicate that field strengths over $\gamma \simeq 100$ would be needed to align particles with the electric field.

To check this, we performed simulations of cubes containing 8 point dipoles, and studied alignment of particles in a string as a function of the field strength. Neighboring particles were seen to align in strings at field strengths higher than

$\gamma \simeq 30$, but for lower field strengths, no clear correlations in the orientations of neighboring particles were visible. Since the energy calculations show that the alignment effect decreases in strength on increasing the number of point dipoles per particle, we conclude that for a field strength lower than $\gamma = 30$, using multiple point dipoles per particle is not likely to significantly influence the aligning of cubes in the string fluid phase or hexagonal columnar phase.

7.4 Conclusions & outlook

We investigated the phase behavior of sharp-edged colloidal cubes in an external electric field. Our experiments illustrate that a single cube does not show any preferential orientation in an electric field. At low field strengths, string fluid phase was observed. Our preliminary results suggesting for indications of formation of a hexagonal columnar phase of an orientationally disordered cubes at moderate field strengths and volume fractions, and a bct phase at higher field strengths. Additionally, we predicted the phase behavior of hard colloidal cubes in an external electric field using Monte Carlo simulations in the NPT ensemble. The resulting phase diagram contains bct and simple cubic crystal phases, a hexagonal columnar phase, and a string fluid phase. The experimental γ values are not consistent with the simulations but our experimental results are in a qualitative agreement with the predicted phase diagram.

As far as we know, real space phase behavior studies of sharp-edged cubes in an electric field have not been reported before. We believe that our sharp-edged cubic particles could be coated with silica [29] after which the $NaMgF_3$ cubes can then be selectively removed by chemical etching so that these systems can be used for 3D real space studies. Coating of silica with octadecanol is a well established technique to keep the interactions short ranged and the particles dispersable in organic solvents [29].

Acknowledgements

I would like to thank Frank Smallenburg for performing simulations and for helpful discussions. I would also like to thank Stéphane Badaire for particle synthesis and Bo Peng for SEM measurements.

References

[1] E. Duguet, A. Desert, A. Perro, and S. Ravaine, *Design and elaboration of colloidal molecules: an overview*, Nature **40**, 941 (2011).

[2] S. M. Yang, S. H. Kim, J. M. Lim, and G. R. Yi, *Synthesis and assembly of structured colloidal particles*, J. Mater. Chem. **18**, 2177 (2008).

[3] S. Glotzer and M. J. Solomon, *Anisotropy of building blocks and their assembly into complex structures*, Nature Materials **6**, 557 (2007).

[4] A. Stein, F. Li, and N. R. Denny, *Morphological control in colloidal crystal templating of inverse opals, hierarchical structures, and shaped particles*, Chem. Mat. **20**, 649 (2008).

[5] S. Y. Sung Yong Park, K. R. Lytton-Jean, B. Lee, S. Weigand, G. C. Schatz, and C. A. Mirkin, *DNA-programmable nanoparticle crystallization*, Nature **451**, 553 (1996).

[6] C. A. Mirkin, R. L. Letsinger, R. C. Mucic, and J. Storhoff, *A DNA-based method for rationally assembling nanoparticles into macroscopic materials*, Nature **382**, 607 (1996).

[7] M. R. Jones, R. J. Macfarlane, B. Lee, J. Zhang, K. L. Young, A. J. Senesi, and C. A. Mirkin, *DNA-nanoparticle superlattices formed from anisotropic building blocks*, Nat. Mate. **9**, 913 (2010).

[8] K. D. Hermanson, S. O. Lumsdon, J. P. Williams, E. W. Kaler, and O. D. Velev, *Dielectrophoretic assembly of Electrically functional microwires from nanoparticle suspensions*, Science **294**, 1082 (2001).

[9] R. M. Erb, H. S. Son, B. Samanta, V. M. Rotello, and B. B. Yellen, *Magnetic assembly of colloidal superstructures with multipole symmetry*, Nature **457**, 999 (2009).

[10] H. R. Vutukuri, A. F. Demirors, P. Bo, P. D. J. van Oostrum, A. Imhof, and A. van Blaaderen, submitted.

[11] M. E. Leunissen, H. R. Vutukuri, and A. van Blaaderen, *Directing Colloidal Self-Assembly with Biaxial Electric Fields*, Adav. Mat. **21**, 3116 (2009).

[12] I. Sevonkaev, D. V. Goia, and E. Matijevic, *Formation and structure of cubic particles of sodium magnesium fluoride (neighborite)*, J. Colloid and Inter. Sci. **317**, 130 (2007).

[13] L. Rossi, S. Sacanna, W. T. M. Irvine, P. M. Chaikin, and D. J. Pine, *Cubic crystals from cubic colloids*, Soft Matter **7**, 4139 (2011).

[14] Z. Pu, J. Cao, J. Yang, K. Huang, and C. Hu, *Controlled synthesis and growth mechanism of hematite nanorhombohedra, anorods and nanocubes*, Nanotechonology **17**, 799 (2006).

[15] K. S. Cho, D. V. Talapin, W. Gaschler, and C. B. Murray, *Designing PbSe Nanowires and Nanorings through Oriented Attachment of Nanoparticles*, J. Am. Chem. Soc. **127**, 7140 (2005).

[16] S. J. Bettina, J. Carol, and F. A. Escobedo, *Phase behavior of colloidal hard perfect tetragonal parallelepipeds*, J. Chem. Phys. **128**, 044909 (2008).

[17] S. J. Bettina, S. Abraham, and F. A. Escobedo, *Cubatic liquid-crystalline behavior in a system of hard cuboids*, J. Chem. Phys. **120**, 9383 (2004).

[18] U. Agarwal and F. A. Escobedo, *Mesophase behaviour of polyhedral particles*, Nature Materials **10**, 230 (2011).

[19] X. Zhang, Z. Zhang, and S. C. Glotzer, *Simulation Study of Dipole-Induced Self-Assembly of Nanocubes*, The J. Phys. Chem. C **111**, 4132 (2007).

[20] E. van den Pol, A. V. Petukhov, D. M. E. Thies-Weesie, D. V. Byelov, and G. J. Vroege, *Experimental Realization of Biaxial Liquid Crystal Phases in Colloidal Dispersions of Boardlike Particles*, Phy. Rev. Lett. **301**, 258301 (2009).

[21] R. Blaak, D. Frenkel, and B. M. Mulder, *Do cylinders exhibit a cubatic phase?*, J. Chem. Phys. **110**, 11652 (1999).

[22] M. H. Lewis and M. W. A. Bright, *TRansformation twinning in synthetic neighborite*, The American Mineralogist **56**, 1519 (1971).

[23] P. P. Ewald, *Die Berechnung optischer und elektrostatischer Gitterpotentiale*, Annalen der Physik **369**, 253 (1921).

[24] B. Frenkel, D. anf Smit, *Understanding Molecular Simulations: From Algorithms to Applications*, Academic Press, New York, 2002.

[25] J. de Graaf, M. Dijkstra, and R. van Roij, submitted.

[26] U. Dassanayake, S. Fraden, and A. van Blaaderen, *Structure of electrorheological fluids*, J. Chem. Phys. **112**, 3851 (2000).

[27] B. W. Kwaadgras, M. Verdult, M. Dijkstra, and R. van Roij, *Polarizability and Alignment of Dielectric Nanoparticles in an External Electric Field: Bowls, Dumbbells and Cuboids*, J. Chem. Phys. **135**, 134105 (2011).

[28] A.-P. Hynninen and M. Dijkstra, *Phase diagram of dipolar hard and soft spheres: manipulation of colloidal crystal structures by an external field*, Phys. Rev. Lett. **94**, 138303 (2005).

[29] C. Graf, D. L. J. Vossen, A. Imhof, and A. van Blaaderen, *A General Method To Coat Colloidal Particles with Silica*, Langmuir **19**, 553 (2003).

Summary

The central theme of this thesis is exploiting the directed self-assembly of both isotropic and anisotropic colloidal particles to achieve the fabrication of one-, two-, and three-dimensional complex colloidal structures using external electric fields and/or a simple in situ thermal annealing method.

Colloids are typically defined as objects having at least one dimension in the size range of a few nanometers to several micrometers that form a dispersed phase when suspended in a continuum phase. As a result of Brownian motion, the colloidal particles are able to explore configurational space, and eventually reach the equilibrium configuration that minimizes the free energy. Spherical colloids have been used successfully as condensed matter model systems in order to study fundamental aspects of phase behavior, and dynamic processes such as glass transitions. An important feature of the colloidal particles is the possibility of controlling the size, shape, and composition. The interactions between the particles can also be manipulated by means chemical (e.g. charge, polymer coating) and physical (e.g. flat and rough surfaces) modification of surface of the particles and physical properties of the dispersing medium. The interactions between the colloidal particles can be altered by external fields such as electric fields, magnetic fields, and optical fields.

In this thesis, we have used external electric fields to impart anisotropy into systems consisting of both isotropic and an-isotropic particles. If there is a mismatch in permittivity between the particles and the suspending medium, the colloids acquire an induced dipole moment. A major advantage of this approach is that the interactions are tunable and fully reversible. Moreover, a large number of parameters can be used to control and tune particle interactions and subsequent self-assembly in AC electric fields, including field strength and frequency, particle shape, particle and solvent dielectric properties. Interestingly, the relatively simple anisotropic dipolar interaction already gives rise to several new phases in a uniaxial field.

In Chapter 2, we developed facile methods to fabricate colloidal analogues of polymer chains in all three stiffness regimes that can be observed on a single particle level, even in concentrated systems without using molecular tracers. We demonstrated that the methods simply rely on a combination of induced dipolar interactions by external fields to assemble the particles into strings and a simple bonding step (a simple in situ thermal annealing method or a seeded growth of a thin layer) to keep the particles together even after the field is switched off. In addition, we discussed the generality of our methods by using it to build several other colloidal polymer analogues, such as block-copolymer chains made by combining rigid and flexible strings, spherocylinders formed by heating rigid chains and both a-tactic and iso-tactic chains from dimer particles as the monomer units. We strongly believe that our method can, in principle, be used with any type of colloidal particles. We obtained control over the length, and the flexibility

of the bead chains. Additionally, we demonstrated by changing the flexibility of these chains we can tune the model system from a stiff biopolymer into a variant closer to a 'chemical' polymer. Next, we quantified the flexibility of both rigid and flexible bead chains by estimating the persistence length and the bond angle distributions of the rigid and flexible bead chains.

In Chapter 3, we demonstrated how our simple in situ thermal sintering method can be applied to a wide range of assembled systems such as, but clearly not limited: to close and non-close packed assemblies which are driven by different types of interactions, for instance, a weak attraction between oppositely charged particles e.g., CsCl morphology crystals, and a strong dipolar interaction resulting in quite different 3D bct crystals and maze like structures. Additionally, these bonded structures can easily be survived a subsequent drying step without loss of colloidal stability. We characterized these structures before and after the bonding using confocal and electron microscopy. An interesting feature of our method is that the permanently bonded and dried structures could be used either as seeds for crystal nucleation and growth studies or for a successive self-assembly process.

In Chapter 4, we exploited our simple thermal sintering method further for synthesizing polyhedral polymeric colloidal particles such as rhombic dodecahedron particles. Here, we varied the shape and the volume fraction of the assembled spherical particles after bonding by extend heating in such a way that mass transport between the particles does not take place. Next, these structures were disassembled by sonication at room temperature. The resulted particle shapes are remarkably smooth and stable in the solvent.

The anisotropy of induced dipole-dipole interactions gives rise to an entirely different suspension structure, even though the particles themselves remain spherical. In the low-field regime, the stable structure is a string fluid phase that consisted of chains of particles parallel to the applied field direction but no positional ordering in the lateral direction. In Chapter 5, we controlled the lateral position of the strings of particles with micrometer-scale precision by a combination of structured wall and electric dipoles. Our preliminary results strongly suggested that our method can be used to fabricate 3D assemblies with a desired lattice spacing by simply varying the ionic strength and the particle size. In this fashion non-closed packed structures can be achieved.

In Chapters 6 and 7 attention was shifted to directed self-assembly of anisotropic particles in external electric fields. The self-assembly of gold nano-sheets as a function of salt with electric fields was studied in Chapter 6. In the absence of salt, the repulsion overwhelms the attraction at all separations, and the particles remain isotropically dispersed. We calculated the interaction potential between two gold platelets in water as a function of the inter-platelet distance for different salt concentrations. The calculated potential curves revealed that the potential energy has a secondary minimum at an inter-particle distances between 50 nm to 200 nm for $\geq$ 0.2 mM dispersions, whereas at lower salt concentrations this minimum is comparable to the thermal energy. As a result of the secondary min-

imum between the particles, these platelets assembled into reversible worm-like columns at moderate salt concentrations. We found that the response of the gold platelets strongly depends on the ionic strength of suspension in an electric field, just as the phase behavior. In the absence of salt, the particles were aligned with their longest axis in the field direction in a head-to-toe arrangement. However, in the presence of enough salt the worm-like chains were aligned perpendicular to the applied field direction.

Finally, in Chapter 7, we studied the effect of external electric fields on the phase behavior of sharp-edged colloidal cubes using optical microscopy and Monte Carlo simulations. In contrast with most anisotropic particles, the potential energy of a single cube in an electric field is independent of its orientation. This was experimentally demonstrated with micron-sized cubes of single crystalline neighborite ($NaMgF_3$) in a MHz electric field. However, the dipolar attractions induced by the external electric field between particles can lead to alignment when two or more particles are in close proximity. Our preliminary results suggested the indications of formation of a hexagonal columnar phase of an orientationally disordered cubes at moderate field strengths and volume fractions, whereas a body-centered tetragonal (bct) phase was observed at higher field strengths. Additionally, we predicted the phase behavior of hard colloidal cubes in an external electric field using Monte Carlo simulations in the NPT ensemble.

Samenvatting

Het centrale thema van dit proefschrift is het benutten van de gestuurde zelforganisatie van isotrope en anisotrope colloïdale deeltjes voor de productie van complexe één-, twee- en driedimensionale colloïdale structuren, met behulp van zowel externe elektrische velden als een eenvoudige in-situ warmtebehandeling.

Colloïden worden gewoonlijk gedefinieerd als objecten die ten minste in één dimensie een afmeting hebben in de orde van enkele nanometers tot enkele micrometers. Bovendien dienen zij een gedispergeerde fase te vormen wanneer ze in een medium (een continue fase) worden gebracht. Ten gevolge van de Brownse beweging kunnen de colloïdale deeltjes in principe alle samenstellingen uit de ruimte van mogelijke configuraties aannemen, maar zij eindigen in een van de evenwichtsconfiguraties met minimale vrije energie. Bolvormige colloïden werden en worden succesvol gebruikt als modelsystemen voor gecondenseerde materie. Met zulke modelsystemen kan men fundamentele aspecten van fasegedrag te bestuderen, evenals dynamische processen zoals glasovergangen. Een belangrijk voordeel van colloïdale deeltjes is de mogelijkheid hun grootte, vorm en samenstelling te aan te passen. Daarnaast kunnen de interacties tussen de deeltjes gemanipuleerd worden door middel van chemische modificatie (bijvoorbeeld via hun lading of een polymeerlaag) en fysische modificatie (bijvoorbeeld door het aanbrengen van gladde of ruwe oppervlakken) van het deeltjesoppervlak, en door de fysische eigenschappen van het gekozen medium. De interacties tussen de colloïdale deeltjes kunnen ook worden beïnvloed met behulp van externe velden zoals elektrische, magnetische en optische velden.

In dit proefschrift hebben we gebruik gemaakt van externe elektrische velden om anisotro-pie aan te brengen in systemen van zowel isotrope als anisotrope deeltjes. Wanneer er een verschil in permittiviteit bestaat tussen de deeltjes en het medium, wordt in de colloïden een dipoolmoment geïnduceerd. Een groot voordeel is dan, dat de interacties geheel reversibel zijn en zelfs kunnen worden gemanipuleerd. Bovendien kan een groot aantal parameters worden gebruikt voor deze manipulatie van de deeltjesinteracties en daaropvolgende zelforganisatie in elektrische velden, waaronder de veldsterkte en -frequentie, de vorm van de colloïden, en de dielektrische eigenschappen van de deeltjes en het oplosmiddel. Interessant is ook dat de relatief eenvoudige anisotrope dipoolinteractie al resulteert in verscheidene nieuwe fases in een één-assig veld.

In hoofdstuk 2 ontwikkelden we eenvoudige methoden om colloïdale structuren te maken die het analogon zijn van polymeerketens, in elk van de drie regimes van rigiditeit die kunnen worden onderscheiden op het niveau van individuele ketens. Dit kon zelfs worden gedaan in geconcentreerde systemen en zonder het gebruik van moleculaire tracers. We hebben laten zien dat de methoden berusten op een combinatie van twee stappen: een stap waarbij we geïnduceerde dipoolinteracties onder externe velden gebruiken om de deeltjes zich in ketens te laten organiseren, en een eenvoudige verbindingsstap (een simpele in-situ ver-

warmingsmethode of het aangroeien van een dunne laag) om de deeltjes samen te houden ook nadat het veld is uitgeschakeld. Daarnaast hebben we de algemeenheid van onze methoden bestudeerd door er andere colloïdale polymeeranalogieën mee te bouwen. Voorbeelden daarvan zijn blok-copolymeerketens door combinatie van rigide en flexibele ketens, afgeronde cilinders gevormd door het verwarmen van rigide ketens, en zowel atactische als isotactische ketens met dimeren als monomeer-eenheden. We zijn er sterk van overtuigd dat onze methode in principe kan worden toegepast op elk type colloïdale deeltjes. Verder hebben we door de flexibiliteit van deze ketens aan te passen gedemonstreerd dat we het modelsysteem kunnen laten variëren van een rigide biopolymeer tot een variant die meer lijkt op een 'chemische' polymeer. Ten slotte hebben we de flexibiliteit van zowel rigide als flexibele ketens gekwantificeerd door een schatting te maken van hun 'persistence length' en de verdelingen van de bindingshoeken binnen de beide soorten ketens.

In hoofdstuk 3 hebben we getoond hoe onze eenvoudige thermische verhittingsmethode kan worden toegepast op een breed scala aan georganiseerde systemen, zoals bijvoorbeeld (maar zeker niet beperkt tot) geordende systemen met dichtste en niet-dichtste pakkingen. Dergelijke systemen kunnen door verschillende wisselwerkingen tot stand zijn gekomen, bijvoorbeeld door een zwakke aantrekking tussen tegengesteld geladen deeltjes zoals in kristallen met een CsCl morfologie, of door een sterke dipoolinteractie die resulteert in 3D bct kristallen en doolhof-achtige structuren. Daarnaast kunnen deze gebonden structuren een daaropvolgende droogstap doorstaan zonder verlies van colloïdale stabiliteit. We hebben deze structuren gekarakteriseerd voor en na de vorming van de verbindingen, door middel van confocale en elektronenmicroscopie. Een interessant aspect van onze methode is dat de gedroogde, permanent gebonden structuren de kern kunnen vormen voor een zelforganisatieproces, of voor studies naar kristalnucleatie en -groei.

In hoofstuk 4 hebben we onze eenvoudige thermische verhittingsmethode verder benut voor de synthese van polyeder-vormige polymerische colloïdale deeltjes waaronder rombische dodecaëders. We hebben de vorm en volumefractie van de geassembleerde bolvormige deeltjes veranderd door middel van langdurige verhitting, zodanig dat er geen massatransport tussen de deeltjes plaatsvond. Vervolgens werden deze structuren losgemaakt door sonicatie bij kamertemperatuur. De deeltjesvormen die daarvan het resultaat zijn, zijn opmerkelijk glad en stabiel in hun oplosmiddel.

De anisotropie van de geïnduceerde dipool-dipool interacties brengt een geheel andere structuur aan in de dispersie, hoewel de deeltjes zelf bolvormig blijven. Voor lage veldsterkte is de stabiele structuur een vloeistoffase die bestaat uit ketens van deeltjes parallel aan de richting van het aangebrachte veld, maar zonder ordening in de zijdelingse richting. In hoofdstuk 5 laten we zien hoe de laterale positie van de deeltjesketens met een nauwkeurigheid op micrometerschaal gekozen kan worden door een combinatie van elektrische dipolen en een

gestructureerde wand. Onze voorlopige resultaten geven sterk de indruk dat onze methode kan worden gebruik voor het vervaardigen van 3D assemblages met een gewenste 'lattice spacing' door eenvoudigweg de ionische sterkte en deeltjesgrootte te wijzigen. Op deze manieren kunnen niet-dichtste pakkingen worden verwezenlijkt.

In hoofstukken 6 en 7 werd de aandacht verlegd naar gerichte zelforganisatie van anisotrope deeltjes in externe elektrische velden. De zelforganisatie van gouden nanoplaatjes als functie van de zoutconcentratie in elektrische velden werd bestudeerd in hoofdstuk 6. In afwezigheid van zout domineert de afstoting de aantrekking op elke deeltjesafstand, en dan blijven de deeltjes isotroop gedispergeerd. We berekenden de interactiepotentiaal tussen twee goudplaatjes in water als functie van de afstand tussen de plaatjes voor verschillende zoutconcentraties. De berekende potentiaalcurven onthulden dat de potentiële energie een secundair minimum heeft bij een afstand tussen de deeltjes van 50 nm tot 200 nm voor $\geq$ 0.2 mM dispersies, terwijl bij lagere zoutconcentraties dit minimum vergelijkbaar is met de thermische energie van de deeltjes. Als gevolg van het secundaire minimum (tussen de deeltjes) assembleerden deze plaatjes in reversibele wormachtige kolommen bij gemiddelde zoutconcentraties. We ontdekten dat de reactie van de goudplaatjes in een elektrisch veld, evenals het fasegedrag, sterk afhangt van de ionische sterkte van de suspensie. In afwezigheid van zout lagen de deeltjes in een kop-staart rangschikking met de lange as in de richting van het veld. In aanwezigheid van genoeg zout waren de ketens loodrecht echter op de richting van het aangebrachte veld gericht.

Tot slot bestudeerden we in hoofdstuk 7 het effect van externe elektrische velden op het fasegedrag van scherpgerande colloïdale kubussen door middel van optische microscopie en Monte Carlo simulaties. In tegenstelling tot wat het geval is bij de meeste anisotrope deeltjes, is de potentiële energie van een enkele kubus in een elektrisch veld onafhankelijk van diens oriëntatie. Dit werd aangetoond met kubussen van een micron gemaakt uit enkelvoudig kristallijn neighboriet ($NaMgF_3$), in een elektrisch veld met een frequentie van 1 MHz. De dipoolinteracties die worden geïnduceerd tussen de deeltjes in een external elektrisch veld kunnen echter wel voor gelijkgerichtheid zorgen als twee of meer deeltjes zich dicht bij elkaar bevinden. Onze voorlopige resultaten wezen op de vorming van een hexagonale columnaire fase van kubussen met ongeordende oriëntaties bij lage veldsterktes en volumefracties, terwijl een 'body centered tetragonal'(bct) fase wordt gevormd bij hogere veldsterktes. Daarnaast voorspelden we het fasegedrag van harde kubussen in een extern elektrisch veld door middel van Monte Carlo simulaties in een NPT ensemble.

Acknowledgements

It is my great pleasure to express my gratitude towards all the people who have been instrumental in the journey of my PhD.

First and foremost, I would like to express my heartfelt thanks and deep sense of gratitude to my research advisor Prof. Dr. Alfons van Blaaderen whose help, stimulating suggestions, encouragement, and constructive criticism helped me during all the time of research work. Despite being very busy, you have always found time to answer my questions and listen to my problems. Alfons, I would like to thank you for giving me the opportunity and freedom to work in one of the leading soft condensed matter groups in the world. Your enthusiasm and knowledge were a great source of inspiration, scientifically and beyond. Next I would like to extend my gratitude to my co-advisor Dr. Arnout Imhof. Arnout, you were always ready for a discussion, thanks for numerous interesting discussions, for your suggestions and patience. I would also like to thank Marjolein Dijkstra, Rene van Roij, Krassimir Velikov, and Paul van der Schoot for fruitful discussions.

My scientific adventure began in the group of Prof. V. Kumaran, IISc, Bangalore, where I did my masters thesis and had some taste of basic research. Kumaran sir, you were the real source of inspiration and motivation for me to pursue a PhD.

I feel privileged to have been working with my esteemed collaborators inside and outside the SCM group in Utrecht. It's a great pleasure to thank all the people who synthesized the beautiful and colorful particles which have benefited me: Johan, Stéphane, Bo, Teun, Didi, Yu Ling, Carlos, and Gulşen. Johan, thanks for your unconditional support by supplying particles and also for the very useful discussions and suggestions. Stéphane, it was a great learning experience working with you, hopefully our work will end up in a nice publication, and also thanks for teaching me how to synthesize gold platelets, Merci! Mirjam, Ahmet, and Yu Ling, thanks for introducing me to the induced dipolar world! Frank, Edward, and Raghunath thanks for useful assistance in the persistence length calculations. Frank, thanks for our numerous stimulating discussions on 'torturing' the colloids with electric fields:). Ahmet, Bo, and Peter, thanks for our pleasant collaborations on colloidal beads chain work. Johan and Teun thanks for the fabrication of nice CsCl structures. Teun, thanks for our numerous car trips to various places around Utrecht and also for teaching me how to survive in the Dutch society in the beginning! Djamel, it was fun working with you, thanks for our work on μ-gravity experiments on earth! Anke, thanks for our pleasant collaborative work on 'kogelvormige' particles in electric fields. Bas, thanks for the help in the DLVO potential calculations. Arjen and Rien thanks for the help with the DSC measurements. Hans, Bo, and Carlos, thanks for the SEM measurements. I would like to thank Michel, Teun, and Thijs for their help with particle tracking. My thanks also go to Hans, Peter, Carlos, Gulşen, and Judith for the great technical support I received over the years. I want to thank Marlous for the Dutch translation of the thesis summary on a short notice. I am very thankful to my students Ernest

and Stephanie. Special thanks go to Ahmet, Anke, and Mirjam for the nice office atmosphere and also for the useful conversations. I would like to thank the people from the FOM personnel department: Maria Teuwissen, Annette Bor, and Manon Quik. You guys were always helpful and easy to approach. I would also like to thank my 'paranimfs'.

I would like to give special thanks to Joost, Peter, and Laura, who have patiently proofread some of my thesis chapters and provided me with insightful comments during the past few months. Special thanks also go to Anjan, not only because I could speak to you in my mother-tongue but also for the numerous dinners we shared especially during the thesis writing. Eduardo, Chantal, and Andrea thanks for a fabulous and memorable trips to Sicily and Alhambra, Granada, Gracias! Allesandro, I enjoyed the trip to Copenhagen, Grazie! Esther and Peter, thanks for organizing group outings to the 'Wadlopen (walking in mud!!)' and Efteling.

I would like to give a 'BIG THANK' to all past and present members of the SCM group for the beautiful atmosphere, both scientifically and socially.

Coming to non-scientific life in Utrecht, it has been full of fun, excitement and new friendships. Surely, my Indian friends played a big role in my non-scientific life in Utrecht. Due to their warm affection I never felt home sick. The journey was so overwhelmingly joyful with the association of many friends and most importantly due to Narasimha-Pranitha, Rajesh-Sasi, Vijay-Priya, Pavan-Bindu, Ippili-Geeta, Shyam-Prasanna, Madhu-Lavanya, Ashish-Radhika, Gupta-Suhasini, Sai, Satya, and Raghu. Special moments such as our frequent get together in Vijay's house at Indian Festival celebrations and followed by delicious Indian food. I thank you all for all your help, friendship and for many qualities that I have learned from you. I will always cherish your hospitality whenever I visited your houses. I would also like to thank Carl, Anne, Ana, Daniela, Tab, Rik, Gijs, Laxmi, Jissy, Deepa, Priya-Esther, Divya, Devashish, Raja, Helene, and Viviana, for their friendship and help. Anne, thanks for introducing me to the traditional Dutch dish 'Stamppot', Bedankt!!. I would also like to thank the people of The Netherlands for their friendly and frank nature-Utrecht truly feels like a second home now!

Finally, I extend whole hearted thanks to my parents, who taught me the value of hard work by their own example. I would like to share this moment of happiness with my parents, my brother, my sisters, my brother-in-law, and my cute and smiley niece and nephews. They rendered me enormous support during the whole tenure of my research.

Hanumantha Rao

List of publications

This thesis is partly based on the following publications:

- H. R. Vutukuri, A. F. Demirörs, B. Peng, P. D. J. van Oostrum, A. Imhof, and A. van Blaaderen, *Colloidal analogues of charged and uncharged polymer chains with tunable stiffness*, submitted - Chapter 2.
- H. R. Vutukuri, J. Stiefelhagen, and T. Vissers, A. Imhof, and A. van Blaaderen, *Bonding assembled colloids without loss of colloidal stability*, Advanced Materials, **24**, 412(2012) - Chapter 3.
- H. R. Vutukuri, A. Imhof, and A. van Blaaderen, *A facile method for creating polyhedral colloidal latex particles*, in preparation -Chapter 4.
- H. R. Vutukuri, Y. L. Wu, A. Imhof, and A. van Blaaderen, *Epitaxial growth of 3D colloidal structures in electric fields*, in preparation -Chapter 5.
- H. R. Vutukuri, S, Badaire, A. Imhof, and A. van Blaaderen, *Directed self-assembly of highly anisotropic gold platelets in an electric field*, in preparation -Chapter 6.
- H. R. Vutukuri, S, Badaire, A. Imhof, and A. van Blaaderen, *Colloidal cubes in electric fields*, in preparation -Chapter 7.

Other publications

- M. E. Leunissen, H. R. Vutukuri, and A. van Blaaderen, *Directing Colloidal Self-Assembly with Biaxial Electric Fields*, Advanced Materials, **21**, 3116(2009).
- D. El. Masri, T. Vissers, S, Badaire, J. Stiefelhagen, H. R. Vutukuri, P. Helfferich, T. H. Zhang, W. K. Kegel, A. Imhof, and A. van Blaaderen, *Rotational averaging-out gravitational sedimentation of colloidal dispersions and phenomena*, submitted.